Data-driven Approach to Predict the Static and Fatigue Properties of Additively Manufactured Ti-6Al-4V

by

Antriksh Sharma

A Thesis Presented in Partial Fulfillment
of the Requirements for the Degree
Master of Science

Approved July 2020 by the
Graduate Supervisory Committee:

Yongming Liu, Chair
Qiong Nian
Yang Jiao

ARIZONA STATE UNIVERSITY

August 2020

ABSTRACT

Additive manufacturing (AM) has been extensively investigated in recent years to explore its application in a wide range of engineering functionalities, such as mechanical, acoustic, thermal, and electrical properties. The proposed study focuses on the data-driven approach to predict the mechanical properties of additively manufactured metals, specifically Ti-6Al-4V. Extensive data for Ti-6Al-4V using three different Powder Bed Fusion (PBF) additive manufacturing processes: Selective Laser Melting (SLM), Electron Beam Melting (EBM), and Direct Metal Laser Sintering (DMLS) are collected from the open literature. The data is used to develop models to estimate the mechanical properties of Ti-6Al-4V. For this purpose, two models are developed which relate the fabrication process parameters to the static and fatigue properties of the AM Ti-6Al-4V. To identify the behavior of the relationship between the input and output parameters, each of the models is developed on both linear multi-regression analysis and non-linear Artificial Neural Network (ANN) based on Bayesian regularization. Uncertainties associated with the performance prediction and sensitivity with respect to processing parameters are investigated. Extensive sensitivity studies are performed to identify the important factors for future optimal design. Some conclusions and future work are drawn based on the proposed study with investigated material.

ACKNOWLEDGMENTS

I would like to extend my heartiest appreciation and sincere thanks towards my advisor Dr. Yongming Liu for his valuable suggestions and critiques throughout the development of this research. His patience, motivation, and immense knowledge brought this research to its logical end.

I would also like to offer my special thanks to the committee members, Dr. Qiong Nian and Yang Jiao who found my research work interesting and contributed towards the improvement of the thesis through their insights and review.

I am particularly grateful to my parents and my little sister for their continuous encouragement and unfailing support for the betterment of my research.

Lastly, I am thankful to my friends and colleagues who were there by my side in times of stress, anxiety, and distress to push me through those difficult situations.

TABLE OF CONTENTS

CHAPTER Page

CHAPTER Page

APPENDIX Page

LIST OF TABLES

Table Page

Table Page

LIST OF FIGURES

Figure Page

Figure Page

Figure Page

CHAPTER - 1

INTRODUCTION

1.1 General Background

The ingenious innovations happening in the industrial sector and fast-growing competition in the global market from the past few decades have encouraged the engineering sector to devote extra attention to building products with high added value and exceptional capabilities to perform under extreme working conditions. In some cases, the required properties and shapes cannot be attained by conventional manufacturing techniques, such as turning, milling, boring, drilling, grinding, and abrasive jet machining. Each manufacturing process is capped by the number of resources employed and its continuity depends on the profit gained from its manufacturing be it in terms of money, increased component life, or customer satisfaction. The cost of a finished product is a total of the costs of metal extraction, manufacturing process, and post-manufacturing process. The extraction cost determines the cost for extracting the mineral from its ore, the post-manufacturing determines the topology and morphology of the final product however the cost of manufacturing is depended on how the manufacturing is done, how much material wastage happens during that process, and how much energy is consumed for carrying out that process. For instance, the cost of production of titanium alloys is a factor of the cost involved with the extraction process of titanium mineral from its ore (Kroll's Process) and the cost of the fabrication process which may require high energy consumption, protective environment, and significant material wastage [1], [2]. These factors, therefore, limit the usage of titanium alloy to a still broader utilization [1]. To reduce these capping factors, research has been focused on developing efficient alternate manufacturing procedures [3].

1.2 Manufacturing Processes

To date, the manufacturing of metals, composites, and alloys is conducted broadly in two manners. One is a subtractive manufacturing method and the other is an additive manufacturing method.

Subtractive Manufacturing:

As the name suggests, subtractive manufacturing is a process where the material is removed from a solid block, bar, rod of plastic, metal, or other materials to shape them into the required dimensions by removing material using conventional machining processes like turning, milling, boring, drilling, grinding, and abrasive jet machining, etc. Other than these techniques, CAD software is also used in conjunction with non-conventional machining processes like Electron discharge machining (EDM), laser cutting, water jet cutting, and Computer numerical control (CNC) machining, etc.

Additive Manufacturing (AM) or 3D printing:

Unlike subtractive manufacturing where the material is removed from a large casted piece, the additive manufacturing process is based on adding material layers one at a time where each successive layer bind to the preceding, layer by layer until the part is complete. AM also uses CAD models which are utilized by 3D printers to deposit the material, or selectively melt and fuse the powder to create the part. However, some cleaning and finishing processes are required after the part has been manufactured by 3D printing to achieve their final dimensions before they are ready to use [4].

Subtractive manufacturing processes no doubt have their advantages but there are certain aspects to 3D printing which gives it the edge over the former. First and foremost, it opens a platform for manufacturing a vast variety of materials like plastics, resins, ceramics, glass, concrete, and metals and mostly all the manufacturing involves a few basic steps [5]. Unlike subtractive machining, AM doesn't have to deal with a unique process & equipment and tool for different materials [6]. Thirdly, 3D printers can perform the needful without or minimal human intervention although many still require supervision to ensure the printing process is accurate [6]. Fourthly, AM provides flexibility in the complexity and customization of the design without affecting the production cost which is far greater than subtractive machining where manufacturing complex shapes put a heavy toll on the manufacturing tool [6], [7]. Lastly, AM is found to be environmentally suitable as it results in a reduction of energy consumption and emission of CO_2 along with minimal wastage of material [8]. Also, in some AM processes like Powder-Bed-Fusion (PBF) techniques, the Powder (manufacturing material) can be reused to obtain efficient AM in some materials [9], [10]. 3D printing still lacks behind the alternate on a few fronts such as initial expenditure, manufacturing time, and small size production [11].

Some of the advantages of AM in varied streams are presented hereunder [12]–[19]:

- Aerospace:
  - Improved development cycles and complex design parts
  - Consolidation of design and spares manufacturing

  - Less material wastage and in-process quality assurance
  - Aircraft brakes, heat pipes, joints, passenger doors, engine nacelle, ailerons, spoilers, flaps, undercarriage doors, wingtips, rotor blades, stabilizers, fuselage skin are a few of many in-use 3D printed aerospace components.
- Sports:
  - Lightweight equipment and enhanced customization
  - Better safeguard and accessories
  - Data collection with a simulating and scanning equipment
  - Footwear, golf balls, surfing and skating boards, speed boats, scuba diving tanks, race cars, baseball bats, hockey sticks, skis, and many more are in practice.
- Automotive:
  - Design and concept of communication and prototyping validation
  - Preproduction sampling, tooling and customized parts
  - Driveshafts, fan blades, accelerating pedals, air filter housing, radiator end caps, mirror housing, brake shoes, belts, interior panels, bumper fuel tanks, bicycle, tire frames, and truck body are a few of in-use 3D printed automotive components.
- Medical:
  - Heart valves, pacemakers, attachment wires, surgical instruments, wheelchairs
  - 3D printed biocompatible medical implants, prosthetics, and hearing aids
  - Dental bridges, aligners, crowns, orthodontic appliances, and stone models
- Military:
  - Modeling, test units, and prototyping

- Replacement parts, tooling, and maintenance
- Structural components for defense systems
- Localized production and freedom of design and customization
- Helmets, bulletproof vests, impact-resistant vehicles, engine and equipment foundations, rudders, hovercrafts are some of the in-use 3D printed military components

1.3 Material Selection

As mentioned earlier additive manufacturing can work with plastics, resins, ceramics, glass, concrete, and metals. Mechanical properties of metals or alloys to be used play a major role in deciding its application in industry. Ti-6Al-4V is one of the most sought far titanium alloys in diverse fields of engineering owing to its high strength, low density, low coefficient of thermal expansion, outstanding corrosion resistance, high cycle fatigue resistance, and biocompatibility. These characteristics of titanium alloys help in taking a decisive role in applications that warrant high reliability and end-use of the products such as in surgery and medicine, aerospace, automotive, chemical plant, power generation, oil and gas extraction, sports, and other major industries.

In most of the industrial and allied engineering applications, titanium has replaced heavier materials. Further, titanium alloy has proved to be stronger, reliable, and more durable thereby giving it an edge over other available choices. The density of titanium is about 60% that of steel, this makes it lighter and potential material for aerospace applications [12]. The advantage of high strength, low density, low coefficient of thermal expansion, and good corrosion resistance tempts the use of titanium and its alloys in automobiles as well.

This may help to reduce fuel consumption, improve the efficiency of the engine, and reduce the noise; however, being expensive material it is not commonly used in ordinary cars, though it finds its application in luxury cars, special purpose cars, and sports cars [13].

With the advent of the latest machines and advancements in manufacturing techniques, the use of implants has become very common. However, these implants must be in line with the requirements of human beings. These must possess biomechanical properties comparable to those parts which need to be replaced and must be compatible without any side effects. The essential requirements for all medical implants include good corrosion resistance, good biocompatibility, bio-adhesion, and machinability [20]–[22]. To ensure that the implants satisfy these requirements, materials being used are checked for genotoxicity, carcinogenicity, reproductive toxicity, cytotoxicity, irritation, sensitivity, and residues of sterilization [23], [24]. Modern-day medical implants have to pass strict regulations, and these must ensure the safety, effectiveness, and compatibility of the patients. Titanium and its alloys have been widely accepted as an implant for orthopedic and dental applications over the last few decades [25]. Among the different types of titanium alloys, Ti-6Al-4V remains the most widely used material for possessing appropriate properties, such as higher strength, lower modulus of elasticity, better corrosion behavior, and superior biocompatibility compared to other metallic biomaterials [26], [27]. High corrosion resistance is primarily due to the spontaneous formation of the protective passive TiO_2 film on titanium surfaces [28].

At times the damaged components or parts might not be readily available for replacement e.g. an implant for one person may not be suitable to another. Similarly, many industrial and engineering applications may require a specific type of components and parts to be fabricated and replaced. Such customized parts can be fabricated through Additive Manufacturing. The present work, therefore, focuses on various types of Additive Manufacturing Techniques for fabricating parts using Ti-6Al-4V powder.

This study includes six main chapters. Followed by the Introduction, Chapter 2 discusses the literature review where detailed information about titanium and its alloys is discussed. It also covers various AM techniques and post processes utilized to manufacture Ti-6Al-4V alloy. Chapter 3 presents the data-driven approach using multi-regression analysis and Artificial Neural Network (ANN) to estimate the static and fatigue properties of Ti-6Al-4V alloy manufactured by different 3D printing processes. Chapter 4 shares the open literature data collection for tensile and fatigue properties of the Ti-6Al-4V alloy fabricated using the different AM processes. The results of the model developed in Chapter 3 are then presented in Chapter 5. Finally, Chapter 6 presents the conclusions drawn and future work associated with the study.

CHAPTER - 2

LITERATURE REVIEW

2.1 Titanium and its Alloys

2.1.1 History and Properties of Titanium

It was in 1791 when the then-unknown element was first discovered by a British chemist, William Gregor, who preferred to call it ‘Gregorite’. Later in 1795, a Prussian chemist, Martin Heinrich Klaproth, independently discovered the same element and entitled it ‘Titanium’. However, extraction of titanium from its ore wasn’t achieved until 1910 when pure metallic titanium was first prepared by heating titanium tetrachloride with sodium in a steel bomb. It was in 1932 when Wilhelm Justin Kroll came up with a process, now known as Kroll’s Process, to reduce titanium from titanium tetrachloride ore using Calcium which brought titanium outside of the laboratory and into the commercial market. With further modifications to the process, he observed that using Magnesium instead of Calcium as a reducing agent makes the process commercially more efficient. Kroll’s process to date is the most widely used method for obtaining titanium from titanium tetrachloride [3],[29].

Titanium has an atomic number of 22 and falls under the d-block transition elements category as per the periodic table. Titanium is the ninth most plentiful element and the fourth most abundant structural metals in Earth’s crust ranked just below aluminum, iron, and magnesium. The only downside is that it is never found in the pure state and the extraction process makes it expensive on top of which it is seldom found in high concentrations. Titanium is a non-ferrous metal and with a density of 4.51 g/cm^3, it can be classified as heaviest lightweight metal [29].

Being a low-density element (approximately 60% density of steel), backed up by non-magnetic and good heat-transfer behavior titanium in itself posts a tough competition to other vastly used materials like steel and aluminum. However, its coefficient of thermal expansion is nearly half of that of aluminum and lower than steel. To compensate for such shortcomings, titanium alloys are used instead of titanium element in the industry very variedly. Some of the physical and mechanical properties of element titanium are presented in Table 2.1 [30]:

Table 2. 1 Physical and mechanical properties of pure titanium

Property	**Description or value**
Atomic number	22
Atomic weight	47.90
Atomic volume	10.6 *W/D*
Color	Dark gray
Crystal Structure	
Alpha (≤882 °C)	Close-packed hexagonal
Beta (≥882 °C)	Body-centered cubic
Density	4.51 g/cm^3
Melting point	1668 ± 10 °C
Solidus/liquidus	1725 °C
Boiling point	3260 °C
Specific heat (at 25 °C)	0.5223 kJ/kg · K
Thermal conductivity	11.4 W/m · K
Heat of fusion	440 kJ/kg (estimated)
Heat of vaporization	9.83 MJ/kg
Specific gravity	4.5
Hardness	70 to 74 HRB
Tensile strength	240 MPa
Young’s modulus	120 GPa
Poisson’s ratio	0.361
Coefficient of linear thermal expansion	8.41 μm/m · K

2.1.2 Titanium Crystal Structure and Alloying

Pure titanium exhibits various crystallographic forms with each modification stable within a certain temperature ranges, thus, defining it as an allotropic element. Similar properties are shown by certain other elements like Ca, Fe, Co, Zr, Sn, Ce, and Hf. At room temperature, titanium exhibits hexagonal close packing (hcp) which is also called the α-phase titanium or simply α-titanium. There occurs a crystallographic transformation when titanium is solidified from a liquid or when titanium is heated to a temperature above 882 ± 2 °C. This transformed structure of titanium is a body-centered cubic (bcc) also called the β-phase titanium or simply β-titanium [30]. Both of these crystal structures can be seen in Figure 2.1 with the shaded plane representing the most densely populated plane.

A complete transformation from one crystallographic form to the other is called allotropic transformation and the temperature at which this transformation takes place is referred to as transus temperature. Based on these two crystal structures, generally accepted stable classes of titanium alloys are 'alpha', 'alpha+beta', or 'beta'.

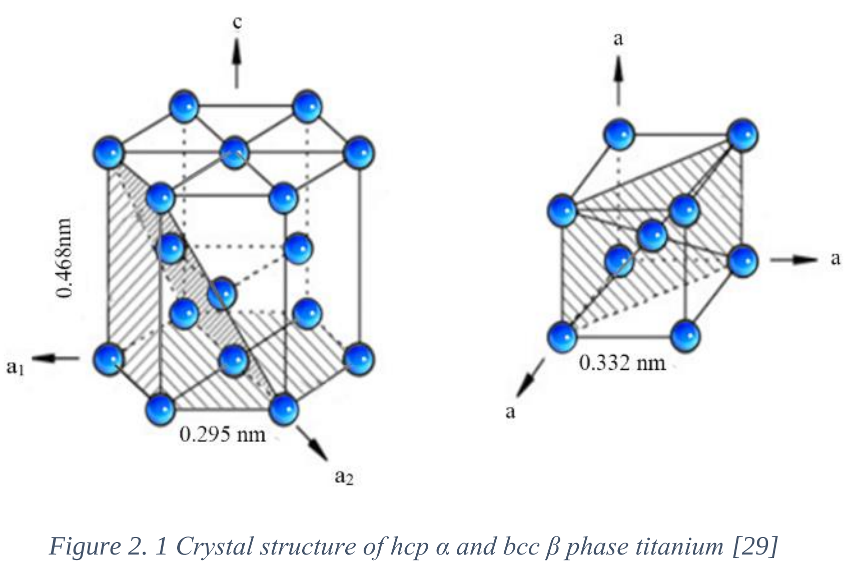

Figure 2. 1 Crystal structure of hcp α and bcc β phase titanium [29]

Due to the allotropic behavior of titanium, it is employed in different applications. However, at room temperature, the stable form of titanium is the alpha form while at a temperature higher than 882 ± 2 °C, the stable form of titanium is the beta form and therefore, at lower temperatures, titanium cannot be utilized for the beta phase applications and similarly at high temperature, the alpha phase applications cannot be utilized. However, by alloying titanium metal with other elements like aluminum, tin, vanadium, manganese, oxygen, iron, molybdenum, or chromium, etc., alloy crystal structure can be stabilized at room temperature and in turn making it possible to manufacture near-alpha, alpha, mixed alpha-beta, near-beta, and beta structure titanium alloys at room temperature. Table 2.2 shows a few examples of titanium alloys for each of the stable titanium phase and the possible property trends that can be observed with different alloy crystal structures.

Alloying elements are classified based on their influence on the α/β-transition temperature as α stabilizers, β stabilizers, and neutral. α stabilizers tend to increase the transition temperature and hence results in a stable alpha crystal structure alloy. Aluminum, oxygen, nitrogen, and carbon are examples of α stabilizers. On the other hand, elements that depress the transition temperature lead to a stable beta crystal structure alloy. Vanadium, iron, chromium, nickel, cobalt, and molybdenum are examples of β stabilizers. Neutral elements present no effect on the stability of any phase. Tin and zirconium are examples of such alloying elements. Mechanical properties of each phase alloy are somewhat representative of the stabilizing element involved. β-stabilizing elements introduce high density to the alloy resulting in a higher strength while α stabilizing elements are equipped with low density but moderate strengths and higher ductility. The properties of the α+β phase alloys lie in between both extremes as presented by Table 2.2 [30]. However, properties like fracture toughness and fatigue life get affected by heat treatment and other post-manufacturing processes, and therefore, they cannot be related directly to either stabilizing elements.

Table 2. 2 Titanium alloy microstructures and consequent property trends

Titanium Alloy Microstructures				
α	Near α	α+β	Near β	β
α stabilizers: Al, O, N or C Neutral elements: Zr, Sn	1-2% of β stabilizers are added along with larger amounts of α stabilizers	Equally favoring α and β stabilizers	1-2% of α stabilizers are added along with larger amounts of β stabilizers	β stabilizers: Mo, V, Fe, Cr, Mn or Si
Unalloyed Ti Ti-5Al-2.5Sn Ti-8Al-1Mo-1V	Ti-6Al-2Sn-4Zr-2Mo Ti-8Al-1Mo-1V	Ti-6Al-4V Ti-6Al-6V-2Sn	Ti-8Mn Ti-8Mo-8V-2Fe-3Al	Ti-3V-11Cr-3Al Ti-11.5 Mo-6Zr-4.5Sn
Property Trends				
Density →				
Heat treatment response →				
Strain rate sensitivity →				
Strength →				
Fabricability →				
← Weldability				
← Creep strength				
← Oxidation behavior				
← Corrosion behavior				

2.1.3 Classification of Titanium Alloys

As mentioned earlier depending on the proportion of each phase present, titanium alloys are classified as near-alpha, alpha, alpha-beta, near-beta, and beta phases. The near-α alloys have 1-2% of the β-stabilizers approximately and 5-10% β phase. α-alloys have no β stabilizers and consequently no β phase. α+β alloys have higher amounts of β-stabilizers resulting in 10-40% of the β phase. Similarly, near-β/metastable and β alloys have higher amounts of the β-stabilizers and constitute a predominant β-phase [31].

Figure 2.2 illustrates the possibilities of making each titanium phased alloy based on an α-stabilizing element, aluminum (Al), and a β-stabilizing element, vanadium (V) using a schematic 3D phase diagram. The alpha alloys comprise of unalloyed titanium and titanium alloys having aluminum or any neutral interstitial occupancy.

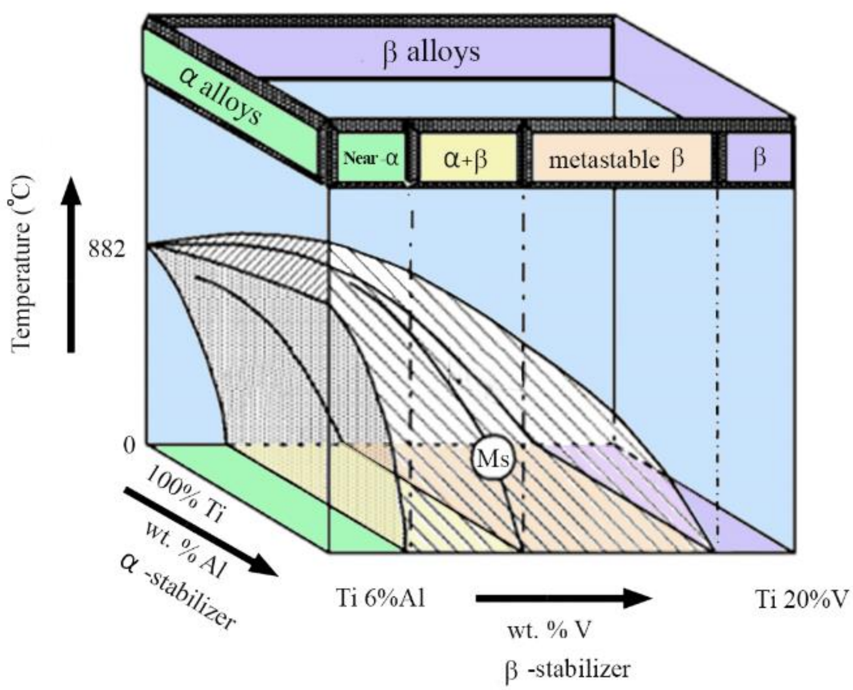

Figure 2. 2 3D representation of titanium alloys in relation with an α-stabilizing (Al) and a β-stabilizing element (V) [29]

Minor addition of the vanadium drives the alloy to near alpha titanium alloys. Having a blend of aluminum equally dominant as vanadium results in an α+β alloy group where β volume fraction ranges from 10-40% at room temperature. This α+β alloy phase stays until at quenching, the alloy is no longer able to transform into martensite (Ms). As this volume fraction of vanadium is passed, the β-phase becomes dominant and alloy, still being in two phases, obtains a metastable/near beta state. Lastly, a single-phase beta alloy is obtained when vanadium has complete dominance over the interstitial sites of titanium. Each of the titanium alloys with their properties has been discussed in the following section in detail.

<u>Unalloyed titanium or Commercial Purity (CP) titanium:</u>

CP titanium is the weakest form of titanium yet shows the most corrosion resistance. It is represented in four grades specifically 1, 2, 3, and 4 based on the nitrogen, carbon, hydrogen, oxygen, and iron present in the interstitial sites. Since CP titanium has α-stabilizing or neutral elements in interstitial sites backed by their stable hcp crystal structure at room temperature, it can be regarded as α-phase titanium. These α-stabilizing or neutral element additions suffice titanium utilization in various applications, for instance, oxygen, nitrogen, and iron as the interstitial elements greatly strengthen pure titanium. High purity grade-1 CP titanium equipped with lesser oxygen, nitrogen, and iron percentage depict lower strength and hardness and a consequent lower transformation temperature than those with higher amounts of interstitial elements. Following the same trend, grade-4 CP titanium has the lowest corrosion resistance but the highest strength and hardness. A general representation of the composition of CP titanium grades and their tensile properties is shown in Table 2.3. CP titanium is employed in the form of a coil, bar, wire, strands, and cables in a variety of medical and industrial applications like pacing leads, needles, woven wire mesh, eye-glass frames, orthodontic appliances, ligature clips, and multiple orthopedic appliances.

Table 2. 3 Composition and tensile properties of distinct grade CP titanium [32]

Grade	Max. Weight %					Tensile Properties		
	N	C	O	Fe	H	UTS (MPa)	YS (MPa)	El (%)
1	0.03	0.10	0.18	0.20	0.015	241	172	24
2	0.03	0.10	0.25	0.30	0.015	345	276	20
3	0.05	0.10	0.35	0.30	0.015	448	379	18
4	0.05	0.10	0.40	0.50	0.015	552	483	15

Alpha titanium alloys:

Having neutral stabilizers or a higher concentration of alpha stabilizers, these titanium alloys exhibit hcp crystal structure at room temperature. Other than having low to medium strength, good notch toughness, oxidation resistance, and reasonable ductility they exhibit good resistance against creep at a higher temperature than the rest of the titanium alloy class. Therefore, alpha alloys developed using aluminum, tin, and zirconium as stabilizing elements are well suited for high temperature and cryogenic applications. However, at high temperatures, a reduction in ductility and toughness is observed because of an excess of interstitial sites getting occupied. They intrinsically exhibit good weldability which brings in the fact why they do not respond to heat treatment. Hence, their properties cannot be enhanced by modification of microstructure and to get around these hindrances, extra low interstitial (ELI) alloys with reduced interstitial site occupancy are prepared. Ti-5Al-2.5Sn-ELI is such an example of an alpha alloy used excessively in cryogenic applications because it can retain its ductility and toughness as a result of reduced interstitial site occupancy [30]. Mechanical properties of a few alpha phase Ti alloys are presented in Table 2.4.

Table 2. 4 Mechanical Properties of a few α alloys [33]

Alloy	UTS (MPa)	YS (MPa)	El (%)	Hardness (HV)
Ti-2Bi	360	310	25	210
Ti-10Bi	520	425	15	300
Ti-20Bi	585	535	3	365

Near-alpha titanium alloys:

Near alpha titanium alloys are a result of the addition of a small amount of β-stabilizers to an alpha alloy composition and are also called super-alpha titanium alloys. These are excellent for high temperature (500-550 °C) applications due to near excess α-stabilizers.

Table 2. 5 Mechanical Properties of a few near-α alloys [29]

Alloy	UTS (MPa)	YS (MPa)	El (%)	Hardness (HV)
Ti-6-2-4-2-S	1010	990	13	340
TIMETAL 834	1010-1050	900-950	10-16	-
TIMETAL 1100	1030	910	6-12	350

Also, due to the presence of a small amount of β phase, its high temperature creep resistance and oxidation resistance are accompanied by a higher strength compared to the alpha alloys. Some microstructural grain changes can also be observed upon heat treatment.

Compressor discs in a gas turbine, compressor blades for jet engines, and skins for airframes, etc. are found to exploit the abilities of Ti–6Al–5Zr–0.5Mo–0.25Si, Ti-8A1-1Mo-1V, and Ti-6A1-2Nb-lTa-0.8Mo near-alpha titanium alloy [30]. Mechanical properties of a few near-alpha titanium alloys are presented in Table 2.5.

Alpha+beta titanium alloys:

With a further increase of beta stabilizers, equally dominant alpha and beta phases can be obtained in the titanium alloy. An increase in the beta phase accounts for the reduction in the alpha phase and hence alpha+beta titanium alloys exhibit lower creep strength and weldability than near-alpha and alpha phase alloys. However, they come with a perfect blend of properties from alpha and beta phases and hence are very well suited for a balanced set of properties where high tensile strength vs fracture toughness, high tensile strength vs high cycle fatigue, and good creep resistance vs low cycle fatigue strength are the deciding criteria of material selection. They show good formability and are heat treatable hence, a wide variety of microstructures can be tailored by manipulating thermodynamic processing parameters as per the requirement. Solution heat treatment, quenching, and age hardening can be used to increase the strength of alpha+beta alloys as per the end-use application. For example, Ti-6-2-2-2-2 finds its applications in high-temperature (400 °C) conditions like gas turbine engines while Ti-6-2-4-6 is utilized as high strength and high toughness alloy. Titanium alloy market is captured by alpha+beta alloys and specifically Ti-6Al-4V marks more than half of the alpha+beta titanium alloy production. It is stronger than CP titanium and exhibits lower Young's modulus than stainless steel thus acting as a straight competitor. Ti-6Al-4V finds its applications majorly in the aerospace, biomedical, marine, and power generation industries [3]. Table 2.6 illustrates the mechanical properties of a few alpha+beta phase titanium alloys.

Table 2. 6 Mechanical Properties of a few α+β alloys [29]

Alloy	UTS (MPa)	YS (MPa)	El (%)	Hardness (HV)
Ti-6-2-2-2-2	1100-1300	1000-1250	8-15	-
Ti-6-4	900-1200	800-1100	13-16	300-400
Ti-6-2-4-6	1100-1200	1000-1100	13-16	330-400
Ti-6-6-2	1000-1100	950-1050	10-19	300-400
Ti-17	1100-1250	1050	8-15	400

<u>Beta and near-beta titanium alloys:</u>

Beta and near-beta alloys are formed when an excess of beta phase is observed in titanium alloy which lowers the temperature of allotropic transition. Accompanied by rich β-stabilizers and minimal or no amounts of α-stabilizers, beta and near-beta alloys are characterized by high hardenability resulting in strength levels over 1300 MPa. Because of their attractive combination of fatigue resistance, toughness and strength, corrosion resistance, and creep resistance against intermediate temperatures, these alloys have gained attention over the past few decades. They have high density, poor oxidation resistance, moderate weldability, and higher formulation cost that alpha+beta alloys. Also, excess β-phase invites more slip systems which makes them susceptible to faster crack growth rates. Beta and near beta alloys are seen to contribute to the aerospace industry majorly. Some microstructure modifications make them and effective choice in the automotive industry and moderate temperature gas turbine engines. Ti–13 V–11Cr–3Al, Ti–8 V–6Cr–4Mo–4Zr–3Al (Beta C), and Ti–15Mo–2.7Nb–3Al–0.2Si (TIMETAL 21S) are some examples of beta alloys [34]. Table 2.7 illustrates the mechanical properties of a few metastable beta and beta phase titanium alloys.

Table 2. 7 Mechanical properties of a few metastable β and β alloys [29]

Alloy	UTS (MPa)	YS (MPa)	El (%)	Hardness (HV)
SP700	960	900	8-20	300-500
Beta III	900-1300	800-1200	8-20	250-450
Beta C	900-1300	800-1200	6-16	300-450
Ti-10-2-3	1000-1400	1000-1200	6-16	300-470
Ti-15-3	800-1100	800-100	10-20	300-450

2.1.4 Ti-6Al-4V, an α+β Titanium Alloy

Ti-6Al-4V also known as Ti64 or Grade 5 titanium is the most commonly used alpha+beta titanium alloy dominating more than 50% of titanium alloy manufacturing because of its excellent balance of properties [12]. Aluminum, the α-stabilizing element contributes nearly 6 wt.% while vanadium, the β-stabilizing element contributes to 4 wt.%. The chemical composition of cast Ti64 according to ASTM standards is shown in Table 2.8.

Table 2. 8 The chemical composition of Ti-6Al-4V alloy [35]

Element wt. (%)	Al	V	Fe	O	N	C	H	Ti
Min.	5.50	3.50	0	0	0	0	0	Remainder
Max.	6.75	4.50	0.30	0.20	0.10	0.05	0.015	Remainder

Ti64 has been contributing to the aircraft and aerospace industry as a structural material for a long time [3]. It gives in a good balance between strength, ductility, fatigue, and fracture toughness properties along with low density, high corrosion resistance, and the ability to alter microstructure after heat treatment. Therefore, Ti64 becomes an optimum choice for applications like airframes, bolts, seat rails, cabin brackets, bleed pipes, pressure vessels, aircraft gas turbine engines, fan blades and cases, surgical implants, prosthetics, suspension, racing prototypes, automotive parts, and marine equipment. Ti64 doesn't exhibit fixed mechanical properties per se. Mostly its properties are adjusted by the post-manufacturing heat treatment like annealing, stress-relieving, solution heat treatment, and aging treatment, etc. to suit the purpose.

2.1.4.1 Ti64 alloy microstructure:

Being an alpha+beta alloy, Ti64 contains both alpha-phase (hcp) and beta-phase (bcc) crystal structures. In hcp crystal structure, lattice parameters are observed to be 'a = 0.293 nm and c = 0.467 nm' [36] against 'a = 0.295 nm and c = 0.468' nm in pure titanium [3]. At room temperature, the measure lattice parameters for bcc crystal structure in Ti64 were 'a = 0.323 nm' compared to 'a = 0.332 nm' measure at the β-transus temperature in pure titanium [29] which maybe because of the high temperature required to attain β-phase crystal structure.

The size and arrangement of alpha and beta phases in the microstructure are determined by the rate at which the alloy is cooled from the beta phase region. Different heating conditions and cooling rates can give rise to different microstructures namely fully lamellar, fully equiaxed, and bi-modal (duplex), martensite, and widmanstätten. A brief description of each of these microstructures is presented in the following section.

1. <u>Fully lamellar microstructure:</u>

As the name suggests, lamellar structures have the alpha phase distributed in plates-like shapes. Such a microstructure can be achieved by a series of processes that can be better understood in Figure 2.3. When heated enough above the beta transus temperature, the alloy possesses a complete beta phase dominance or a homogeneous beta phase. This process is called homogenization. Next, the alloy is deformed by either by rolling or forging at temperatures near the beta transus temperature (can be in either beta or alpha-beta phase fields).

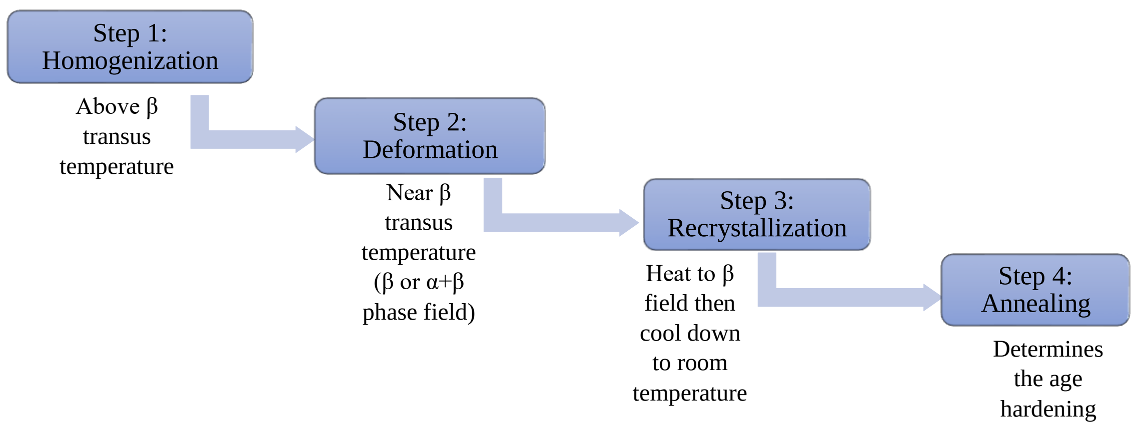

Figure 2. 3 Processing route resulting in a fully lamellar microstructure

Afterward, the alloy is heated back to the beta phase field and cooled down to room temperature at a controlled cooling rate. This cooling rate acts as the deciding factor for the distinguishable microstructure parameters. From Figure 2.4, the alpha lamellae width, alpha colony size, and width of the alpha layer at beta grain boundaries can be observed to have decreased with the increase in cooling rate [37]. Finally, recrystallization at 30-50 °C above the beta transus temperature ensures that unnecessarily segregates are eliminated and a solid phase equilibrium between alpha and beta phases is obtained.

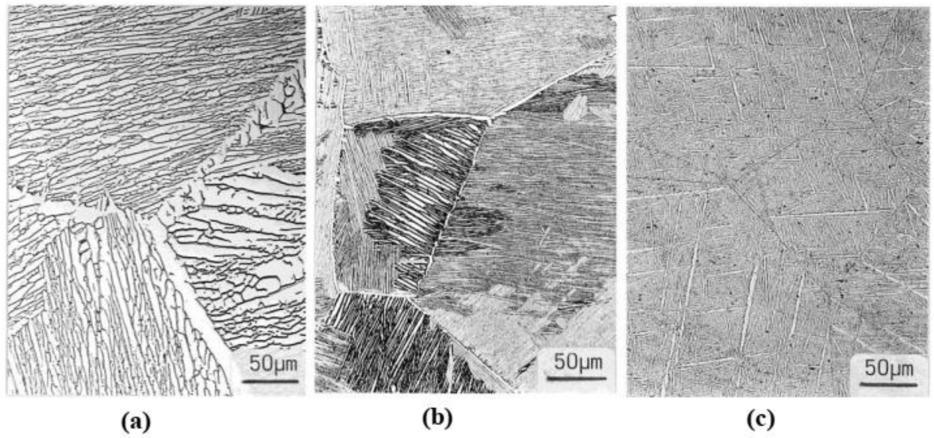

Figure 2. 4 Effect of cooling rate on the lamellar microstructures: (a) slow; (b) intermediate; (c) quenching [37]

The martensitic microstructure is one of the forms of fully lamellar microstructures that are produced as a result of very fast cooling (water quenching) from temperatures above the martensite start temperature. Due to the high-temperature variations, the bcc beta crystals completely transform into hcp alpha crystals by a diffusionless process leaving no retained beta phase [29],[38]. The alpha phase is supersaturated in beta stabilizing elements. Figure 2.4 (c) is an example of a martensitic microstructure.

2. Widmanstätten microstructure:

Also known as the 'basketweave' microstructure, it is also an extension of the fully lamellar microstructure and is obtained when Ti64 alloy is cooled at critically slow rates (air cooling) from the beta phase region. When the temperature of alloy starts to drop below the beta transus temperature (about 980 °C for Ti64), the hcp alpha phase starts to appear in the form of plates parallel to the special plane in the beta phase. Phase development begins with nucleation with an alpha phase nucleus. Alpha phase shows more affinity towards similar phase crystals and hence the plane parallel growth is more compared to plane perpendicular growth resulting in a plate-like region. The growth continues until another beta crystal special plane comes along and hinders the plan parallel growth. Six non-parallel alpha phase sets are formed as a result of six potential non-parallel growth planes sites in the beta grains. Figure 2.5 shows the formation of the Widmanstätten microstructure [30], [39], [40].

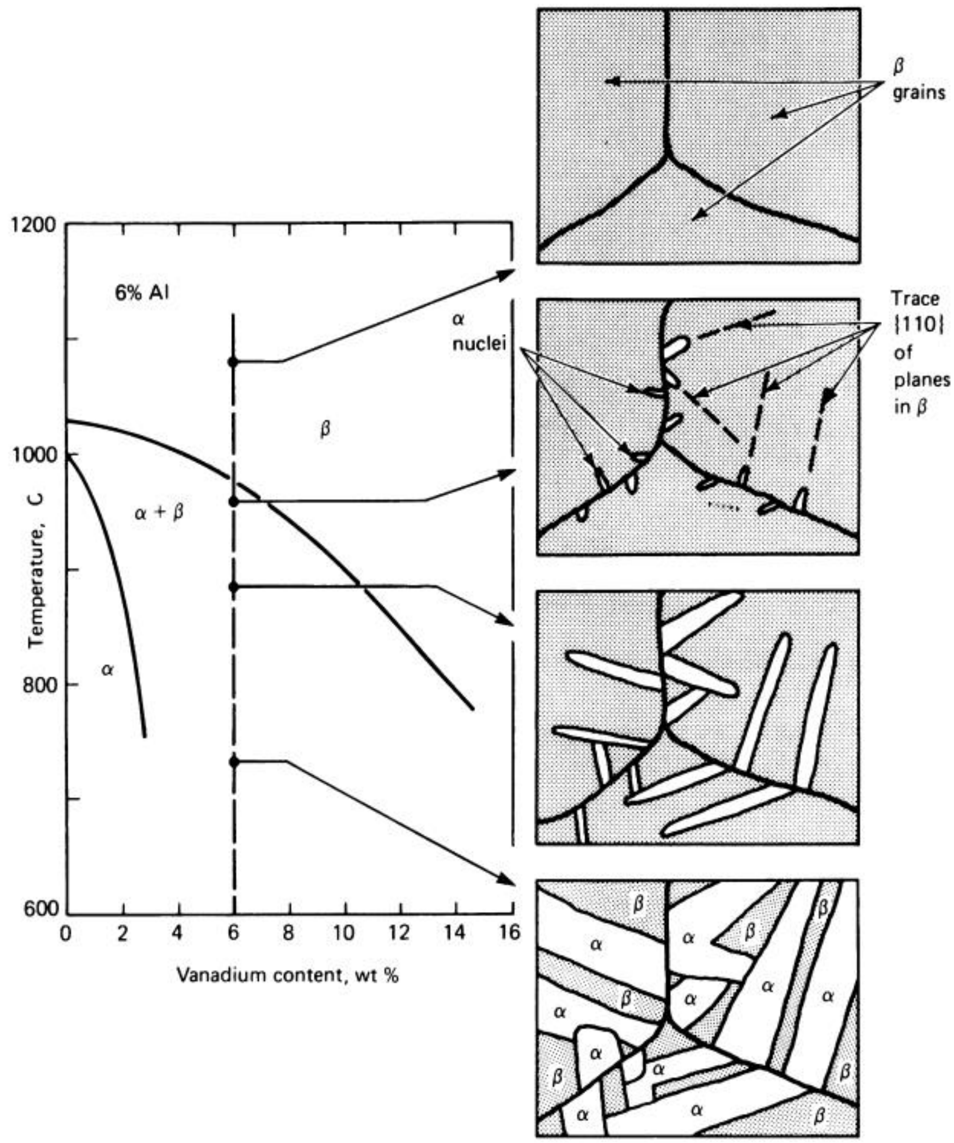

Figure 2. 5 Schematic representation of the formation of Widmanstätten microstructure [30]

3. <u>Bi-modal (duplex) microstructure:</u>

The process route schematics shown in Figure 2.6 can be used to understand the procedure for a duplex microstructure. Similar to the lamellar microstructure process, the duplex microstructure is achieved in four different stages beginning with the homogenization process with heating the alloy well above beta transus temperature. Stage two is conducted in the alpha+beta phase field generally and the plastic deformation of alpha lamellae is the objective of this stage.

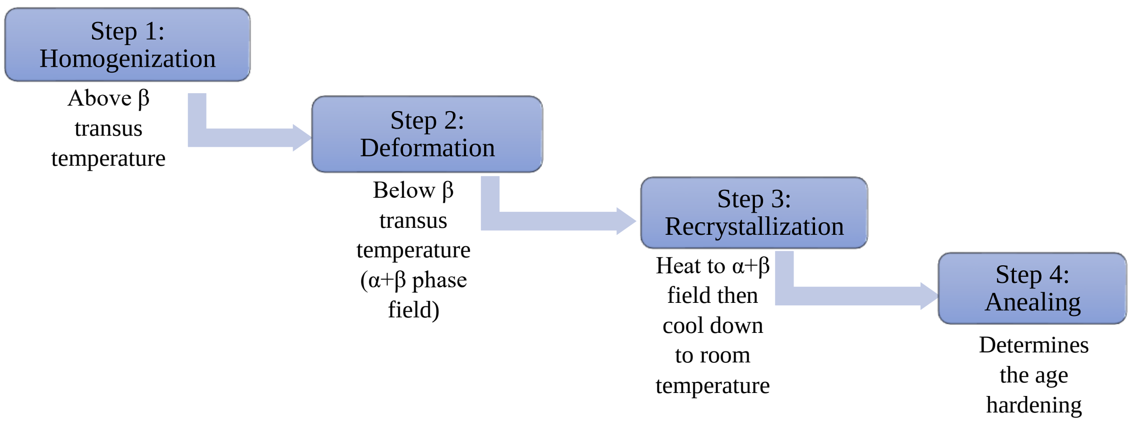

Figure 2. 6 processing route resulting in a duplex microstructure

In the third stage, recrystallization is performed. This recrystallization aids the alpha phase to generate new equiaxed grains at the expense of the deformed lamellae ones in the previous stage and therefore, the final stage incorporates both equiaxed and lamellae alpha grains as can be seen in Figure 2.7. The critical parameter here is the cooling rate at which the alloy is cooled after this homogenization process which determines the width of lamellae alpha grains. Their deformation acts as the basis of the generation of equiaxed alpha grains during the recrystallization process. Figure 2.7 shows the duplex microstructure as a result of two different cooling rates after homogenization.

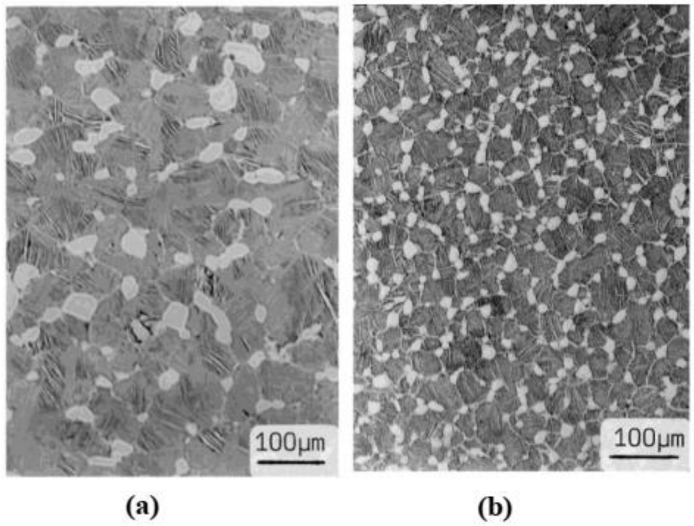

Figure 2. 7 Effect of cooling rate on the duplex microstructures: (a) slow; (b) fast [37]

4. <u>Fully equiaxed microstructure:</u>

When the alpha phase is existent only as equiaxed grains, see Figure 2.8, then the microstructure is called fully equiaxed. These can be developed following the same approach as of the bi-modal microstructure with small modifications. To establish all the alpha phase in equiaxed form, the lamellae alpha grains would have to be converted into equiaxed grains. This can be achieved by two methods.

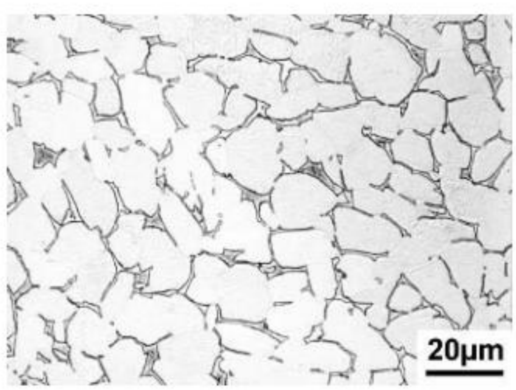

Figure 2. 8 Fully equiaxed microstructure obtained after slowly cooling from the bi-modal recrystallization annealing temperature [29]

One way is to perform the recrystallization process at such a low temperature that the alpha phase exists in high enough equilibrium volume fraction to develop the equiaxed microstructure at the expense of so far deformed lamellar structure. The other is to impose a sufficiently lower cooling rate recrystallization annealing temperature. This would allow only equiaxed alpha grains to grow during the cooling process and no alpha lamellae will be formed resulting in a fully equiaxed microstructure [3].

2.1.4.2 Tensile properties of different microstructure Ti64

The following section discusses the tensile behavior of each of the above-discussed microstructures of Ti64 alloy. Table 2.9 represents the tensile behavior of lamellar microstructure Ti64 alloy with respect to the cooling rate.

Table 2. 9 Tensile behavior of the lamellar Ti64 microstructures against the cooling rate [41]

	Cooling rate (°C/min)	UTS (MPa)	YS (MPa)	El. (%)
Lamellar Microstructure Ti-6Al-4V	2000	1095	1035	13
	500	1040	970	15
	50	980	910	16

Depending on the cooling process, the mechanical properties of fully lamellar microstructure Ti64 alloys vary because the microstructure gets changed as a result of the cooling process as depicted in Table 2.9. Mechanical performance of the fully lamellar microstructure is strongly affected by the alpha plate thickness which is determined by the cooling rate after the homogenization step. Faster cooling rates develop decreased alpha plate thickness resulting in a proportionate decrease in the effective slip length [42]. Since, the yield strength is a measure of resistance to the dislocation motion upon loading, therefore, with a reduction in slip length, yield strength increases. Hence, faster cooling rates produce higher strength Ti64 alloys as evident from the values for water quenched fully lamellar microstructure in Table 2.9. However, in the case of tensile ductility, it is observed to increase with the increase of cooling rate at first and then declines. This phenomenon is supposed to happen because of a change in the fracture mode from transcrystalline dimple type at lower cooling rates to intercrystalline dimple type at higher cooling rates [3]. Figure 2.9 can be used as an estimate for the strength and ductility behavior of lamellar alloys with cooling rates.

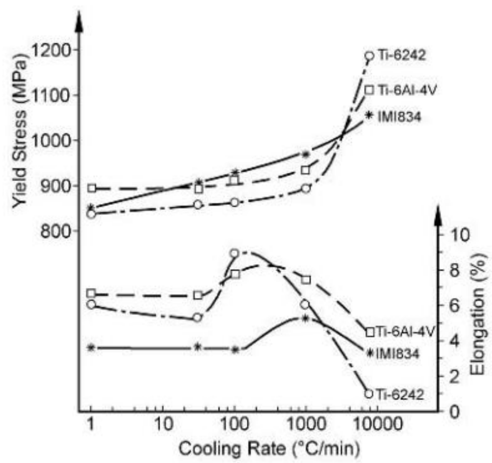

Figure 2. 9 Effect of cooling rate on strength and ductility of lamellar microstructures [3]

Another impacting parameter on the mechanical behavior of lamellar microstructure alloys is beta phase grain boundaries [43]. Beforehand short beta grain boundaries act as sites from where dislocation propagation becomes easier as least energy expense is required in the process thus preferred [42]–[44]. Long prior beta grain boundaries hinder dislocation propagation and therefore, long beta grain boundaries result in reduced ductility.

Two important factors determining the mechanical behavior of bimolar microstructures are the size of beta grain and the alloy element partitioning effect. Commercially prepared bimolar alloys are usually well processed generating an almost perfect recrystallized microstructure where the beta grain size is nearly equal to the distance between primary alpha grains. This implies that the volume fraction and the size of primary alpha grains can be used as a measure for the beta grain size in bimolar microstructures. Less the size of beta grains, more is the size and volume fraction of alpha grains, in turn, shorter the effective slip length, therefore, an increase in the yield strength and ductility are observed. However, the alloying element partitioning effect also plays some role in deciding this mechanical behavior of the alloy. An increase in the volume fraction of the primary alpha phase leads to an increase in the partitioning effect which is responsible for a slightly lower inter-lamellar strength and becomes a deciding factor unlike in the fully lamellar microstructure. [3]. For small primary alpha concentrations, alpha plate thickness behaves as the dominating factor, and the alloy strength increases while for large concentrations, the partitioning effect overshadows the former leading to a decrease in the alloy strength. Hence, to attain a high strength microstructure, there needs to be a balance between the partitioning effect and beta grain size consideration. Bimolar microstructures are accompanied by a much smaller effective slip length due to some amounts of equiaxed alpha grains getting built on top of the lamellar grains. The smaller slip length determines the increment in the ductility compared to lamellar structures [42].

Table 2. 10 Yield strength and area reduction for an equiaxed Ti64 alloy against change in α-grain size [3]

	α-grain size (μm)	Yield Strength (MPa)	Area Reduction (%)
Equiaxed Microstructure Ti-6Al-4V	2	1120	50
	6	1065	40-50
	12	1030	40

The primary factor for determining the tensile properties of the equiaxed microstructures is the alpha grain size which determines the effective length, in turn, determining the tensile behavior of the alloy. The relationship of tensile properties to the alpha grain size in equiaxed microstructures behaves similar to that of the tensile properties and alpha plate thickness in lamellar microstructures. They present very high tensile ductility of the order of bimodal microstructures or even higher. Table 2.10 shows the variation of yield strength and area reduction with respect to α-grain size for an equiaxed Ti64 alloy.

2.2 Additive Manufacturing (AM) or 3D Printing

Additive Manufacturing also known as rapid prototyping, 3D printing, or Solid Freeform Fabrication (SFF) is a layer on layer fabrication technique wherein the material to be deposited is melted by a focused heat source such as laser power or electron beam. Latest AM techniques allow materials (say Ti-6Al-4V) to be used in the powdered form and each layer of powder is fused by an appropriate power source. Laser beam source is used to produce high precision small parts whereas electron beam AM is used for bigger and parts with the rougher surface [45].

2.2.1 History of Additive Manufacturing

Origin of Additive manufacturing falls back to late 1970s when the first AM concept was introduced by Ross Housholder in 1979 which he referred to be utilizing a molding process for forming a three-dimensional article in layers [46]. In 1981, Hideo Kodama was the first scientist to actually develop a functioning model of AM with photo-hardening thermoset polymer which utilized a mask pattern to control the exposure of UV rays [47]. In 1982, Alan Herbert, following a similar approach but independently, developed, and tested a prototype part [48], [49]. The first commercialized AM machine was introduced by Charles Hull, the stereolithography apparatus (SLA), in 1986 which is recognized as the first 3D printer [48], [50]. It was based on slowly pouring liquid plastic to build plastic layer by layer and hence made it expensive enough to be used by large companies, research groups, and labs only, however, this invention was a major breakthrough as it used digital data files to develop 3D models. In 1988, Scott Crump filed a patent for using CAD/CAM bed fused deposition model (FDM) following adding layers as a basic approach [51]. Soon after, in 1990, Carl Dickard filed a patent for first-ever selective laser sintering (SLS) process which worked by shooting a laser at a powdered material rather than a liquid [52]. Several other 3D printing techniques were introduced to humankind during this period however, not all reached the same popularity. Fewer known techniques are Laminated Object Manufacturing (LOM) by Michael Feygin, Ballistic Particle Manufacturing (BPM) by William Masters, Solid Ground Curing (SGC) by Itzchak Pomerantz, and Three-dimensional printing (3DP) by Emanuel Sachs, etc. Some major patents related to 3D printing marking its history until 1990 have been listed in Table 2.11. From the late 1990s onward, additive manufacturing entered its adolescence stage where the general market wasn't familiar with its concepts and advantages however, it had started to become a hot topic for research scholars. It was the period when 3D printers started becoming available to the market and CAD tools were being developed to use those 3D printers. In 1993, one of the first CAD tools, 'solidscape' was developed. In the early 2000s, AM was first used in medical applications to develop dental implants and prosthetics.

Table 2. 11 Patents related to 3D printing until 1990 [49]

Name	Title	Filed	Country
Housholder	Molding Process	December 1979	U.S.
Murutani	Optical Molding Method	May 1984	Japan
Masters	Computer automated manufacturing process and system	July 1984	U.S.
Andre et al.	Apparatus for making a model in industrial part	July 1984	France
Hull	Apparatus for making three-dimensional objects by stereolithography	August 1984	U.S.
Pomerantez et al.	Three dimensional mapping and modelling apparatus	June 1986	Israel
Feygin	Apparatus and method for forming an integral object from laminations	June1986	U.S.
Deckard	Method and apparatus for producting parts by selective laser sintering	October 1986	U.S.
Fudim	Method and apparatus for production of three-dimensional objects by photosolidification; radiating an uncured photopolymer	February 1987	U.S.
Arcella et al.	Casting shapes	March 1987	U.S.
Crump	Apparatus and method for creating three-dimensional objects	October 1989	U.S.
Helinski	Method and means for constructing three-dimensional articles by particle deposition	November 1989	U.S.
Marcus	Gas phase selective beam deposition: three-dimensional, computer controlled	December 1989	U.S.
Sachs et al.	Three-dimensional printing	December 1989	U.S.
Levent et al.	Method and apparatus for fabrication of three-dimensional articles by thermal spray deposition	December 1990	U.S.

Thereafter, the first-ever functional miniature kidney was developed and now AM is contributing to producing bones, ears, jawbones, blood vessels, vascular networks, tissues and organs, eyeglasses, windpipes, cell cultures, stem cells, and drug delivery devices, etc. and since then AM is actively used to build prototypes in industries taking a bigger leap towards the fabrication of functional and tailor-made parts. It exhibits tremendous potential in different scientific and technological areas name it tooling, manufacturing, medicine, or any other sophisticated material addition process. AM in today's scenario is widely accepted in diverse fields such as automotive industry, aerospace applications, biomedical, etc., however, the end product needs to exhibit sufficient mechanical properties and possess good strength to enable it to become a functioning part. In most of the aforementioned applications, metal is used as the material of choice. Therefore, the AM processes that are most commonly used to produce metal components are considered in the following section.

2.2.2 Additive Manufacturing for Metals and Metal Alloys

Additive manufacturing requires wire or powder form of the material it needs to additively manufacture, therefore, only a handful of materials available are being manufactured by industry. A few of those plastics and metallic materials are listed in Table 2.12.

Out of these, only DED, PBF, sheet lamination, and binder jetting are involved in metal processing. For fabrication of metals and their alloys, majorly DED and PBF processes are utilized however, there have been some studies available with sheet lamination too. Table 2.13 illustrates the majorly employed AM techniques for 3D printing metals and their alloys.

Table 2. 12 Plastic and metallic materials currently available for AM

Plastics Materials	Metallic Materials
ABSAcrylonitrile butadiene styrene (ABS)	Stainless Steel
Polylactic Acid (PLA)	Tool steel
Polyamide	Titanium and titanium alloys
Polycarbonate	Cobalt and chromium alloys
Nylon Plastic	Aluminum alloys
Polyaryletherketone (PAEK)	Bronze alloys
VisiJet®	Inconel
DuraForm®	Silver
PrimeCast®	Gold
Accura plastics	Nickel-titanium superalloys

Table 2. 13 Major Additive manufacturing techniques for metals and their alloys

AM Process type	**Process Concept**	**Technology**
PBF	Selective sintering	Selective Laser Sintering (SLS) Direct Metal Laser Sintering (DMLS)
	Selective melting	Selective Laser Melting (SLM) Electron Beam Melting (EBM)
DED	Blown powder	Laser Engineered Net Shaping (LENS) Direct Metal Deposition (DMD) Fused Deposition Modelling (FDM)
	Wire feed	Wire and Arc Additive Manufacturing (WAAM) Direct Laser Fabrication (DLF)

This study concerns the fabrication of Ti-6Al-4V which is a popular choice for high-density load-bearing applications hence EBM, SLM, and DMLS in PBF and DED which result in dense fabrications via melting and solidification of powder will be discussed in the following sections. WAAM which uses wire as a feedstock unlike PBF techniques and hence counted as a DED process where an electric arc is used to heat the metal to its melting temperature and then directly deposit it to the substrate has also been gaining attention for fabricating Ti64 alloy [53]–[56]. For the comparison purpose, this study includes only those processes where the powder is used as feedstock material.

2.2.2.1 Direct Energy Deposition (DED)

DED is an additive manufacturing process where molten material is directly deposited at the substrate in layers that stack up to generate the whole CAD profile. Unlike PBF, it employs both powder form and wire form as the feedstock. Before the deposition process, the melt is prepared by a laser, electron beam, or electric arc. The substrate is fixed on the worktable and similar to PBF, the chamber is either filled with an inert gas for laser-based proceedings or vacuum to reduce the oxygen content in the chamber for electron beam based proceedings.

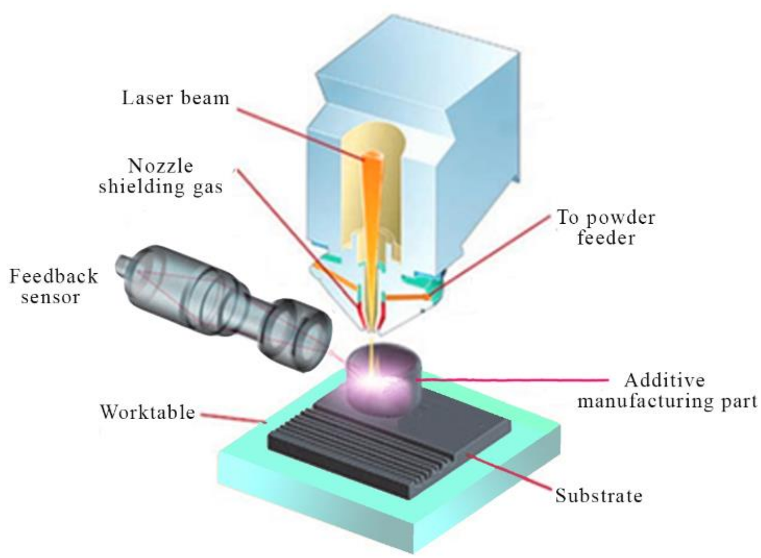

Figure 2. 10 Schematic representation of a DED process [53]

The melt prepared beforehand is then poured on the substrate using a nozzle and the melt solidifies as soon as the nozzle moves away. The nozzle follows a predetermined path to ensure the CAD design to get built. Subsequent layers are then injected into the melt pool one layer at a time to generate the AM part as a whole. Figure 2.10 shows a schematic for a DED process.

Characteristics of DED

DED is compatible to work with a wide variety of metal-based materials like aluminum alloys, stainless steel, titanium alloys, nickel, copper, Inconel, and tungsten, etc. Since the DED systems utilize metal deposition via a nozzle, therefore, complex geometries can be obtained by mounting that nozzle to a multi-axis arm. High-density fabrication can be obtained from a DED process and the ability to control grain structure makes it an ideal fit for repairing in-use metal components. It is a high-speed fabrication process depositing metal directly from a nozzle. The amount of powder needed for depositing a layer can be calculated and the same volume of metal can be melted therefore leading to no material wastage, in turn, reducing the cost of fabrication. One demerit of DED processes is the surface finish and low-resolution product obtained after the fabrication which needs further processing and hence adds to the overall cost of the component.

2.2.2.2 Powder Bed Fusion (PBF)

PBF is an additive manufacturing technique that employs high power energy sources like laser or electron beam for melting or sintering the metal powder. The process begins with fixing up the base plate on which the rest of the build has to be carried on and providing an inert gas atmosphere for laser-based or vacuum to reduce oxygen for electron beam based manufacturing in the closed chamber. Then, a thin layer of spherical powder is optimally distributed, leveled to a predetermined thickness, for reducing the unwanted anomalies in the design. The high energy power source is used to scan the powder selectively melting or sintering the powder to fill in the design provided by the CAD data. After the first layer has attained the required shape, the next layer of powder is spread, and the process is repeated. Since the penetration power of the laser/electron beam is deeper than one layer, each new layer gets welded to the previous layer. At the end of the process, the unused powder can be reused again or mixed with a new powder stack for another manufacturing unit. A schematic representation of a PBF process is shown in Figure 2.11.

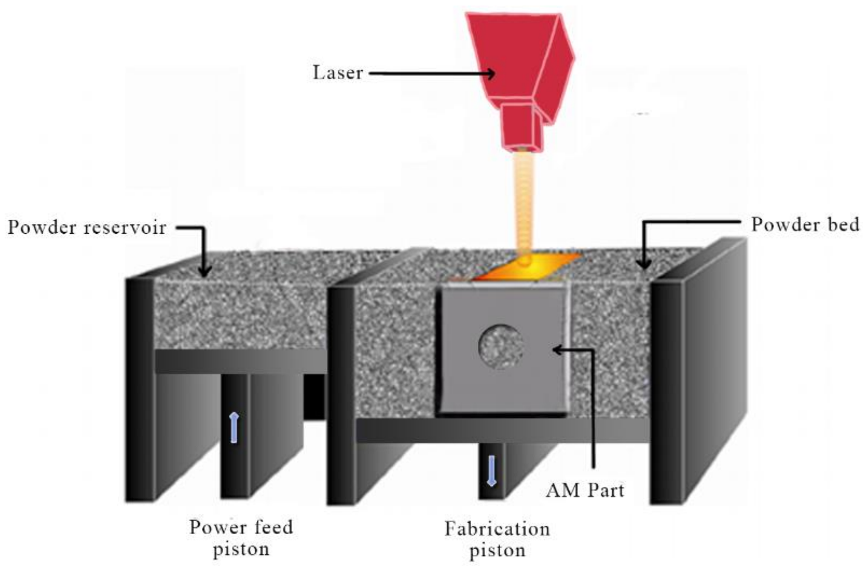

Figure 2. 11 Schematic representation of a PBF process [57]

Microstructure and mechanical properties of the final build are dependent on the processing parameters and the post-fabrication heat-treatments. Figure 2.12 can be used as a reference to understand the various processing parameters involved in a PBF process [57]. A few of them are explained hereunder:

a) Powder layer thickness or sometimes mentioned as layer thickness is the thickness of a powder bed that is prepared for one round of laser or electron beam to scan and melt. It is varied by lowering the worktable on which the powder bed is maintained.

b) Spot size is the diameter of the spot that laser or beam covers in contact with the powder bed. It can be understood as the diameter of the circle that would be formed if the power source is kept still at one spot.

c) Hatch spacing is a parameter that decides the motion of the power source perpendicular to the scan direction. For better melting and layer formation, hatch spacing is kept less than half of the spot size.

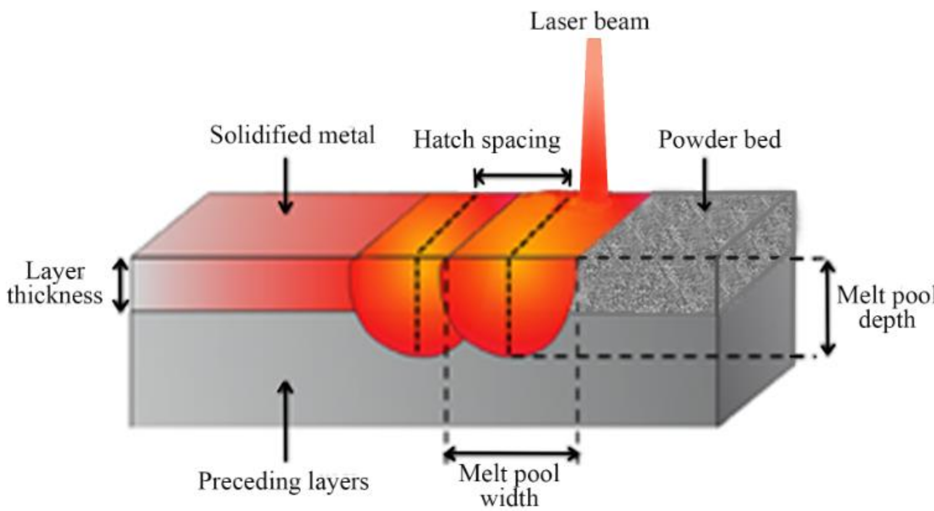

Figure 2. 12 Interaction of energetic beam with powder bed in a PBF process [57]

d) Scan velocity governs the speed of the power source with which it scans and melts the powder prepared on the bed and the consequent direction is called scan direction or beam traverse direction. Build direction is perpendicular to scan direction and direct out of the plane of scanning direction as can be seen in Figure 2.13.

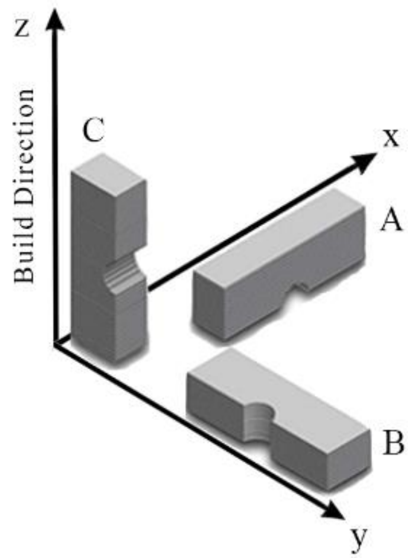

Figure 2. 13 Fabricated part with respect to the scan and build directions

Table 2. 14 A set of different scan strategies employed

	Layer n	Layer n+1
All X	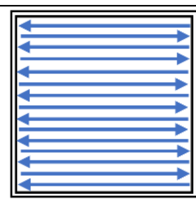	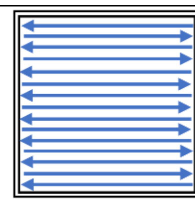
All Y	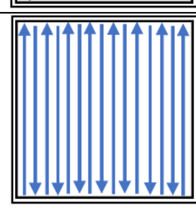	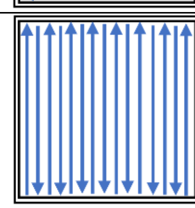
All X multi-scan each layer	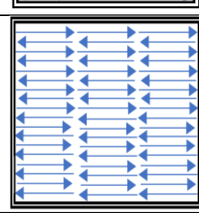	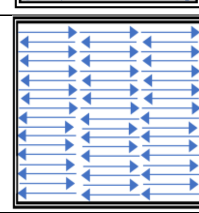
All Y multi-scan each layer	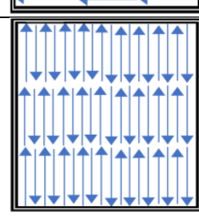	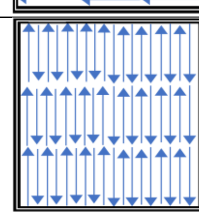

e) Scan strategy determines the method according to which the power source scans on the powder bed, it can be continuous or discontinuous and can be arranged as per the researcher's requirement [58]. A set of scan strategies can be seen in Table 2.14.

A few of most often used PBF techniques are discussed in the following section:

1. Selective Laser Melting (SLM):

SLM is an evolution of the Selective Laser Sintering process developed back in 1996 and is well known for producing complex geometries with mechanical properties comparable to bulk materials. The high-power energy source for this PBF process is a laser that is used to heat the powder layers, see Figure 2.14. After sufficient energy laser beam, the powder material melts forming a liquid pool that cools down and solidifies, forming the first layer.

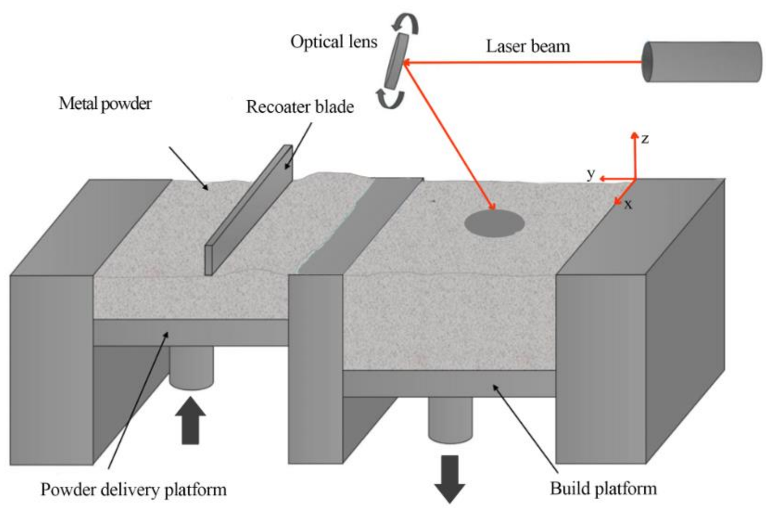

Figure 2. 14 Schematic representation of the SLM process [59]

Thereafter, the build platform is lowered by a definite depth which decides the powder layer thickness for the next layer. General process parameters affecting the part generation by an SLM process are laser power, laser spot diameter or spot size, scanning velocity, scanning strategy, and powder layer thickness which will be discussed in the latter part of this study [60]. Based on the variations of process parameters, different mechanical and physical properties are obtained. In summary, some attributes of the material fabricated by the SLM process are discussed below:

Density: Since SLM is a melting-solidifying process developed for high-density material fabrication, it aims to achieve a 100% density however in the absence of any mechanical pressure, it can never be attained. Despite that SLM is capable of providing as-built densities as high as 97% to 99% of the theoretical bulk material densities. But the inevitable gas bubble entrapment is also observed due to the solidification process leading to inbuilt defects and residual porosities. To cope with this issue Laser Surface Re-Melting (LSR) is done where each layer after getting built is rescanned by the laser to remelt the solidified region so that under the effect gravity, the bubble entrapments leading to porosities can be removed [61].

Surface quality: SLM does not result in a very good surface finish and most of the SLM fabricated surfaces undergo post-fabrication finishing processes if surface properties are one of the required properties of the fabrication. LSR is also one of the methods to reduce the surface roughness by just re-melting the top layer of the build but it adds up extra time to the manufacturing of a component [62].

Residual Stresses: SLM involves a lot of temperature variations during the process and therefore, distortions and residual stresses are a major concern. Each layer is solidified before the next layer is deposited and it generates high thermal stresses which can mess up the required mechanical properties and dimensions of the fabricated part. It contributes to internal cavities, porosities, warpage, and early crack formation of the components [63].

2. Electron Beam Melting:

EBM is also a PBF additive manufacturing process and follows a similar approach to SLM. But instead of using a laser, an electron beam is utilized as the high-energy power source aided by a vacuum chamber rather than providing an inert gas atmosphere. The electron beam has a better focus, fully electromagnetic control, and higher energy adsorption coefficient than lasers [45]. The vacuum chamber ensures that gases in the chamber wouldn't interfere with the electron beam and a high work temperature can be maintained which in-turn gives a deeper melt-pool and lower thermal gradients. One more variation in EBM is that it works with two layers of scanning. One is a pre-melting scan and the other is the melting scan. The pre-melting scan is generally done at high scan speeds and lower beam current to make sure that the powder bed gets heated up for the melting scan. After the pre-melting scan, scan speed and beam current is adjusted again according to the microstructure and mechanical properties of the resulting component. Similar to SLM, after each layer scanning, the worktable is lowered equal to the powder layer thickness needed for the component fabrication, and the process is repeated, however, the process is comparatively slower and expensive. Processing parameters for a typical EBM process are the beam current, scanning speed, hatch spacing, spot size, layer thickness, accelerating voltage, scanning strategy. Since EBM involves an additional pre-melt scanning as well, therefore, it adds up some extra processing parameters to the fabrication however, their effects could be considered minimal. A schematic representation of an EBM process can be seen in Figure 2.16.

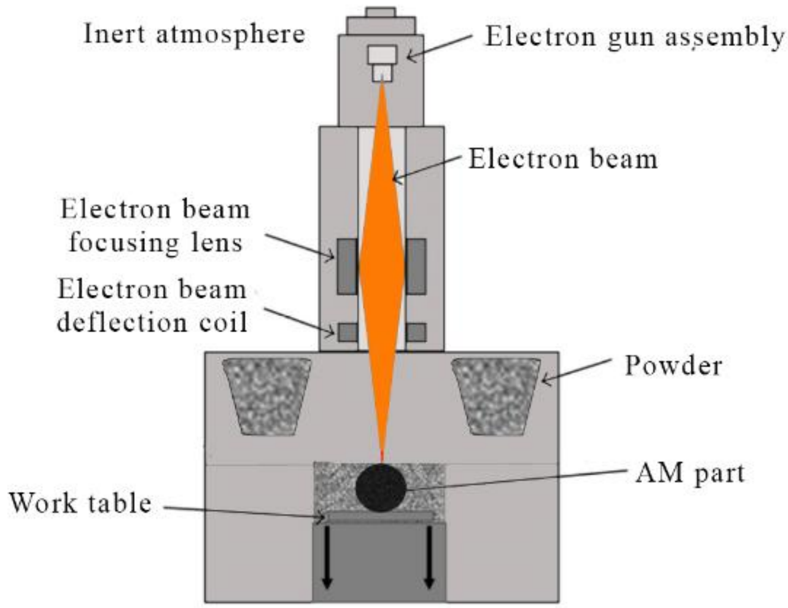

Figure 2. 15 Schematic representation of an EBM process [64]

Some attributes of the material fabricated by the EBM process are discussed below:

Density: Similar to SLM, this process also leads to high-density fabrications but the issue with EBM is that it can only be used with a handful of materials where titanium alloys are set at most comfortable priority to work with EBM.

Surface roughness: EBM works at speeds as high as 1000 m/s, which is nearly 1000 folds of that of SLM, and beam power of the range of 4 kW resulting in a surface generation that is generally twice as rough as that of SLM. But with post-processing, this surface can be smoothened.

Residual stresses: EBM process doesn't require post-heat treatment processes because it generally produces fewer thermal stresses than SLM. EBM apparatus requires support structures that not only account for the build platform, overhanging, and anchor parts but also act as heat sinks for molten powder, therefore, leading to lower thermal stresses and prevents warpage.

3. <u>Direct Metal Laser Sintering:</u>

DMLS uses lasers as the high-power energy source and operates on similar conditions as SLM. In some of the cases, DMLS is also referred to as SLM because both the processes are similar in practice however with just a fundamental difference. DMLS utilizes the effect of sintering and not the melting of powder [65]. DMLS is a sintering process whereas SLM is a melting process [66]. Sintering is generally carried at a temperature lower than the melting temperature (called sintering temperature) where the grain viscosity drops with temperature causing an interfacial kitting of the grains without fully melting them. DMLS can be used for fabricating almost all metals and their alloys whereas SLM only works bet with pure metals added to the fact that lesser energy is required for reaching the sintering temperature than to reach the melting temperature. Using the laser as a heating source asks for an inert atmosphere and after the first layer has been developed, the worktable is pushed down depending on the powder layer thickness required for the fabrication process. Major processing parameters affecting the build of a DMLS equipment are the laser power, scan speed, hatching space, layer thickness, spot size, and scanning strategy.

Some attributes of the material fabricated by the DMLS process are discussed below:

Density: Since complete melting is not being done in this process, the final product turns out to be more porous than SLM and EBM fabrications. But post-processing can be used to reduce the porosity and fabricated parts have comparable strengths to their counter cast materials.

Surface roughness: Like SLM, the surface finish of the as-built DMLS parts is not very good, therefore, post-treatments have to be employed to achieve a finished surface. However, while compared with EBM, as-built surfaces of DMLS have less surface roughness.

Residual stresses: Similar to SLM, high-temperature variations lead to high thermal stresses and warpage, therefore, additional structures are built around the chamber to transfer the heat away from the powder material. A typical comparison of the above mentioned PBF techniques is summarized in Table 2.15 [64],[67].

Table 2. 15 A typical comparison of process parameters for SLM, EBM, and DMLS processes

Parameter	SLM (ReaLizer SLM50)	EBM (Arcam EBM S12)	DMLS (EOS M 280)
Heat source type	Laser beam	Electron beam	Laser
Source power (W)	120	3500	200-400
Scanning speed (m/s)	0.3-1.0	> 1000	< 7.0
Spot size (μm)	small	large	small
Powder layer thickness (μm)	20-100	50-200	20-100
Build Environment	Argon	Vacuum	Argon
Pre-scan heating (°C)	100-200	700-900	100-200

2.2.3 Research and Research gap

Each of the additive manufacturing processes provides the industry with its own merits and demerits. Some of them can be rectified or adjusted using proper post-fabrication treatments but in the remaining cases, the industry has to settle by finding the best possible combination out of those merits and demerits. AM processes have gone through a lot of variations in procedure, post-fabrication treatments, and material selection, etc. However, we still have limited knowledge of these processes. A glimpse of the research history available on the above discussed AM processes is presented in the following section.

In a comprehensive review work, Liu and Shin [53] presented a comparison on the AM of Ti-6Al-4V through three different fabrication processes namely DED, SLM, and EBM. The authors reported that the presence of α′ martensite in DED and SLM processes increases the ultimate tensile and yield strength considerably but decreases the ductility of the as-built components as compared to the EBM fabricated parts that present a similar strength value of Ti-6Al-4V components. The authors opined that the presence of α′ martensite due to the former processes also helps in lower crack thresholds and offers higher fatigue strength in comparison to components fabricated through the EBM process.

Review work of Agius et al. [68] discusses the fatigue and fracture mechanical behavior of Ti-6Al-4V fabricated by the SLM process. The authors summarized that the stress raisers near the defects may influence the crack nucleation stage and subsequently the rate at which the slip activates in the fabricated parts. The reported work offers sufficient insight to utilize the fundamentals related to microstructure, build orientation, defect percentage in developing fatigue resistance materials.

Chern et al. [69] compiled uniaxial fatigue data and correlated the effects of build orientation, surface roughness, and hot-isostatic pressing to the fatigue properties, defects, and failure mechanisms in Ti-6Al-4V fabricated through EBM process. The authors suggested that annealing may not be advantageous for fatigue in the EBM process as the residual stresses are relieved in-situ, though HIP has been reported to be an effective method to increase fatigue resistance. The authors also observed that the parts fabricated in vertical orientation are more likely to exhibit crack initiation due to the rough surface produced.

Izadi et al. [70] summarized the influence of build and process parameters on the metallic parts fabricated by LENS and stressed the need for prediction towards the influence of the build process for fabricating industrial parts. The authors identified laser power, powder feed rate, scan speed, and hatch distance to be the most influential variables that impact the build quality. The authors were the view that a mathematical model that reflects the build process and algorithm to predict the influence of control parameters may help the research community in a great way.

Guzanová [71] investigated the influence of various processing parameters on the hardness of Ti-6Al-4V manufactured by the DMLS process and concluded that annealing leads to a reduction in hardness, moreover, the ANOVA analysis reflected the significant effect of laser power on the hardness. The authors also observed a considerable difference in the hardness values of the materials build in parallel and perpendicular direction.

Cao et al. [72] have compiled the research work related to fatigue behavior of additively manufactured Ti-6Al-4V and inferred that SLM based parts show better fatigue properties than the EBM build components due to reduced surface roughness and less porosity. However, they concluded that the fatigue strength of AM-manufactured Ti-6Al-4V may not be sufficient for fatigue applications until subsequent post-processing such as HIP, surface machining, and polishing are carried out.

Based on the literature it can be observed that the processing parameters in any additive manufacturing process play a significant role in deciding the mechanical properties of the manufactured part. Further, it is also reported that the availability of an appropriate mathematical model or algorithm may help the research community in deciding the process and its usability in manufacturing a particular component for a specific application based on the mechanical properties desired [73],[74].

In this work, therefore, an attempt has been made to predict the mechanical properties of Ti-6Al-4V obtained through different additive manufacturing processes such as EBM, SLM, and DMLS. The data collected from various research papers have been compiled in tabular form in the fourth chapter of this study, the prediction model and the results are also highlighted in further chapters.

CHAPTER - 3

METHODOLOGY

3.1 Introduction

This study aims to collect and analyze the data pertaining to Ti-6Al-4V alloy, available in the open literature, and to develop a model that assists in estimating the mechanical properties of the alloy manufactured by a certain AM process. The mechanical properties that are being taken into account here are the tensile properties (ultimate tensile strength, yield strength, and elongation at fracture) and the fatigue properties (S-N curve). Since the properties of the alloy are determined by the process parameters considered while additively fabricating it, therefore, to properly estimate the alloy behavior, process parameters associated with different manufacturing processes must be considered as the input parameters. It has been seen that due to high-temperature gradients involved in these processes, a separate stress-relieving process has to be carried out, thus, adds up the heat treatment parameters to the influencing factors. Once the alloy is fabricated and post-processing is complete, it becomes accessible for lab testing. For typical tensile testing, the load is gradually increased, and the strain developed in the alloy is noted. Both values are plotted against each other to get the ultimate tensile strength (UTS), the yield strength (YS), and the percent elongation (El) of the material.

In fatigue properties, an attempt to estimate the S-N curve is made. S-N curve is used to determine the fatigue life of the alloy for certain alternating stress values. General factors affecting the fatigue life of an AM fabricated test sample are its surface roughness, process parameters for fabrication, inherent defects from the fabrication, geometry of the sample, the test stress ratio (R), and the test frequency. A representation of what is expected from the model is shown in Figure 3.1

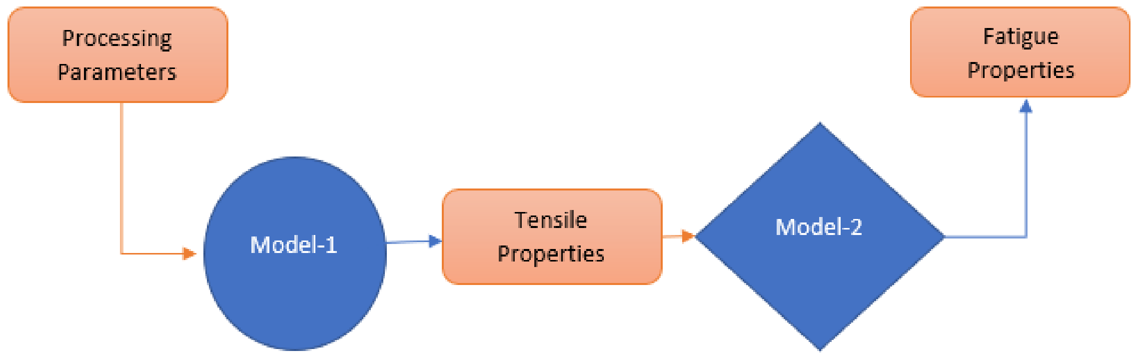

Figure 3. 1 Schematic representation of the complete model

3.2 Model Conceptualization

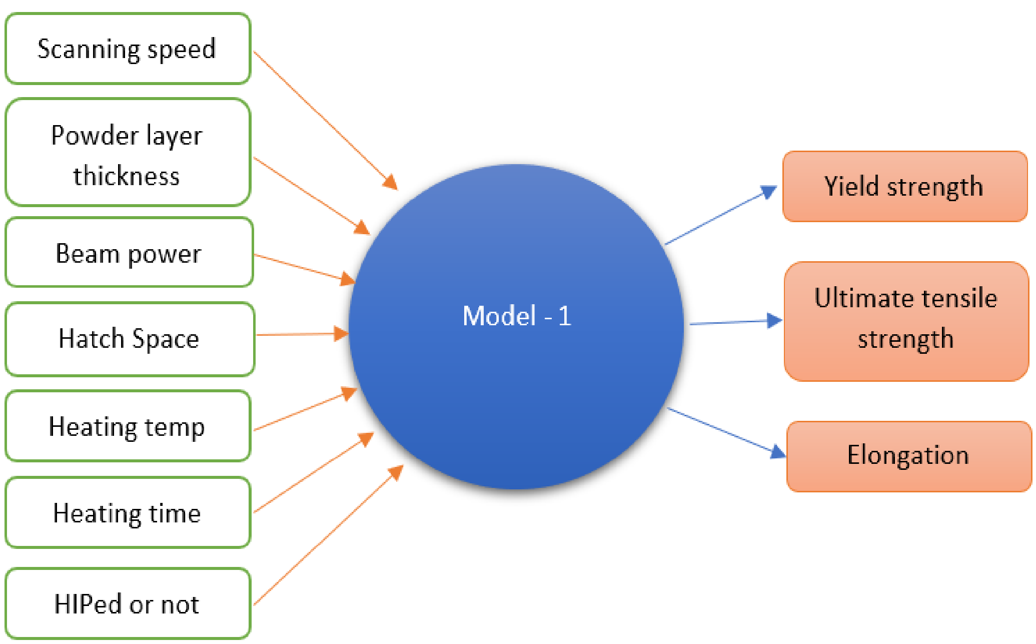

Figure 3. 2 Inputs and outputs for Model-1

Not all the experimenters make available the processing parameters data when they are publishing the fatigue or tensile test results, therefore, to work with the available data, a different approach had to be taken. Hence, two separate estimation models are prepared which can later be combined to estimate the whole set of mechanical properties of Ti64 alloy fabricated by selected AM processes. The first model, Model-1 utilizes the process parameters and heat treatments, if any, influencing the AM part as input parameters and the tensile properties (the ultimate tensile strength, the yield strength, and the elongation) are evaluated as outputs as can be seen from the schematic drawn in Figure 3.2.

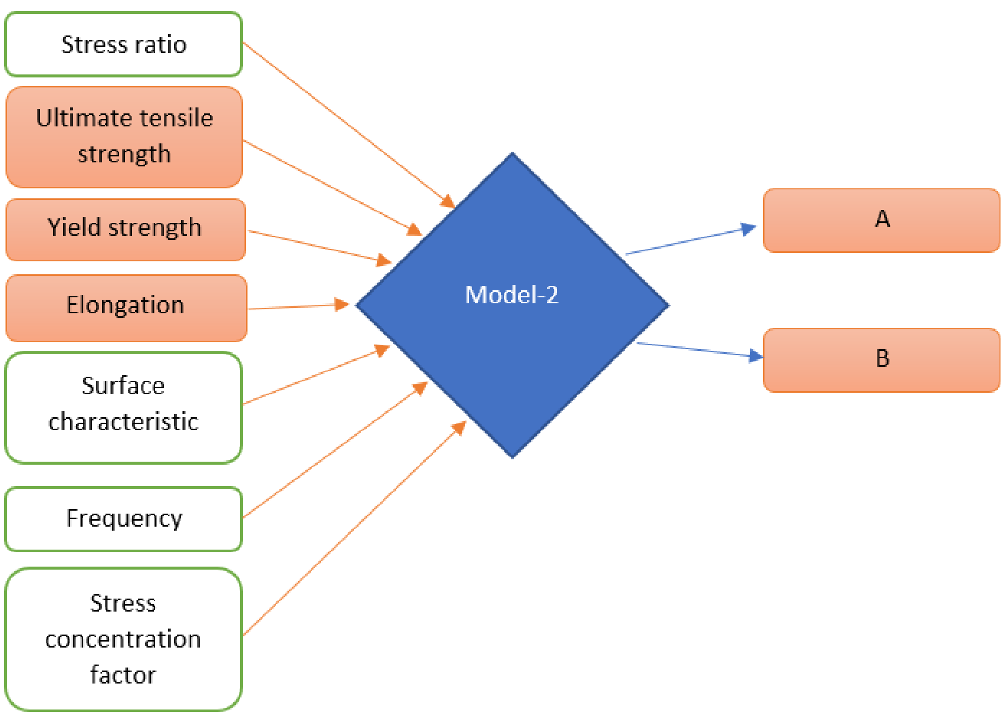

Figure 3. 3 Inputs and outputs for Model-2

The second model, Model-2 considers the ultimate tensile strength, yield strength, elongation, surface characteristics, and fatigue test parameters (frequency and stress ratio) as input parameters and aims to predict the SN curve as the output of the fabricated Ti64 alloy. A schematic representation of Model-2 is shown in Figure 3.3.

For using the S-N curve in the model, instead of using the graphical representation, the power law or scaling law has been employed to reduce the S-N curve into two constants A and B, where A determines the intercept of the S-N curve on the stress amplitude axis and B is the law's exponent. One representation of such a conversion from Figure 3.4 is shown below.

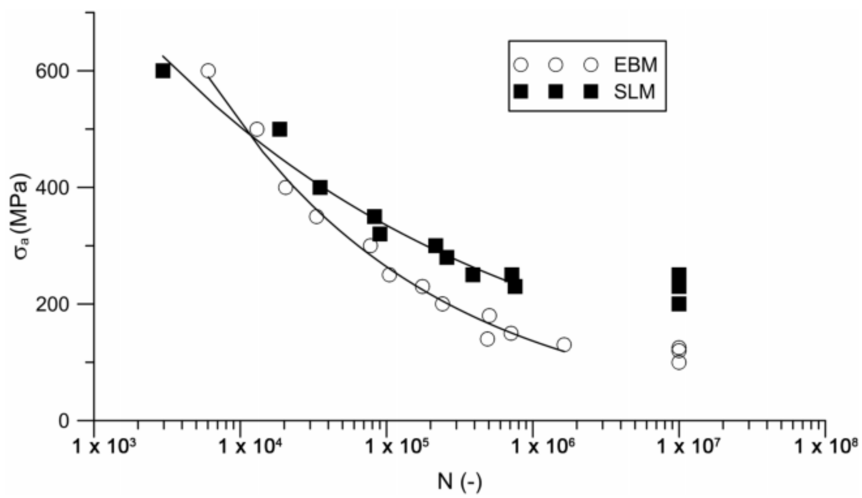

Figure 3. 4 S-N curves for Ti64 fabricated by SLM and EBM processes. [75]

Table 3.1 represents the digitized forms of the stress amplitude and the number of cycles to failure values for Ti64 alloy fabricated by certain SLM and EBM processes. Using these digitized values, power law can be employed to generate the two constants, A and B, mentioned above. Figure 3.5 shows the plots generated from the power law and it can be observed that they look potentially identical to the S-N plots represented in Figure 3.4. All the available S-N curves were digitized in order to generate the power law values and the related data can be found in the Appendix.

Table 3. 1 Digitized S-N curve value and corresponding power law for Tii64 alloy fabricated by SLM and EBM process

SLM Process		EBM Process	
N	S (MPa)	N	S (MPa)
3007.662	599.139	6033.797	600
18722.03	498.906	12873.74	498.69
35108.18	399.385	20324.36	399.127
83573.39	350.478	33358.52	349.345
90255.36	319.728	76926.5	299.563
219754.5	299.754	104977.7	249.782
259321.1	279.846	175681.4	231.441
392402.7	250.874	239743.5	200
720878.3	249.613	501674.4	179.913
761632.1	230.921	487263.3	138.865
9964673	249.978	711738.9	149.345
9961421	229.482	1625438	130.131
9956737	199.944	10000000	124.017
Power law conversion $S = 1368.4 * N^{-0.119}$ Where, A = 1368.4; B = -0.119		Power law conversion $S = 4334.5 * N^{-0.241}$ Where, A = 4334.5; B = -0.241	

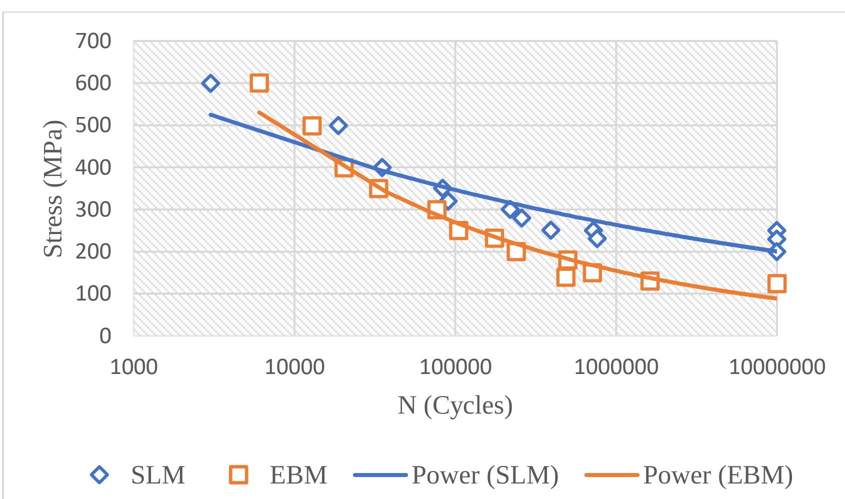

Figure 3. 5 S-N plots generated for above digitized SLM and EBM processes using the power law

It is also not always possible to attain all the data that fulfills the model requirements from the literature. As mentioned earlier, one of the influencing parameters is the surface roughness parameter in Model-2 where due to unavailability of proper numeric values of the surface roughness, a binary choice had to be made, therefore, the model incorporates for value ‘1’ if the surface is processed (machined) and ‘0’ if the surface is the same as obtained after fabrication (rough). Similarly, ‘1’ was assigned for the cases where the sample went through Hot Isostatic Pressing and ‘0’ otherwise.

One similar case to the above-discussed situations is the case for the heat treatment parameter in Model-1 where some samples were heat treated as a post-process and some were not, however, for the data sets where except for the heat treatment, all the remaining Model-1 parameters were same, the output results were coming differently. Meaning, the binary choice here would not have been the best resort because useful information as such ‘the impact of heating temperature and time on the tensile properties of the fabricated component’ would get completely lost in the collateral. The best solution to such a condition would be to develop a decision tree-based model where the input heat treatment is kept in binary information. If the sample has been heat-treated, it takes 1 and if not, it takes 0. Then for the heat-treated sample, separate temperature and time inputs would be asked, and the model would proceed further. In the cases where heat treatment is not done, the model ignores that option and moves on with further processing. This process calls for two bifurcations of the data set collected, one with heat treatment and another without heat treatment hence reduces the total number of data sets to efficiently predict the model. Due to the unavailability of required data sets, to account for this situation, four compensating sets, (heating temperature, heating time) to fit an as-fabricated sample into the data along with the heat-treated sample, were prepared and checked with SLM process data (heaviest data set available) to see which one of them gives the best result in the model output. The heating temperature is kept at 30 °C considering that the sample is kept at room temperature instead of an elevated temperature like heat treatment processes and heating time is varied from 0.5 to 4 hours depending on the general heating temperature range observed from the collected data. This was also an attempt to consider the 'as-fabricated' condition equivalent to a situation where it can be represented as a combination of heating temperature and time which could be useful for future research regarding similar studies. These compensating sets in the form of (heating temperature in °C, heating time in hours) are (30,0.5), (30,1.5), (30,3), (30,4).

3.3 Model Development

Since it is unknown whether the input parameters behave linearly or have a complex relationship with the output parameters, therefore, the two model development approaches worked on in this study are 'regression analysis' for the linear relationship consideration and 'Artificial Neural Network (ANN)' for the complex relationship consideration. Both these models are discussed in the following section.

3.3.1 Regression analysis

Regression analysis is a very efficient method to identify trends in data sets. It usually presents with a relationship between dependent variables and independent variables meaning how much movement will the independent variable experience if the dependent variable is moved by a certain amount. There are different types of regression analysis namely, linear, polynomial, logistic, stepwise, ridge, lasso, and elastic net regression. Here, regression analysis is aimed to understand if there exists any linear relationship between the input and output parameters. Also, since the model is equipped with multiple inputs, a multi-input regression analysis is considered.

Multi-regression analysis:

Simple linear regression analysis is used to relate a single dependent variable, say 'X', to a single independent variable, say 'Y', and in general terms, it is represented as-

$$Y = \beta * X + \varepsilon$$

where, β is a constant, scaling X to a relatable Y value and ε is the additional term which could compensate for either error in the relationship or the intercept that the plot related to the above equation makes on Y-axis.

Multi-regression analysis behaves similar to simple linear regression analysis, the only difference is that instead of one single dependent variable, it accounts for multiple dependent variables, and each of them is presented to have a linear relationship with the independent variable. A typical representation of a multi-regression analysis looks like-

$$Y = \beta_1 * X_1 + \beta_2 * X_2 + \beta_3 * X_3 + \ldots. + \beta_n * X_n + \varepsilon$$

Where, X_1, X_2, X_3 … X_n are the independent variables (also known as covariates) and β_1, β_2, β_3 … β_n are their corresponding coefficients or weights that define how influencing each variable is for estimating the dependent variable. There are two ways to proceed with a multi-regression analysis. One is 'forward substitution' where the regression equation is built by adding covariates influencing the dependent variable to the equation one by one from initially having no covariates on the right-hand side and the other is 'backward selection' where regression equation initially has all the covariates and they are removed from the equation one by one depending on their influence. The former is used when there are a smaller number of covariates (say 4) to add to the equation. Since Model-1 and Model-2 in this study deal with a larger number of covariates therefore, the backward selection is used to obtain the regression equation for different output variables.

Understanding the multi-regression analysis output:

The output of a regression analysis can provide a lot of information about the data served to it. In this study, JMP pro is used for exploring the linear relationship between the input parameters and output parameters for both Model-1 and Model-2. Modeling begins with fitting the data to the model. For that purpose, the results generated from a typical regression analysis are presented in Figure 3.6.

1. RSquare and RSquare Adj:

RSquare and RSquare Adjusted are both a measure of identifying how well the regression model fits the data given to it. In other terms, it represents the percentage of variance in the dependent variables that can be explained by the independent variables. RSquare Adj is a measure that compensates for the increased number of covariates assuming they in themselves are not independent of each other and hence add in a small amount of penalty to the RSquare value. RSquare Adj value is always smaller than RSquare value accounting for the increased covariates penalty.

Summary of Fit

RSquare	0.56933
RSquare Adj	0.534276
Root Mean Square Error	81.61722
Mean of Response	1089.072
Observations (or Sum Wgts)	94

Analysis of Variance

Source	DF	Sum of Squares	Mean Square	F Ratio
Model	7	757324.2	108189	16.2413
Error	86	572877.8	6661	Prob > F
C. Total	93	1330202.1		<.0001*

Parameter Estimates

Term	Estimate	Std Error	t Ratio	Prob>|t|
Intercept	1294.8803	69.23243	18.70	<.0001*
Speed	-0.067892	0.038268	-1.77	0.0796
Power	0.7479009	0.215442	3.47	0.0008*
Hatch	-0.252816	0.36832	-0.69	0.4943
Thickness	-3.498455	1.066508	-3.28	0.0015*
Heat Temp	-0.275589	0.030677	-8.98	<.0001*
Hiped	-13.33061	39.54932	-0.34	0.7369
Heat Time	5.8446224	6.285698	0.93	0.3551

Figure 3. 6 A regression analysis output generated by JMP Pro 14

For a better fit model in case of multi-regression analysis ideally, RSquare Adj value is 1 meaning a 100% explanation of dependent variable variance by the independent variables collectively. For comparing the MATLAB obtained model results, the R-value of the models developed by regression analysis would be considered which is merely the square-root of the RSquare Adj value in this case.

2. Prob > |t|:

Prob > |t| represents the P-value for the two-tailed test. Each of the covariates is associated with a two-tailed hypothesis test linked to them where the null hypothesis is that the covariate is not significant to the regression model and the alternate hypothesis is that the covariate is significant to the regression model. For a covariate to be included in the regression equation, it needs to reject the null hypothesis and become significant to the regression model. For a standard α level of 0.05, each of the P-values significant to the regression model must show a less than 0.05 value in that column. The covariates having a P-value of more than 0.05 are to be removed from the regression equation. For instance, in Figure 3.6, covariate, HIPed, Heat Time, Hatch and Speed have a P-value larger than 0.05 and therefore they are insignificant to the regression model. However, this doesn't essentially mean that each of these covariates is to be removed from the model at once and that is because of the interdependence of the covariates on each other. Therefore, the covariate with maximum P-value is removed and the model is re-run and the process is repeated until all the P-values come under the 0.05 threshold. All the covariates remaining after this analysis are a part of the regression equation for the model as can be seen in Figure 3.7.

Summary of Fit

RSquare	0.547592
RSquare Adj	0.532512
Root Mean Square Error	81.77161
Mean of Response	1089.072
Observations (or Sum Wgts)	94

Analysis of Variance

Source	DF	Sum of Squares	Mean Square	F Ratio
Model	3	728408.4	242803	36.3119
Error	90	601793.6	6687	Prob > F
C. Total	93	1330202.1		<.0001*

Parameter Estimates

Term	Estimate	Std Error	t Ratio	Prob>|t|
Intercept	1237.9958	30.93906	40.01	<.0001*
Power	0.418811	0.119445	3.51	0.0007*
Thickness	-2.376572	0.809399	-2.94	0.0042*
Heat Temp	-0.271142	0.026376	-10.28	<.0001*

Figure 3. 7 Significant covariates for the regression model case in Figure 3.6

3. Estimates:

After confirming all the significant variables in the regression model, now the coefficients or the weights of those covariates is to be decided. The ‘Estimate’ column is used for that purpose. The intercept estimate decides the Ɛ term while the remaining estimates decide the β_1, β_2, β_3 … β_n terms in the regression equation.

So, for this typical case, the regression equation looks like:

Output = 1237.996 + 0.418 * Power – 2.376 * Thickness – 0.271 * Heat Temp

Shortcomings of the multi-regression analysis

1. Multi-regression analysis works best with more than 100-150 data sets at the least; however, data sets available for the study are less.
2. Since a few of the input parameters are represented as a ‘Yes’ or ‘No’ condition that is in numerical terms as ‘1’ or ‘0’ therefore, they are not accounted as developing a linear relation with the output parameter value and therefore, get completely disregarded from the regression equation.

3.3.2 Artificial Neural Network

ANN is a black-box model, for predicting complex and nonlinear patterns, demonstrating point to point data covering the whole process. ANN is a machine learning approach that models the human brain and generates artificial neurons as replication of the working of a biological neuron. ANN model consists of several processing elements utilizing training data information to iterate input parameters and to evaluate the response of model as output, infer unseen relationships on unseen data and make a generalized model predict the unseen data based on the relationship between output and input experimental data sets. Implementation of ANN is a discretized approach in which processing element is activated once for each sample of a vector of input values. The neural network in a person's brain is a huge interconnected network of neurons where learning occurs by repeatedly activating neural connections, reinforcing those connections, and involving feedback based on which the outcome gets strengthened. ANN uses a learning algorithm to mimic the behavior of the brain and neurons working to train the model. An ANN is specified by:

- An architecture: A set of neurons and links connecting neurons including activation and learning algorithms
- A Neuron model: The information processing unit of the Neural Network

3.3.2.1 ANN Architecture

The model ANN is specified by three entities: interconnections, activation functions, and learning rules.

1) Interconnections

Interconnections can be defined as processing elements in the ANN connected to each other. Processing elements combine together to form layers of the network.

- *Input Layer:* This layer is also called the buffer layer which accepts input features from the data set. No computation is performed at this layer and the nodes here just pass on the features to the hidden layer.
- *Hidden Layer:* This layer acts as the backbone of the model's computational and processing power. Nodes of this layer are not exposed to outside the model, they are the part of the abstraction provided by any neural network. The hidden layer

performs all sorts of computation on the features entered through the input layer and transfer the result to the output layer.

- *Output Layer:* This layer results in the information learned by the network as the output.

Neurons are represented as nodes in the model, and their shape and size depend on the requirement of the model. Each node gets multiple weighted inputs, to which activation function is applied for the summation of these inputs to generate an output. Within each node, there is a set of inputs, weights, and a bias value. Weight is a parameter of the neural network model which transforms input data within the network's hidden layers. The inclusion of bias values in node enhances the flexibility of the node. Input layer nodes receive input features from the data set and pass that information without any processing to the hidden layer which sums up the weights of nodes and biases initialized randomly. The output of the hidden layer calculated is then passed over to the activation function which produces an output of the model [76].

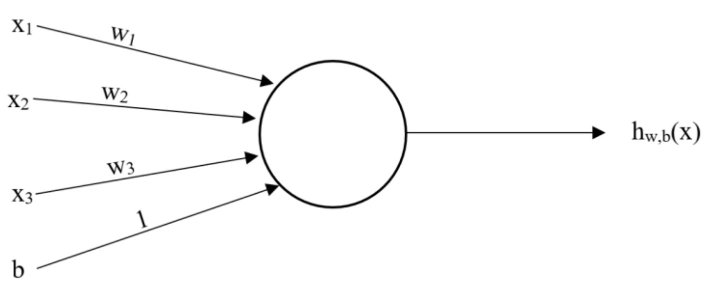

Figure 3. 8 Depiction of node and input variables

Figure 3.8 depicts a node with an input parameter leading to an output where the circle represents the node, taking weighted inputs, and some of this input is given to the activation function. The output of activation function is represented as $h_{w,b}(x)$.

Weighted input to the node in this diagram would be

$$x_1w_1 \ + x_2w_2 + x_3w_3 + b$$

Where w_i are the weight values and b is the bias value.

Data Preprocessing:

The training data set given as input to the nodes of the input layer is normalized first. An adequate normalization is a linear scale conversion that assigns the same absolute values to the data set features with the same relative variations applied to all the features. Data needs to be normalized before training a neural network model. Normalization ensures that the magnitude of the values that a feature assumes is more or less the same. It scales all the data set to be given to the model. Normalization assures that there are both positive and negative values used as input for the hidden layer which makes learning a more flexible and faster convergence for the model. Network performance is enhanced when input variable ranges are equalized by normalization.

Z-score normalization:

This is also known as the standard scaler approach. In this normalization, data is normalized using distributed mean and standard deviation calculations for each feature.

$$x' = \frac{x - x_{mean}}{SD}$$

Where x' is the normalized output, x is the original feature vector, x_{mean} is the mean of that feature vector, and SD is the standard deviation. This standardization makes the values of each feature in the data to have zero mean and unit variance [76].

2) <u>Activation Function</u>

This is also called a transfer function. The activation function of a node results in the output of that node whenever a set of inputs is given. It represents the rate of activation potential of firing for a particular node. Purpose of the activation function is to introduce non-linearity into the output of a neuron, thus increasing the power of multi-layered neural networks, enabling them to easily compute arbitrary and complex functions, Activation function decides whether a neuron should be activated or not by calculating weighted sum and further adding bias with it. Weights are updated on the basis of the error at the output with backpropagation

Rectified linear unit (ReLU):

It gives an output x, if x is positive, and 0 otherwise. ReLU is less computationally expensive and much faster because it involves simpler mathematical operations. The function and its derivative, both are monotonic. However, it doesn't map the negative values appropriately.

3) <u>Learning Rule</u>

The learning rule updates the weights and bias levels of a network when the network simulates the given data set. The learning rule helps the network to learn from existing conditions and improve its performance. A learning rule accepts existing weights and biases of the network and compares the expected result obtained from the output layer and actual result of the network to give new and improved values for weights and bias, acting as an iterative process. Depending upon the process to develop the network, there are three main models of machine learning- unsupervised learning, supervised learning, reinforcement learning.

Supervised Learning:

Supervised learning generates a function that maps inputs to desired outputs. This technique is designed to learn by example. The process of adjusting the weights in a neural network to make it approximate to a particular function is called training. When training a supervised learning algorithm, the training data will consist of inputs paired with the correct outputs. Training data consist of input parameters affecting the fatigue properties and output parameters as the properties of the material as can be seen in Figure 3.9. During training, the algorithm will search for patterns in the data that correlate with the desired outputs [76]. The objective of the supervised learning model is to predict the output for the newly presented input data.

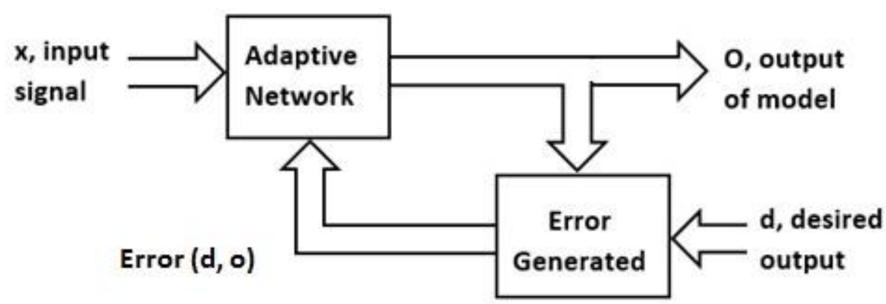

Figure 3. 9 Supervised learning mechanism

Delta Learning Rule:

It is also called Widrow Hoff Rule. It depends on supervised learning. This rule states that the modification in the sympatric weight of a node is equal to the multiplication of error and the input. If the difference is zero, no learning takes place; otherwise, adjusts its. The aim of applying the delta rule is to reduce the difference between the model output and expected output, Figure 3.10 shows the mechanism of delta learning rule. Mathematical formula of delta learning rule [76]:

$$\Delta w_{ij} = \lambda . x_j . E_j$$

Where, Δw_{ij} = weight change for i^{th} node of the hidden layer from j^{th} input node;

λ = the positive and constant learning rate;

x_j = the input value from pre-synaptic neuron depicted as node "j";

Ej = the error between the desired output (d_i) and the model output (o_i)

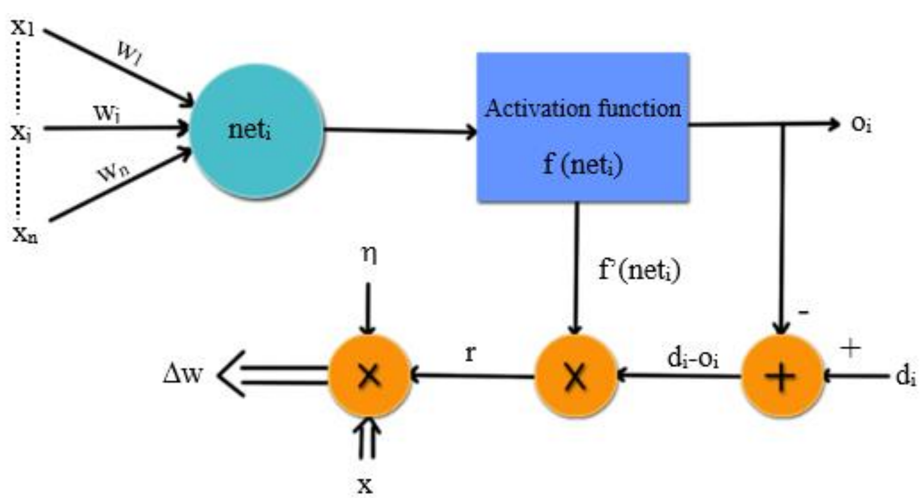

Figure 3. 10 Delta learning rule mechanism

The updating of weight can be done in the following two cases:

Case-I − when **d ≠ o**, then, w(new)=w(old)+ Δw

Case-II − when **d = o**, then, no change in weight

Gradient descent method:

This method uses the derivative of the loss function with respect to the weights of the network. It decreases the output error by adjusting the weights.

$$E_i = L(d_i, o_i)$$

E is the loss(error) for the model output o_i and desired value d_i. This learning algorithm minimizes sum squared error by making appropriate iterative adjustments to the weights w_{ij} If weights are repeatedly adjusted by small steps against the gradient, the result moves through weight space, descending along the gradients towards a minimum of the error function. If we want to change the value of weights to minimize the error function, there are three cases for the derivative of the loss function with respect to the weights

Case 1: If $\frac{dE}{dw} > 0$, E increases as w increases, hence weight should be decreased

Case 2: If $\frac{dE}{dw} < 0$, E decreases as w increases, hence weight should be increases

Case 3: If $\frac{dE}{dw} = 0$, E is at a maximum or minimum value; weight should not be changed

Hence, the error is reduced by changing weight by the amount Δw

$$\Delta \mathrm{w} = \mathrm{w(new)} - \mathrm{w(old)} = -\eta \frac{dE}{dw}$$

Where η is a positive constant specifying how much weight should be changed, and $\frac{dE}{dw}$ describes the direction to go in. Repeating this iterative algorithm, the error will keep decreasing towards a minimum with gradient lines flattening out, known as gradient descent minimization, see Figure 3.11. The backpropagation method is used for figuring out the gradient of a neural network [76].

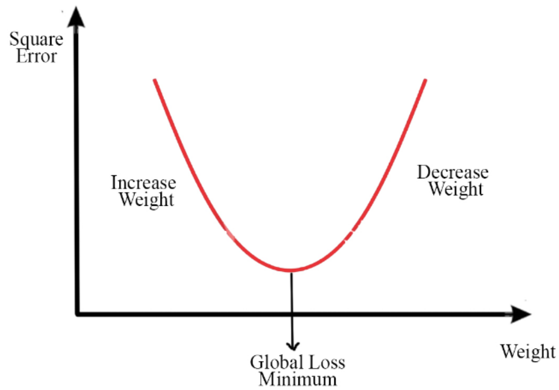

Figure 3. 11 Gradient descent method

Backpropagation

Backpropagation is the algorithm for computing the gradient. It generalizes the gradient computation in the delta rule. Backpropagation is an algorithm that is widely used in the training of feedforward neural networks for supervised learning. Backpropagation efficiently computes the gradient of the loss function with respect to the weights of the network for a single input-output example. The backpropagation algorithm works by computing the gradient of the loss function concerning each weight by the chain rule called delta rule or gradient descent, iterating backward one layer at a time from the last layer to avoid redundant calculations of intermediate terms in the chain rule. The weights that minimize the error function is the solution to the learning problem.

3.3.2.2 Multilayer Perceptron Model (MLP)

This model is called Multilayer Perceptron because it contains many perceptrons that are organized into layers. MLP is a class of feedforward artificial neural network used for function approximation. MLP consists of at least three layers of nodes explained in interconnections. Each node in the hidden layer and the output layer uses a nonlinear activation function. MLP uses a supervised learning technique for training, called backpropagation [76]. An MLP neuron is free to either perform classification or regression depending upon its activation function.

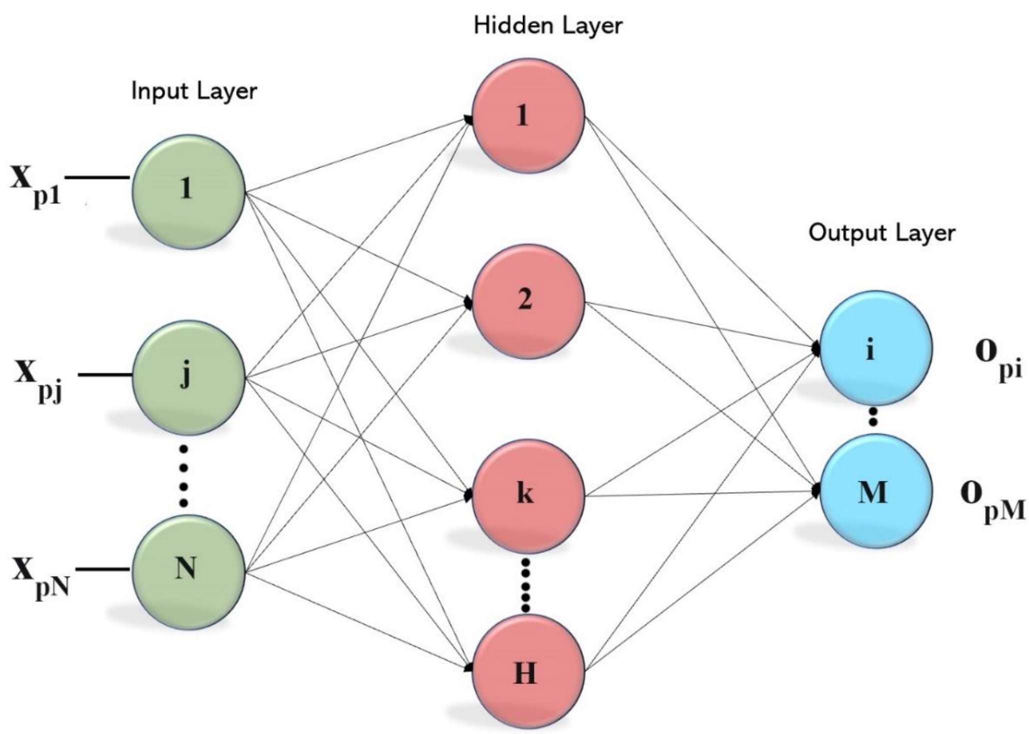

Figure 3. 12 Architecture of Multilayer Perceptron Model

In the diagram given above, input layer consist of "N" nodes and "j" represents one of the node input layer receiving input from p^{th} sample of the dataset, the hidden layer consists of "H" nodes with "k" represented as one of its nodes, and the output layer consist of "m" nodes where "i" represents one of its nodes.

The flowchart below can be used to understand the steps to train the MLP Model:

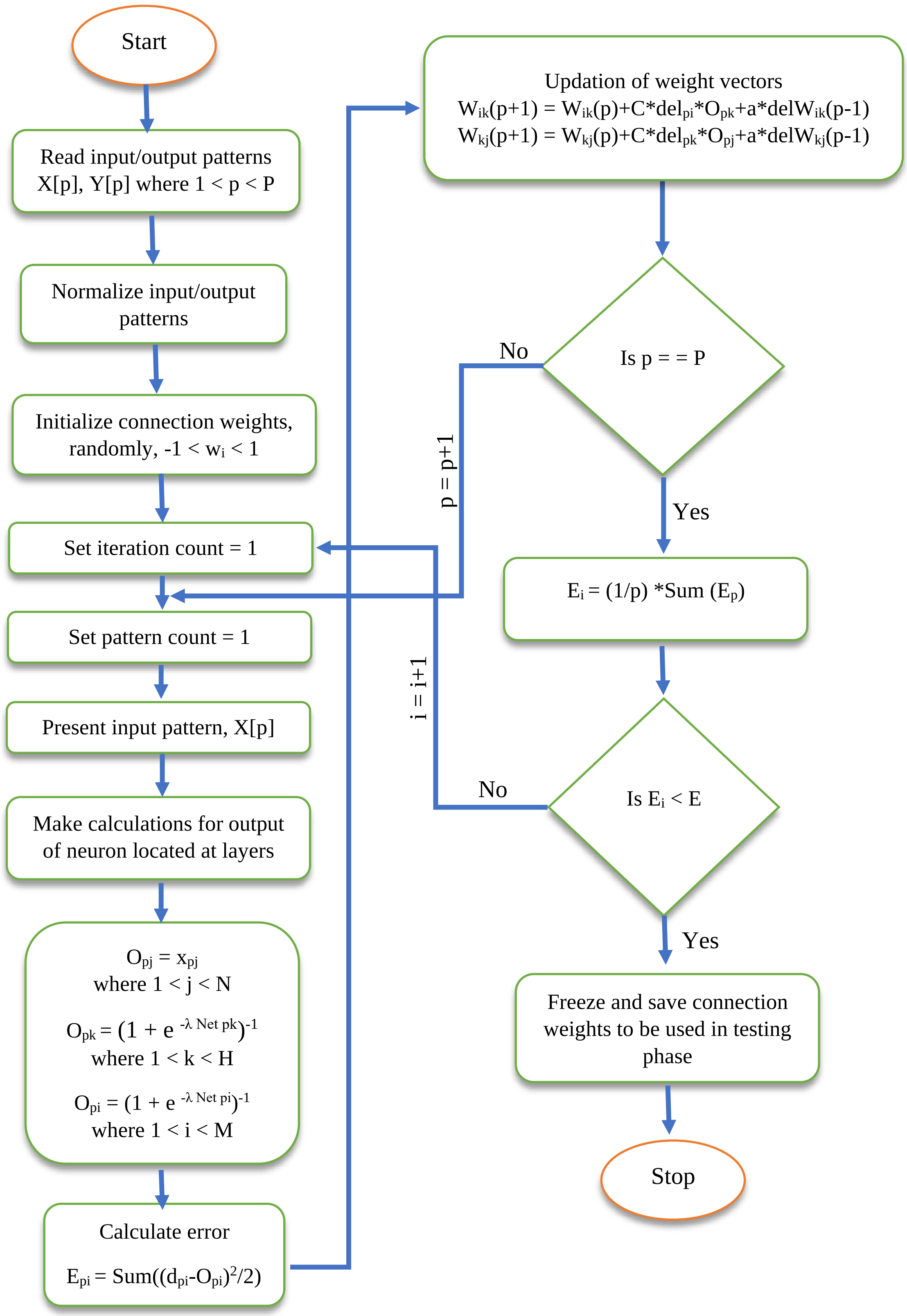
Start
Read input/output patterns
X[p], Y[p] where 1 < p < P
Normalize input/output patterns
Initialize connection weights, randomly, -1 < w_i < 1
Set iteration count = 1
Set pattern count = 1
Present input pattern, X[p]
Make calculations for output of neuron located at layers
$O_{pj} = x_{pj}$
where 1 < j < N
$O_{pk} = (1 + e^{-\lambda \text{ Net } pk})^{-1}$
where 1 < k < H
$O_{pi} = (1 + e^{-\lambda \text{ Net } pi})^{-1}$
where 1 < i < M
Calculate error
$E_{pi} = \text{Sum}((d_{pi}-O_{pi})^2/2)$
Updation of weight vectors
$W_{ik}(p+1) = W_{ik}(p)+C*del_{pi}*O_{pk}+a*delW_{ik}(p-1)$
$W_{kj}(p+1) = W_{kj}(p)+C*del_{pk}*O_{pj}+a*delW_{kj}(p-1)$
Is p = = P
No
p = p+1
Yes
$E_i = (1/p) *\text{Sum}(E_p)$
Is E_i < E
No
i = i+1
Yes
Freeze and save connection weights to be used in testing phase
Stop

1. Preprocessing of data

   Input and output data are normalized first using z-score normalization, before giving them as input to the model. Based on these normalized input-output instances, the model is trained and tested to capture the non-linear system.

2. Initialization of connection weights

   Connection weights corresponding to nodes of hidden and output layers can be initialized from -1 to 1 or from -0.5 to 0.5 with uniform distribution.

3. Calculation of output of layers

   - Calculation of output at the input layer

     The output of node "j" is calculated as $O_{pj} = X_{pj}$, the value received at input layer nodes is passed on as it is to the hidden layer for all values of "j" from I to N

   - Calculation of output at the hidden layer

     $Net_{pk} = \sum W_{kj} O_{pj} - b_k$

     This net value is passed on to the activation function,

     if activation function is sigmoidal, $O_{pk} = (1 + e^{-\lambda \, Net\, pk})^{-1}$

     if activation function is ReLU, $O_{pk} = Net_{pk}$ for $Net_{pk} > 0$ else $O_{pk} = 0$

     that is, $O_{pk} = f(Net_{pk})$, where f is the activation function for all values of "k" from 1 to H

   - Calculation of output at the output layer

     $Net_{pi} = \sum W_{ik} O_{pk} – b_i$

     if activation function is sigmoidal, $O_{pi} = (1 + e^{-\lambda \, Net\, pi})^{-1}$

if activation function is ReLU, $O_{pi} = Net_{pi}$ for $Net_{pi} > 0$ else $O_{pi} = 0$

that is, $O_{pi} = f(Net_{pi})$, for all values of "i" from I to M

4. Calculation of error

   The output obtained from the output layer of the model is compared with the desired output, mentioned in the data set, and error in the result for every node is calculated.

$$E = \sum \frac{1}{2} (d_{pi} - O_{pi})^2$$

   Initially, long steps are taken, as learning is matured, the step size is reduced which reduced the learning rate.

5. Weight updation by backpropagation

   For updating the weights of the output layer, the gradient descent method is used, in which the gradient of the error with respect to weight to be updated is calculated as

$$\frac{dE}{dw} = - (d_i - O_i)\, f'(Net_i) O_{pk}$$

$$\Delta w = -\eta \frac{dE}{dw}$$

$$W_{ik}(new) = W_{ik}(old) + \Delta w$$

A similar procedure is used for weight updation of nodes of the hidden layer, and this process continues for every iteration until error obtained is less than a specified value. Once the error of a particular iteration is less than the specified one, weights at that iterations are frozen to be used in the testing phase for predicting the output.

3.3.2.3 Required Model

An ANN model designed for the prediction of fatigue properties of a material is based on a multilayer perceptron since it is used for function approximation and implies supervised learning. Since data is sufficiently not available, the prediction process is divided into two models, first model results in predicting the values of Ultimate Tensile Strength (UTS), Yield Strength (YS) and elongation which is used as input for the second model to predict the fatigue properties with given input parameters.

<u>Model-1:</u>

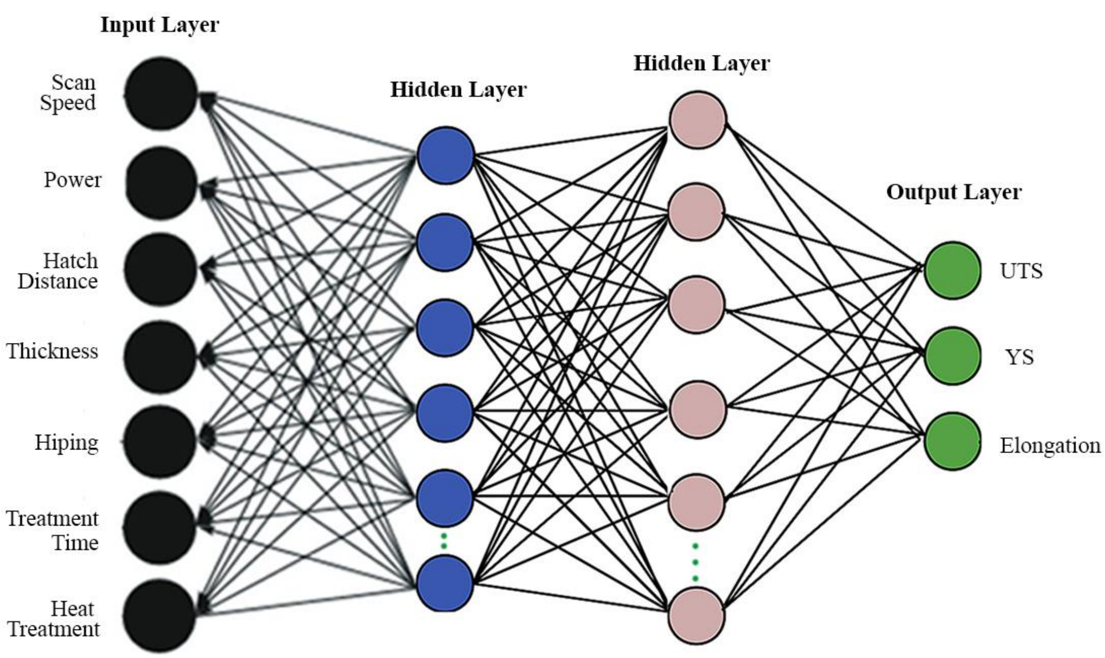

Figure 3. 13 Architecture of the MLP model for predicting UTS, YS, and Elongation

The model is depicted in Figure 3.14. The first layer consists of 7 nodes, with the ReLU activation function, giving input to the hidden layer with 16 nodes, activation as ReLU. If the degree of non-linearity is higher, a greater number of hidden layers or nodes are required. Hence, the second hidden layer consists of 64 nodes to make network dense and improve the performance. The last layer, output layer consists of 3 nodes, UTS, YS, elongation. Input data is normalized using z-score normalization and delta learning rule is used for supervised learning, with backpropagation method depending on gradient descent rule for weight updation. This model is compiled, fitted and the output is predicted for unseen data, and the graph is plotted between predicted output and desired output, to calculate the error.

Model-2:

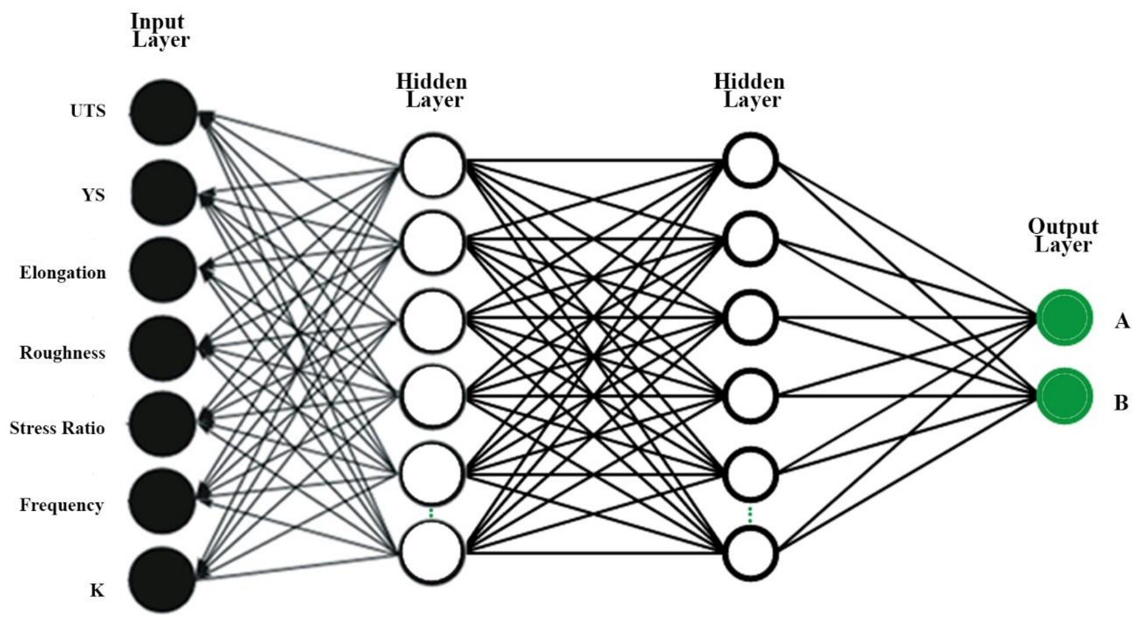

Figure 3. 14 Architecture of the MLP model for predicting Fatigue properties

The model shown in Figure 3.15 consists of 7 input nodes as UTS, YS, elongation, surface, roughness, frequency, k, and 2 output nodes as A and B for fatigue properties. Data received from the input layer is given to the hidden layer consisting of 16 nodes with ReLU activation. The second hidden layer also consists of 64 nodes, making the network dense.

Input data is normalized, and normalized data is compiled by the model. With the help of gradient descent, the model decides whether to increase or decrease weight in the backpropagation process. This model is fitted and A, B outputs are predicted to obtain the fatigue properties of the material.

CHAPTER - 4

DATA COLLECTION

All the data is collected from the open literature available. Some of the data was not numerically available in the publications and proper plots were provided to depict the data. In such cases a digitizing software is used to access the numerical data. Data for tensile testing of Ti-6Al-4V alloy is available for three different directions namely, flat, edge, and vertical as shown in Figure 4.1. The build direction is the one parallel to the worktable movement. For instance, in Figure 4.1, the table is lowered in the Z-direction after each layer is developed, hence, Z-axis represents the build direction. The data collected and the model built consider only the vertical orientation of the alloy as they result in somewhat minimal tensile properties out of the three build options.

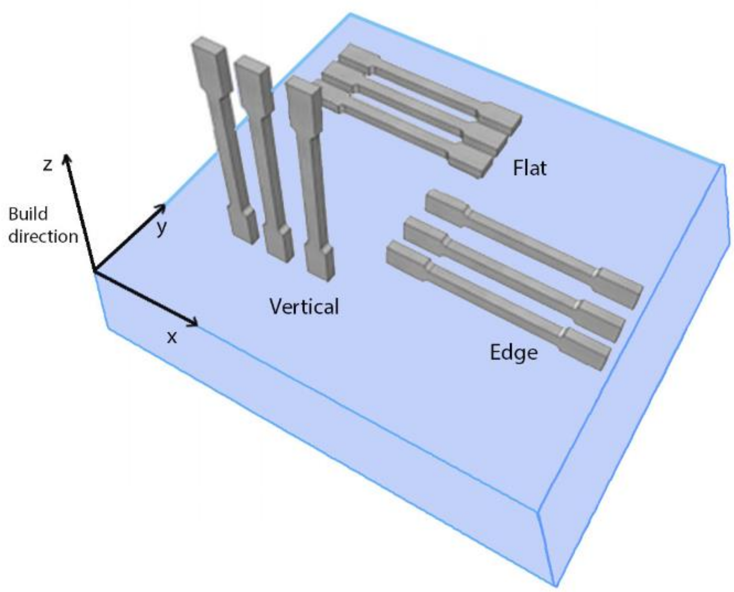

Figure 4. 1 Scanning direction possibilities in an AM process

As mentioned earlier, sometimes SLM and DMLS processes are reported and considered to be the same processes and therefore, researchers use DMLS and SLM interchangeably. This extensive data collection is based on the fact that SLM and DMLS have a fundamental difference of sintering and melting of the powder and therefore, the data is separately collected for DMLS and SLM process. The data could be clubbed together to find out if they both have similar behavior or not however, this study considers them to be different processes and the further proceedings will be carried out based on this consideration.

The open literature data collected is tabulated in the following section:

4.1 Tensile test data of SLM Ti-6Al-4V

SLM tensile data available from the literature was the best set of data out of all the processes discussed. It included variations with scan speed, laser power, powder layer thickness, heating temperature, heating time, and also if the process was HIPed or not see Table 4.1. Some other influencing parameters were also observed however, sufficient data was not presented regarding them in the literature therefore, only the data useful for Model-1 is used from the literature.

Table 4. 1 Data collection (used in model 1-SLM) on tensile behavior of SLM fabricated Ti-6Al-4V alloy

Scanning Speed (mm/s)	Laser Power (W)	Hatch Spacing (μm)	Powder Layer t (μm)	Heat Temp (°C)	Heat Time (hrs)	Hiped or not	UTS (MPa)	YS (MPa)	El (%)	Ref.
1250	200	80	30	820	1.5	No	1045	1010	8	[75]
1600	250	60	30	650	4	No	1170	1124	10.1	[77]
710	175	120	30	800	2	No	NA	NA	NA	[78]
710	175	120	30	920	2	Yes	NA	NA	NA	[78]
200	200	180	50	As-fabricated		No	1035	910	3.3	[79]
960	120	100	30	As-fabricated		No	1237	1098	8.8	[80]
540	120	100	30	As-fabricated		No	1257	1150	8	[80]

400	120	100	30	As-fabricated		No	1148	1066	5.4	[80]
1260	120	100	30	As-fabricated		No	1112	932	6.6	[80]
1500	120	100	30	As-fabricated		No	978	813	3.7	[80]
1000	200	50	50	As-fabricated		No	1243	1153	21.5	[80]
1000	200	50	50	930	2	Yes	922	853	16	[81]
1250	200	120	40	NA	NA	Yes	973	885	19	[81]
1250	170	100	30	650	3	No	NA	NA	NA	[82]
1250	200	120	40	As-fabricated		No	1051	736	11.9	[82]
1250	200	120	40	700	1	No	1115	1051	11.3	[82]
1250	200	120	40	900	2	No	988	908	9.5	[82]
1250	200	120	40	900	2	Yes	973	885	19	[82]
1250	170	100	30	650	3	No	NA	NA	NA	[83]
1250	170	100	30	650	3	No	NA	NA	NA	[83]
1250	170	100	30	650	4	No	1219	1143	4.89	[83]
NA	NA	NA	30	As-fabricated		No	1314.9	1253	4	[84]
NA	NA	NA	30	800	2	No	1228.1	1211	8	[85]
NA	NA	NA	30	1050	2	No	986.4	892	13.8	[85]
NA	NA	NA	30	920	2	No	1088.5	1075	13.8	[85]
NA	NA	NA	30	1050	2	No	1006.8	892	13.5	[85]
NA	NA	NA	30	800	4	No	936.9	862.4	11.4	[86]
NA	NA	NA	60	800	4	No	910.1	835.4	7.2	[86]
NA	NA	NA	60	900	2	No	928	862	9.6	[86]
NA	400	50	60	740	1.5	No	1082.11	NA	14.9	[87]
NA	400	50	60	1200	1.5	No	941.6	NA	11.9	[87]
NA	400	50	60	900	1.5	No	1090.7	NA	17.9	[87]
NA	500	NA	30	670	5	No	1090	1015	10	[88]
NA	500	NA	30	920	2	No	960	850	14	[88]
NA	NA	NA	60	350	2	No	1153.58	1049.7	8.91	[89]
NA	NA	NA	60	420	2	No	1257.22	1159.46	11.47	[89]
NA	NA	NA	NA	670	5	No	1090	1015	10	[90]
NA	NA	NA	NA	920	5	No	950	880	11	[90]
NA	400	32.5	60	850	2	No	912	847.5	4.5	[91]
NA	200	NA	30	650	2	No	1140	1070	NA	[92]
1000	400	160	50	700	1	No	1052	951	3.5	[93]
1200	280	140	30	704	1	No	1093.02	1050.51	15.27	[94]
710	175	120	30	NA	NA	No	1150	1054	9	[95]
686	375	120	90	NA	NA	No	1141	1135	1	[95]
1029	375	120	60	400	2	No	1250	1168	11.4	[95]
600	200	75	25	650	2	No	1174	1037	8.4	[96]
600	200	75	25	920	4	Yes	998	920	15.6	[96]
1600	250	60	30	As-fabricated		No	1271	1115	7.3	[77]
225	195	NA	50	As-fabricated		No	1095	990	8.1	[97]
1600	250	60	30	As-fabricated		No	1267	1110	7.28	[98]
1600	250	60	30	540	5	No	1223	1118	5.36	[98]
1600	250	60	30	850	2	No	1004	955	12.84	[98]
1600	250	60	30	850	5	No	965	909	2	[98]
1600	250	60	30	1015	0.5	No	874	801	13.45	[98]
1600	250	60	30	1020	2	No	840	760	14.06	[98]

1600	250	60	30	705	3	No	1082	1026	9.04	[98]
1600	250	60	30	940	1	No	948	899	13.59	[98]
1600	250	60	30	1015	0.5	No	902	822	12.74	[98]
225	157	100	50	730	2	No	1052	937	9.6	[99]
225	157	100	50	As-fabricated		No	1117	967	8.9	[99]
600	100	105	30	725	8	No	959	950	9.4	[100]
600	100	105	30	974	8	No	912	902	10.09	[100]
600	100	105	30	827	4	No	911	906	9.51	[100]
600	100	105	30	1025	4	No	804	775	14.1	[100]
600	100	105	30	As-fabricated		No	1170.4	1101.68	7.98	[100]
710	175	120	30	640	4	No	1256	1152	3.9	[101]
710	175	120	30	As-fabricated		No	1321	1166	2	[101]
375	100	130	30	As-fabricated		No	1181	1037	7	[102]
1000	150	70	30	As-fabricated		No	1221	1088	6.9	[103]
NA	NA	NA	30	650	4	No	1156	1132	8	[104]
NA	NA	NA	30	890	2	No	998	964	6	[104]
NA	NA	NA	30	As-fabricated		No	1216	1125	6	[104]
710	175	120	30	As-fabricated		No	NA	1096	2.5	[105]
500	110	35 - 95	50	As-fabricated		No	1246	1150	1.4	[64]
1200	280	140	30	920	0.5	No	1079	1029	11	[106]
1200	340	120	60	920	0.5	No	974	881	13	[106]
1200	280	140	30	650	3	No	1237	1161	7.6	[107]
1200	340	120	60	650	3	No	1222	1151	9.8	[107]
1250	250	125	30	As-fabricated		No	1250	1163	10.3	[108]
1250	250	125	30	730	2	No	1134	1054	13	[108]
1250	250	125	30	900	2	No	1046	889	19.2	[108]
375	100	130	30	As-fabricated		No	1220	1120	NA	[109]
125	90	130	30	As-fabricated		No	1250	1125	6	[26]
125	90	130	30	750	2	No	1000	920	12	[26]
375	100	130	30	As-fabricated		No	1220	1120	NA	[110]
58	42	30	50	As-fabricated		No	1117	967	8.9	[111]

4.2 Fatigue test data of SLM Ti-6Al-4V

Fatigue data for SLM was much scattered compared to the tensile data as it can be seen from Table 4.2 that frequencies are ranging from 10 to 19000 Hz. A little information for high-frequency tests was available and therefore, the model would not be very effective in fitting to the real SLM fatigue process, however, if more data was available, a good prediction model could be developed.

Table 4. 2 Data collection (used in Model 2-SLM) on fatigue behavior of SLM fabricated Ti-6Al-4V alloy

UTS (MPa)	YS (MPa)	El (%)	Surface characteristic	Stress ratio (R)	Freq (Hz)	K	A	B	Ref.
1045	1010	8	As-fabricated	-1	100	1	1358.4	-0.119	[75]
1170	1124	10.1	Machined	0	75	1	2040.6	-0.195	[77]
1170	1124	10.1	Machined	0	75	1.75	193.77	-0.051	[77]
1170	1124	10.1	Machined	0	75	2.5	124.63	-0.036	[77]
1035	910	3.3	As-fabricated	-0.2	20	1	7158	-0.346	[79]
1035	910	3.3	Machined	-0.2	20	1	243.35	-0.075	[79]
1237	1098	8.8	As-fabricated	0.1	50	1	873.5	-0.05	[80]
1257	1150	8	As-fabricated	0.1	50	1	1001.5	-0.05	[80]
1148	1066	5.4	As-fabricated	0.1	50	1	669.11	-0.046	[80]
1112	932	6.6	As-fabricated	0.1	50	1	3343.8	-0.206	[80]
978	813	3.7	As-fabricated	0.1	50	1	2403.2	-0.198	[80]
1243	1153	21.5	Machined	0.1	30	1	1121.9	-0.074	[81]
922	853	16	Machined	0.1	30	1	1955	-0.079	[81]
973	885	19	Machined	-1	82	1	2676.3	-0.121	[82]
1219	1143	4.89	As-fabricated	0.1	50	1	2542.8	-0.093	[84]
1314.9	1253	4	As-fabricated	-1	10	1	2622.3	-0.152	[85]
1228.1	1211	8	As-fabricated	-1	10	1	2043.9	-0.124	[85]
986.4	892	13.8	As-fabricated	-1	10	1	7099.3	-0.263	[85]
1088.5	1075	13.8	As-fabricated	-1	10	1	1092.4	-0.033	[85]
1006.8	892	13.5	As-fabricated	-1	10	1	1080.5	-0.046	[85]
936.9	862.4	11.4	As-fabricated	0.1	60	1	798.16	-0.089	[85]
910.1	835.4	7.2	As-fabricated	0.1	60	1	1237.3	-0.119	[85]
928	862	9.6	As-fabricated	0.1	60	1	4685.4	-0.227	[85]
1090	1015	10	As-fabricated	-1	150	1	491.01	-0.045	[88]
960	850	14	Machined	-1	150	1	639.66	-0.032	[88]
1153.58	1049.7	8.91	As-fabricated	0.1	10	1	12772	-0.345	[89]
1257.22	1159.46	11.47	As-fabricated	0.1	10	1	2804.9	-0.139	[89]
1090	1015	10	As-fabricated	-3	150	1	964.33	-0.065	[90]
1090	1015	10	As-fabricated	-1	150	1	595.67	-0.057	[90]
1090	1015	10	As-fabricated	0.1	150	1	249.75	-0.032	[90]
950	880	11	As-fabricated	-1	150	1	330.37	-0.031	[90]
NA	NA	NA	Machined	-1	10	1	2097.9	-0.128	[78]
NA	NA	NA	Machined	-1	19000	1	562.6	-0.032	[78]
NA	NA	NA	Machined	-1	19000	1	845.1	-0.031	[78]
NA	NA	NA	As-fabricated	0.1	50	1	1671.6	-0.136	[83]
NA	NA	NA	Machined	0.1	50	1	564.49	-0.006	[83]

1082.11	NA	14.9	As-fabricated	-1	50	1.1	671.68	-0.101	[87]
941.6	NA	11.9	As-fabricated	-1	50	1.1	806.94	-0.144	[87]
1090.7	NA	17.9	As-fabricated	-1	50	1.1	1203.1	-0.14	[87]
912	847.5	4.5	Machined	-1	NA	1	250.82	-0.018	[91]
1140	1070	NA	Machined	0.1	NA	1	1807.6	-0.142	[92]
1140	1070	NA	As-fabricated	0.1	NA	1	1061.2	-0.047	[92]
1052	951	3.5	Machined	-1	0.25-5	NA	126491	-0.551	[93]
1093.02	1050.5	15.27	As-fabricated	-1	0.4-2	NA	3170.8	-0.218	[94]
1093.02	1050.5	15.27	Machined	-1	0.4-2	NA	2603.8	-0.125	[112]

4.3 Tensile test data of EBM Ti-6Al-4V

As discussed earlier, EBM process is carried out in two sections, first is the pre-scanning where the powder is scanned at higher speed and warmed up for the actual melting process to be carried in the second section. Pre-scanning has its own sets of process parameters like beam current, scanning speed, beam voltage, and powder pre-heating temperature. These parameters sure affect the build of the EBM process however, very few authors have made available the pre-scanning process parameters. The second section comes with additional parameters like scan speed, scan bean current, scan beam voltage, focal offset, line offset, powder layer thickness, and heat treatments at the very last. All this information is necessary to determine the build generated by the EBM process and very less is available in open literature due to manufacturer confidentiality or simply because the information is not essential for the author's study. The Model-1 for EBM, therefore, could not be developed.

4.4 Fatigue test data of EBM Ti-6Al-4V

Similar to SLM, the fatigue data was found in the case of EBM was limited to predict a good model. An attempt has been made to find a relationship of tensile properties with the fatigue properties of Ti-6Al-4V alloy fabricated using the EBM process on the data collected so far, see Table 4.3.

Table 4. 3 Data collection (used in model 2-EBM) on tensile behavior of EBM fabricated Ti-6Al-4V alloy

UTS (MPa)	YS (MPa)	El (%)	Surface characteristic	Stress ratio (R)	Freq (Hz)	K	A	B	Ref.
1036.84	894.34	19.16	As-fabricated	0.1	30	1	3526.9	-0.115	[81]
982.54	959.7	20.56	As-fabricated	0.1	30	1	2122.6	-0.107	[81]
1012	962	8.8	As-fabricated	0.1	50	1	701.49	-0.013	[80]
1011	947	9	As-fabricated	0.1	50	1	812.32	-0.017	[80]
423	420	0.4	As-fabricated	0.1	50	1	688.01	-0.153	[80]
928	869	9.9	As-fabricated	0.1	50	1	854.15	-0.06	[96]
953	879	13.8	As-fabricated	0.1	40	1	1715.5	-0.099	[113]
942	868	12.9	As-fabricated	0.1	40	1	2747.9	-0.101	[113]
953	879	13.8	As-fabricated	-1	133	1	1941.6	-0.131	[113]
942	868	12.9	As-fabricated	-1	133	1	948.64	-0.042	[113]
904	802	13.8	As-fabricated	-1	133	1	1734.3	-0.124	[113]
902	807	14.8	As-fabricated	-1	133	1	870.69	-0.035	[113]
819	771	16.1	Machined	0.1	10	1	2341.2	-0.085	[114]
880	750	16	Machined	0.1	10	1	1546.3	-0.075	[114]
870	788	13.8	Machined	0.1	10	1	1347	-0.066	[114]
896	774	18	Machined	0.1	150	1	2297	-0.082	[115]
833	718	14	As-fabricated	0.1	150	1	3124.2	-0.208	[115]
972	868	15	As-fabricated	0.1	150	1	1937.1	-0.125	[116]
965	869	6	As-fabricated	0.1	150	1	1574.7	-0.158	[116]
1060.93	987.32	14.14	Machined	0.1	20	1	4112.1	-0.183	[117]
1070.33	1026	13.05	Machined	0.1	20	1	3415.6	-0.173	[117]
1033.33	947.32	18.8	Machined	0.1	20	1	2325.4	-0.086	[117]
1090	976	20.1	Machined	0.1	30	1	2300.6	-0.083	[118]
1122	1036	9.8	Machined	0.1	30	1	2006.9	-0.122	[118]
NA	NA	NA	Machined	0.1	<120	1	2558.9	-0.088	[119]
1022.7	931.2	14.7	Machined	0.1	86-146	1	2075.1	-0.114	[120]
910.4	798.4	13.76	Machined	0.1	86-146	1	1305.4	-0.063	[120]
842	782	9.9	As-fabricated	0.1	50	1	3197.6	-0.211	[121]
928	869	9.9	Machined	0.1	50	1	849.2	-0.06	[121]
978.5	881.5	10.7	Machined	0.1	NA	1	1614.5	-0.093	[122]
978	876.5	13.5	Machined	0.1	NA	1	2799.3	-0.103	[122]
987	891	15.7	Machined	-1	20000	1	1070.7	-0.061	[123]

1046	NA	20	As-fabricated	-1	60	1	2419.3	-0.194	[124]
986	NA	22	As-fabricated	-1	60	1	1252.2	-0.129	[124]
986	NA	22	Machined	-1	60	1	966.41	-0.034	[124]
1132	1074	7.2	As-fabricated	-1	100	1	3559	-0.223	[75]
851	812	3.6	As-fabricated	-0.2	20	1	7942.7	-0.327	[125]
1020	950	14	As-fabricated	0	15	1	6757	-0.255	[126]
1000	931	14.3	Machined	-1	20	1	6724.1	-0.303	[127]
1000	931	14.3	Machined	0.5	20	1	2303.8	-0.14	[127]
1000	931	14.3	Machined	0.1	20	1	4292.7	-0.226	[127]

4.5 Tensile test data of DMLS Ti-6Al-4V

From the looks of it, the tensile data available for DMLS process was the one with most sample spaces, however, it seems to cut down important parameters like the hatch spacing, the HIPing process, and the powder layer thickness because after a good look it can be seen that their data is not scattered at all and seems to roughly have the same value for all the data sets, see Table 4.4. In such a case, the regression model simply ignores the parameter because it doesn’t have a linear relationship with the output and the ANN model finds less information to predict the effect of these parameters if an input with a significant variation from these values is provided to it. However, a good variation of laser power and scanning speeds were available, and developing a relationship considering those as major inputs becomes easier.

Table 4. 4 Data collection (used in model 1-DMLS) on tensile behavior of DMLS fabricated Ti-6Al-4V alloy

Scanning Speed (mm/s)	Laser Power (W)	Hatch Spacing (μm)	Powder Layer t (μm)	Heat Temp (°C)	Heat Time (hrs)	Hiped or not	UTS (MPa)	YS (MPa)	El (%)	Ref.
300	130	100	30	As-fabricated		No	1238	1177	6.7	[128]
500	130	100	30	As-fabricated		No	1257	1211	6.2	[128]
700	130	100	30	As-fabricated		No	989	973	3.4	[128]
900	130	100	30	As-fabricated		No	960	936	2.5	[128]

1100	130	100	30	As-fabricated		No	914	893	2.2	[128]
1300	130	100	30	As-fabricated		No	902	877	1.81	[128]
300	170	100	30	As-fabricated		No	1198	1155	5.34	[128]
500	170	100	30	As-fabricated		No	1300	1250	6.26	[128]
700	170	100	30	As-fabricated		No	1247	1206	6.07	[128]
900	170	100	30	As-fabricated		No	1004	967	3.5	[128]
1100	170	100	30	As-fabricated		No	967	1010	2.91	[128]
1300	170	100	30	As-fabricated		No	944	918	2.43	[128]
300	210	100	30	As-fabricated		No	1145	1127	4.37	[128]
500	210	100	30	As-fabricated		No	1244	1165	5.85	[128]
700	210	100	30	As-fabricated		No	1282	1241	6.18	[128]
900	210	100	30	As-fabricated		No	1250	1206	6.11	[128]
1100	210	100	30	As-fabricated		No	1010	978	3.48	[128]
1300	210	100	30	As-fabricated		No	984	957	3	[128]
300	130	100	30	650	2	No	1197	1109	5.84	[128]
500	130	100	30	650	2	No	1210	1147	6.13	[128]
700	130	100	30	650	2	No	943	909	3.45	[128]
900	130	100	30	650	2	No	914	875	2.58	[128]
1100	130	100	30	650	2	No	868	820	2.33	[128]
1300	130	100	30	650	2	No	847	809	1.91	[128]
300	170	100	30	650	2	No	1151	1087	5.39	[128]
500	170	100	30	650	2	No	1243	1180	6.21	[128]
700	170	100	30	650	2	No	1192	1134	6.07	[128]
900	170	100	30	650	2	No	958	912	3.48	[128]
1100	170	100	30	650	2	No	914	880	2.97	[128]
1300	170	100	30	650	2	No	897	860	2.49	[128]
300	210	100	30	650	2	No	1099	1052	4.4	[128]
500	210	100	30	650	2	No	1201	1103	5.42	[128]
700	210	100	30	650	2	No	1233	1177	6.18	[128]
900	210	100	30	650	2	No	1197	1136	6.12	[128]
1100	210	100	30	650	2	No	957	924	3.58	[128]
1300	210	100	30	650	2	No	925	897	3.02	[128]
300	130	100	30	750	2	No	1132	1025	7.75	[128]
500	130	100	30	750	2	No	1124	1032	8.39	[128]
700	130	100	30	750	2	No	911	804	4.39	[128]
900	130	100	30	750	2	No	869	767	3.51	[128]
1100	130	100	30	750	2	No	828	724	3.26	[128]
1300	130	100	30	750	2	No	801	712	2.97	[128]
300	170	100	30	750	2	No	1095	1001	7.29	[128]
500	170	100	30	750	2	No	1171	1087	8.28	[128]
700	170	100	30	750	2	No	1113	1032	8.22	[128]
900	170	100	30	750	2	No	930	815	4.53	[128]
1100	170	100	30	750	2	No	904	778	4.11	[128]
1300	170	100	30	750	2	No	875	749	3.38	[128]
300	210	100	30	750	2	No	1048	947	6.24	[128]
500	210	100	30	750	2	No	1145	1028	7.34	[128]
700	210	100	30	750	2	No	1160	1069	8.17	[128]
900	210	100	30	750	2	No	1127	1038	8.22	[128]

1100	210	100	30	750	2	No	931	809	4.53	[128]
1300	210	100	30	750	2	No	903	783	3.85	[128]
300	130	100	30	850	2	No	1038	926	10.45	[128]
500	130	100	30	850	2	No	1030	934	11.59	[128]
700	130	100	30	850	2	No	823	700	7	[128]
900	130	100	30	850	2	No	784	669	6.27	[128]
1100	130	100	30	850	2	No	742	646	5.11	[128]
1300	130	100	30	850	2	No	719	619	5.01	[128]
300	170	100	30	850	2	No	996	902	10.34	[128]
500	170	100	30	850	2	No	1079	976	12.77	[128]
700	170	100	30	850	2	No	1029	922	11.42	[128]
900	170	100	30	850	2	No	839	732	7.05	[128]
1100	170	100	30	850	2	No	814	699	6.49	[128]
1300	170	100	30	850	2	No	777	674	5.82	[128]
300	210	100	30	850	2	No	964	870	9.29	[128]
500	210	100	30	850	2	No	1038	927	10.86	[128]
700	210	100	30	850	2	No	1059	960	12.54	[128]
900	210	100	30	850	2	No	1030	944	11.54	[128]
1100	210	100	30	850	2	No	841	739	7.5	[128]
1300	210	100	30	850	2	No	804	711	6.6	[128]
300	130	100	30	950	2	No	927	890	9.05	[128]
500	130	100	30	950	2	No	940	879	11.12	[128]
700	130	100	30	950	2	No	803	691	6.31	[128]
900	130	100	30	950	2	No	759	667	5.52	[128]
1100	130	100	30	950	2	No	715	643	4.67	[128]
1300	130	100	30	950	2	No	696	619	4.55	[128]
300	170	100	30	950	2	No	908	849	8.8	[128]
500	170	100	30	950	2	No	973	918	12.4	[128]
700	170	100	30	950	2	No	938	856	10.8	[128]
900	170	100	30	950	2	No	787	733	6.37	[128]
1100	170	100	30	950	2	No	777	720	5.75	[128]
1300	170	100	30	950	2	No	750	673	5.05	[128]
300	210	100	30	950	2	No	892	822	8.7	[128]
500	210	100	30	950	2	No	934	892	10.87	[128]
700	210	100	30	950	2	No	950	907	12.09	[128]
900	210	100	30	950	2	No	931	868	11.08	[128]
1100	210	100	30	950	2	No	825	740	5.77	[128]
1300	210	100	30	950	2	No	781	714	5.5	[128]
1250	200	NA	30	As-fabricated		No	1325	1213	4.5	[129]
300	170	100	30	As-fabricated		No	1199	1154	3.94	[130]
500	170	100	30	As-fabricated		No	1296	1256	3.04	[130]
700	170	100	30	As-fabricated		No	1248	1207	3.2	[130]
900	170	100	30	As-fabricated		No	1140	1087	4.65	[130]
1100	170	100	30	As-fabricated		No	1105	1052	5	[130]
1300	170	100	30	As-fabricated		No	1084	1035	5.45	[130]
300	170	100	30	825	No	No	954	843	13.3	[130]
500	170	100	30	825	4	No	1034	915	11.85	[130]
700	170	100	30	825	4	No	978	867	12.28	[130]

900	170	100	30	825	4	No	900	782	15.25	[130]
1100	170	100	30	825	4	No	873	750	15.58	[130]
1300	170	100	30	825	4	No	841	719	15.98	[130]
NA	200	NA	30	As-fabricated		No	1140	1070	NA	[92]
NA	200	NA	30	650	2	No	1189	1076	13.6	[92]
NA	200	NA	30	As-fabricated		Yes	1022	907	17.7	[92]
1250	340	120	60	As-fabricated		Yes	1196	1056	7	[131]
1250	340	120	60	799	4	No	969	902	11.6	[131]

4.6 Fatigue test data of DMLS Ti-6Al-4V

Most of the work available in the open literature is related to tensile testing of DMLS fabricated Ti64 alloy. There is some data available suiting the input and output parameters this study concerns, however, most of the published work in fatigue study of DMLS fabricated Ti64 alloy is related to understanding the crack propagation.

CHAPTER – 5

RESULTS AND DISCUSSION

As mentioned earlier, to fit the 'as-fabricated data' along with the 'heat treatment' data, four compensating sets of heat temperature and heat time is randomly considered for building Model-1. The SLM tensile data (more promising than the rest considered in this study) is used with all these four variations in MATLAB using the Neural Network tool (nntool) to get an estimate of which compensating set would fit the best for further models. The 'R' value (correlation) obtained from a 'Bayesian Regularization ANN' regression plot is kept as the priority criterion for selection as it determines which model fits the best with the data sets [132], [133].

For this selection, similar to the ANN model, 16 nodes are considered in the first hidden layer and 64 nodes are considered in the second hidden layer. The following section presents the result from each of those tests. The nntool gives correlation value based on all the three output parameters, however, the elongation value is quite smaller compared to the YS and UTS output parameters numerically, thus overall R-value provides less information about the efficiency of the model for estimating the elongation values even if the R-value ≈ 1 for the whole model. Therefore, all the output data is extracted from MATLAB and the correlation information is separately plotted, see Table 5.1-5.4. The overall average value calculated from each of the three correlation is considered for choosing the compensating set for further working.

Compensating set 1: (30, 0.5)

Table 5. 1 Correlation analysis for experimental and predicted output values for compensation set (30, 0.5)

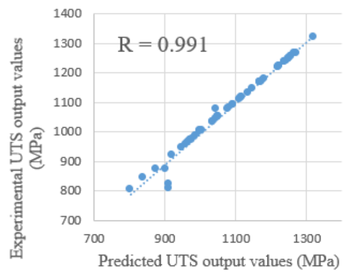

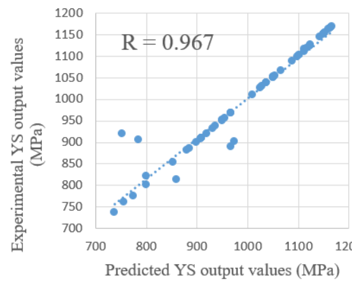

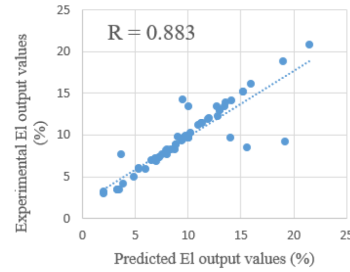

Average R-value = 0.947

Compensating set 2: (30, 1.5)

Table 5. 2 Correlation analysis for experimental and predicted output values for compensation set (30, 1.5)

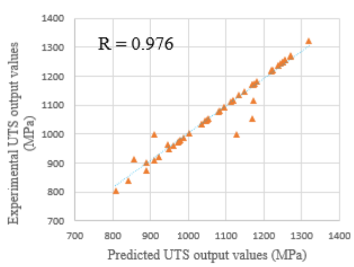

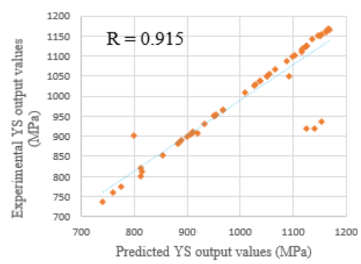

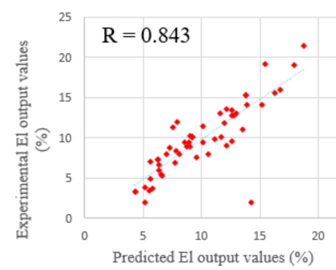

Average R-value = 0.911

Compensating set 3: (30, 3)

Table 5. 3 Correlation analysis for experimental and predicted output values for compensation set (30, 3)

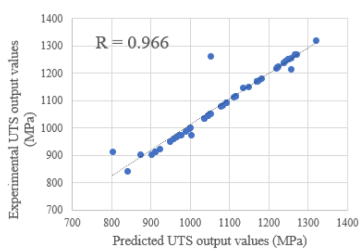

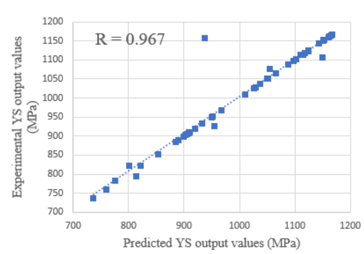

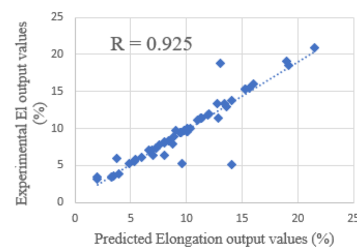

Average R-value = 0.953

Compensating set 4: (30,4)

Table 5. 4 Correlation analysis for experimental and predicted output values for compensation set (30, 4)

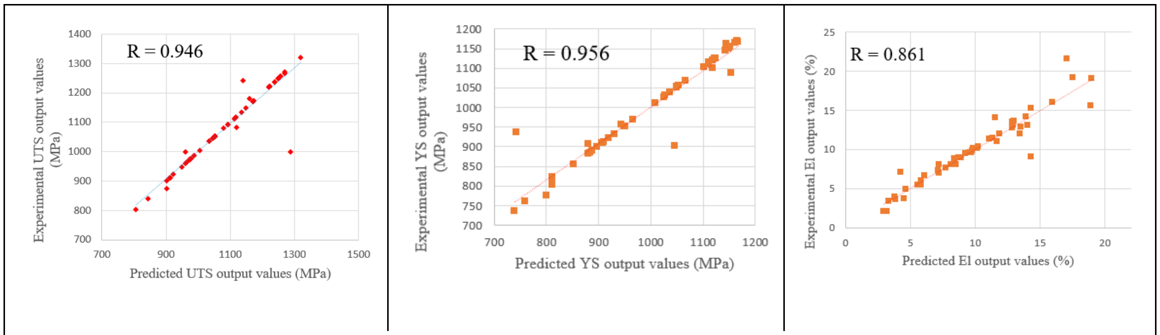

Average R-value = 0.921

From the above analysis, it can be said that here, compensation set 3 (30, 3) fits the model the best and it gives in more than 90% response to each of the output parameters which is acceptable and efficient than the other cases. Therefore, further analysis of tensile data is based on considering the as-built condition as a replacement for a heating temperature of 30°C and a heating time of 3 hours.

5.1 Results for Regression Analysis Model

The following section shows the results for each of the processes with sufficient data to build up a multivariate regression model:

5.1.1 Tensile SLM (Model-1)

Ultimate Tensile Strength

The model fit generated by multi-regression analysis for predicting the UTS can be summarized in Figure 5.1.

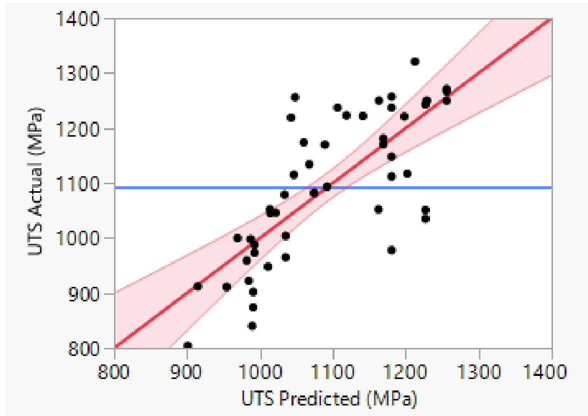

Figure 5. 1 UTS Actual vs UTS Predicted by multi-regression analysis model for SLM fabricated Ti64 Alloys

Summary of Fit

RSquare	0.62179
RSquare Adj	0.557217
Root Mean Square Error	89.24997
Mean of Response	1093.029
Observations (or Sum Wgts)	49

Analysis of Variance

Source	DF	Sum of Squares	Mean Square	F Ratio
Model	7	536920.90	76703.0	9.6293
Error	41	326587.82	7965.6	Prob > F
C. Total	48	863508.72		<.0001*

Parameter Estimates

Term	Estimate	Std Error	t Ratio	Prob>|t|
Intercept	1223.1606	103.2013	11.85	<.0001*
Scan Speed	-0.083301	0.046973	-1.77	0.0836
Laser Power	1.1384334	0.298195	3.82	0.0004*
Hatch Space	-0.19068	0.515149	-0.37	0.7132
Powder Layer Thickness	-3.806539	1.869119	-2.04	0.0482*
HIPed or not	-14.43976	57.42098	-0.25	0.8027
Heating Temp	-0.276868	0.037428	-7.40	<.0001*
Heat Time	8.3803736	9.442221	0.89	0.3800

Figure 5. 2 Initial model fit for estimating UTS of SLM fabricated Ti64 alloys

The initial model fit for can be seen from Figure 5.2. Here it can be seen that ‘HIPed or not’, ‘Heating Time’, ‘Hatch Spacing’, and ‘Scan Speed’ are insignificant in the same order for estimating the UTS value for Model-1 SLM fabrications. Also, the ‘RSquade Adj’ value is close to 0.55 which can be considered lower for estimating a model. The insignificant factors are removed one at a time keeping a check at the RSquare Adj value and the P-values to obtain the following results, see Figure 5.3.

Summary of Fit

RSquare	0.562709
RSquare Adj	0.543696
Root Mean Square Error	90.6024
Mean of Response	1093.029
Observations (or Sum Wgts)	49

Analysis of Variance

Source	DF	Sum of Squares	Mean Square	F Ratio
Model	2	485904.12	242952	29.5966
Error	46	377604.59	8209	**Prob > F**
C. Total	48	863508.72		<.0001*

Parameter Estimates

Term	Estimate	Std Error	t Ratio	Prob>|t|
Intercept	1119.1427	38.15064	29.33	<.0001*
Laser Power	0.5800017	0.182753	3.17	0.0027*
Heating Temp	-0.269394	0.0353	-7.63	<.0001*

Figure 5. 3 Significant covariates for estimating UTS for SLM fabricated Ti64 alloy

Therefore, Significant factors for determining the UTS of an SLM fabricated Ti64 alloy are laser power and heating temperature. careful analysis of Figure 5.3 shows that all the significant covariates have a P-value less than 0.05 thus rejecting the null hypothesis of being insignificant. The RSquare Adj value, however, is 0.543 therefore, it raises the question if the method of predicting UTS by the equation generated by regression any good? To answer that, an F-test needs to be conducted on the results generated. An F-test determines if the model equation is better at predicting the value or concern than taking the mean value of available data. It is another hypothesis test where the null hypothesis is that the regression equation is not better than the mean. To reject this hypothesis, the P-value for F statistics needs to be much lower than 0.05 which can be noted from the ‘Analysis of Variance’ section in Figure 5.3 at the bottom right corner [Prob>F, <0.0001]. Hence, UTS predicted using the multi-regression analysis for SLM fabricated Ti64 alloy can be represented by the following equation:

$UTS_{predicted} = 1199.1427 + 0.58 * \text{Laser Power} - 0.2694 * \text{Heating Temperature}$

The residuals are the deviations of UTS predicted from the UTS experimental. The farther the dots are from the blue line, more is the deviation, see Figure 5.4.

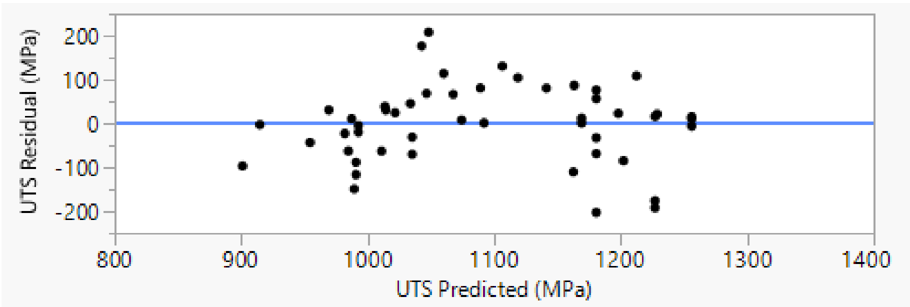

Figure 5. 4 UTS residuals vs UTS predicted for SLM fabricated Ti64 alloy

<u>Yield Strength</u>

The model fit generated by multi-regression analysis for predicting the yield strength can be summarized in Figure 5.5.

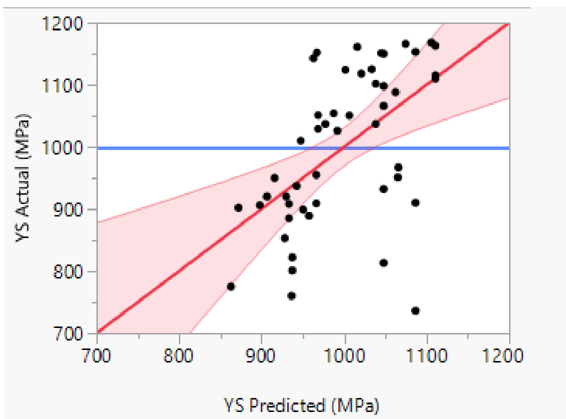

Figure 5. 5 YS Actual vs YS Predicted by multi-regression analysis model for SLM fabricated Ti64 alloys

Similar to the UTS analysis, initial results for the multi-regression analysis of SLM fabricated Ti64, see Figure 5.6, show that the scan speed, hatch spacing, heating temperature, and HIPed or not are insignificant for estimating the yield strength.

Summary of Fit

RSquare	0.405352
RSquare Adj	0.303827
Root Mean Square Error	104.2556
Mean of Response	998.9222
Observations (or Sum Wgts)	49

Analysis of Variance

Source	DF	Sum of Squares	Mean Square	F Ratio
Model	7	303777.68	43396.8	3.9926
Error	41	445638.49	10869.2	Prob > F
C. Total	48	749416.17		0.0021*

Parameter Estimates

Term	Estimate	Std Error	t Ratio	Prob>|t|
Intercept	1100.923	120.5526	9.13	<.0001*
Scan Speed	-0.109726	0.05487	-2.00	0.0522
Laser Power	1.2000067	0.348331	3.45	0.0013*
Hatch Space	-0.386125	0.601762	-0.64	0.5247
Powder Layer Thickness	-4.009003	2.183375	-1.84	0.0736
HIPed or not	-41.66015	67.0752	-0.62	0.5380
Heating Temp	-0.179311	0.043721	-4.10	0.0002*
Heat Time	15.208519	11.02975	1.38	0.1754

Figure 5. 6 Initial model fit for estimating YS of SLM fabricated Ti64 alloys

After removing the insignificant covariates, the results obtained are similar to the UTS results as shown in Figure 5.7, however, the RSquared Adj value drops down to 0.26 which is quite insignificant still the F-statistics confirm that the equation developed for identifying the behavior of yield strength with the considered covariates is better than using the mean value of the data.

YS predicted using the multi-regression analysis for SLM fabricated Ti64 alloy can be represented by the following equation:

$$YS_{predicted} = 995.211 + 0.483 * \text{Laser Power} - 0.176 * \text{Heating Temperature}$$

The residuals resulted from estimating YS by a multi-regression analysis can be seen in Figure 5.8.

Summary of Fit

RSquare	0.289455
RSquare Adj	0.258562
Root Mean Square Error	107.5916
Mean of Response	998.9222
Observations (or Sum Wgts)	49

Analysis of Variance

Source	DF	Sum of Squares	Mean Square	F Ratio
Model	2	216922.18	108461	9.3695
Error	46	532493.98	11576	Prob > F
C. Total	48	749416.17		0.0004*

Parameter Estimates

Term	Estimate	Std Error	t Ratio	Prob>|t|
Intercept	995.21108	45.30441	21.97	<.0001*
Laser Power	0.4830389	0.217021	2.23	0.0310*
Heating Temp	-0.176173	0.041919	-4.20	0.0001*

Figure 5. 7 Significant covariates for estimating YS for SLM fabricated Ti64 alloy

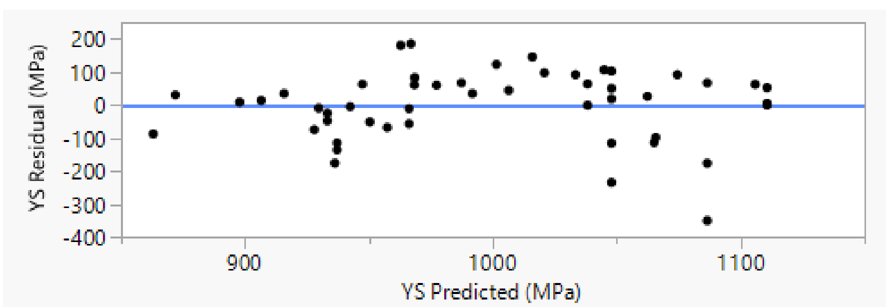

Figure 5. 8 YS residual plots vs YS predicted for SLM fabricated Ti64 alloy

<u>Elongation</u>

The model fit generated by multi-regression analysis for predicting the percent elongation can be summarized in Figure 5.9.

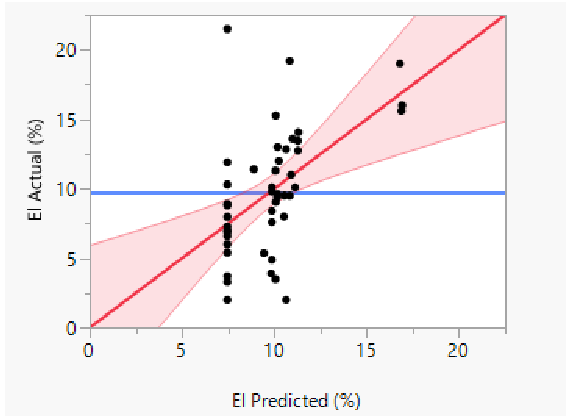

Figure 5. 9 El Actual vs El Predicted by multi-regression analysis model for SLM fabricated Ti64 alloys

Summary of Fit

RSquare	0.380378
RSquare Adj	0.274589
Root Mean Square Error	3.752768
Mean of Response	9.757143
Observations (or Sum Wgts)	49

Analysis of Variance

Source	DF	Sum of Squares	Mean Square	F Ratio
Model	7	354.46674	50.6381	3.5956
Error	41	577.41386	14.0833	Prob > F
C. Total	48	931.88060		0.0042*

Parameter Estimates

Term	Estimate	Std Error	t Ratio	Prob>|t|
Intercept	9.3856865	4.339391	2.16	0.0364*
Scan Speed	0.0010225	0.001975	0.52	0.6075
Laser Power	-0.012653	0.012538	-1.01	0.3188
Hatch Space	-0.018469	0.021661	-0.85	0.3988
Powder Layer Thickness	0.1010901	0.078592	1.29	0.2056
HIPed or not	5.0657196	2.414428	2.10	0.0421*
Heating Temp	0.0040111	0.001574	2.55	0.0147*
Heat Time	-0.775949	0.397025	-1.95	0.0575

Figure 5. 10 Initial model fit for estimating the elongation of SLM fabricated Ti64 alloys

Initial regression analysis results can be seen in Figure 5.10 where RSquare Adj value is 0.27 and the insignificant covariates are hatch spacing, powder layer thickness, beam power, and scanning speed. After removing the insignificant covariates, the final model that included only the significant covariates had an RSquare Adj value of 0.25 and the covariates to be included in the model fit equation were heating temperature, and HIPed or not, see Figure 5.11.

Summary of Fit

RSquare	0.282091
RSquare Adj	0.250878
Root Mean Square Error	3.813606
Mean of Response	9.757143
Observations (or Sum Wgts)	49

Analysis of Variance

Source	DF	Sum of Squares	Mean Square	F Ratio
Model	2	262.87550	131.438	9.0375
Error	46	669.00510	14.544	Prob > F
C. Total	48	931.88060		0.0005*

Parameter Estimates

Term	Estimate	Std Error	t Ratio	Prob>|t|
Intercept	7.3409185	0.929113	7.90	<.0001*
HIPed or not	5.9677129	2.352425	2.54	0.0146*
Heating Temp	0.0038815	0.00147	2.64	0.0113*

Figure 5. 11 Significant covariates for estimating the elongation for SLM fabricated Ti64 alloy

Equation:

$El_{Predicted}$ = 7.341 + 0.0.00388 * Heat temp + 5.967* HIPed or not

The residuals resulted from estimating the elongation by a multi-regression analysis can be seen in Figure 5.12. It is evident that the residuals variation from the zero line is quite significant for the predicted elongation values.

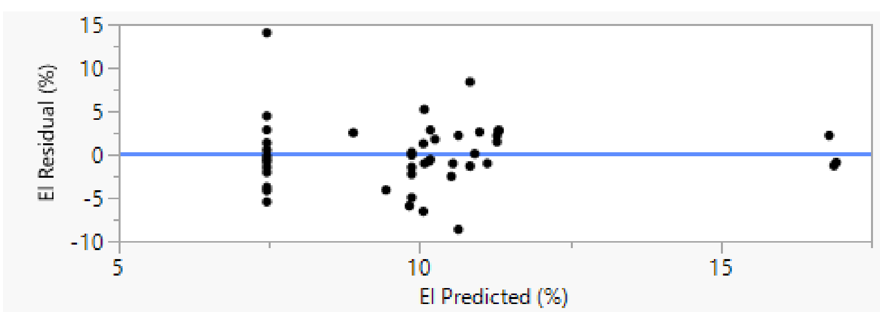

Figure 5. 12 El residuals vs El predicted for SLM fabricated Ti64 alloy

5.1.2 Fatigue SLM (Model-2)

The available data set for Model-2 constitutes only 31 sample space therefore, any good prediction for Model-2 using the multi-regression analysis is next to impossible. Results of the regression analysis for estimating A and B are shown below:

<u>'A'</u>

The results of predicting 'A' from available data sets are not very useful when done by muti-regression analysis as can be seen from the fit provided by JMP for estimating 'A' in Figure 5.13. Suspected reasons for that are the unavailability of sufficient datasets and non-linear behavior of the fatigue properties of Ti64 alloy.

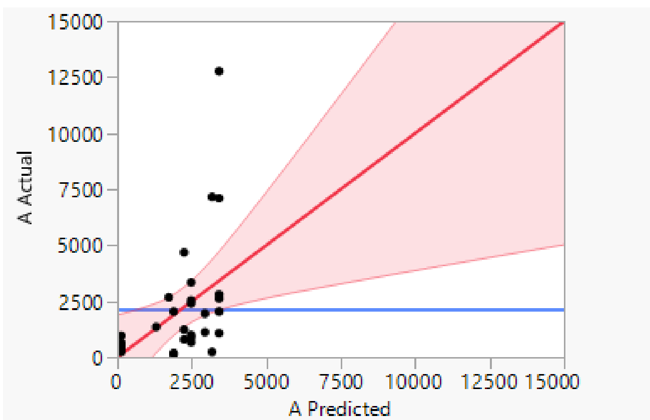

Figure 5. 13 A Actual vs A Predicted by multi-regression analysis model for SLM fabricated Ti64 alloys

From the initial analysis of the regression model, it can be observed that nearly all the covariates, as well as the intercept, are insignificant, and the RSquare Adj value is nearly zero, see Figure 5.14.

Also, the P-value for F-statistics is insignificant implying the values estimated from this method might not be a better estimate than the same if done by taking the mean of available data sets. Figure 5.15 shows the final results of the model predicted by multi-regression analysis that only the frequency set by the user must be significant for the analysis prediction based on the available dataset.

Summary of Fit

RSquare	0.282114
RSquare Adj	0.063627
Root Mean Square Error	2563.509
Mean of Response	2168.155
Observations (or Sum Wgts)	31

Analysis of Variance

Source	DF	Sum of Squares	Mean Square	F Ratio
Model	7	59397380	8485340	1.2912
Error	23	151146345	6571580	Prob > F
C. Total	30	210543725		0.2983

Parameter Estimates

Term	Estimate	Std Error	t Ratio	Prob>|t|
Intercept	5892.4508	5818.129	1.01	0.3217
UTS	7.6962947	15.04956	0.51	0.6139
YS	-10.38392	13.85808	-0.75	0.4613
% El	28.132893	131.1512	0.21	0.8320
Surface Characteristics	-1280.933	1354.083	-0.95	0.3540
Stress Ratio	-89.63946	783.902	-0.11	0.9100
Frequency	-24.23065	10.62249	-2.28	0.0321*
SCF	-117.2532	1900.019	-0.06	0.9513

Figure 5. 14 Initial model fit for estimating A value of SLM fabricated Ti64 alloys

Summary of Fit

RSquare	0.193872
RSquare Adj	0.166075
Root Mean Square Error	2419.213
Mean of Response	2168.155
Observations (or Sum Wgts)	31

Analysis of Variance

Source	DF	Sum of Squares	Mean Square	F Ratio
Model	1	40818600	40818600	6.9744
Error	29	169725126	5852590.5	Prob > F
C. Total	30	210543725		0.0132*

Parameter Estimates

Term	Estimate	Std Error	t Ratio	Prob>|t|
Intercept	3649.2625	709.4533	5.14	<.0001*
Frequency	-23.46159	8.883875	-2.64	0.0132*

Figure 5. 15 Significant covariates for estimating A value for SLM fabricated Ti64 alloy

It can also be seen by the bi-variate plots that only frequency shows a linear relationship (correlation = -0.44) with the A value, see Table 5.5.

Table 5. 5 Bi-variate plots for estimating A value for SLM fabricated Ti64 alloy

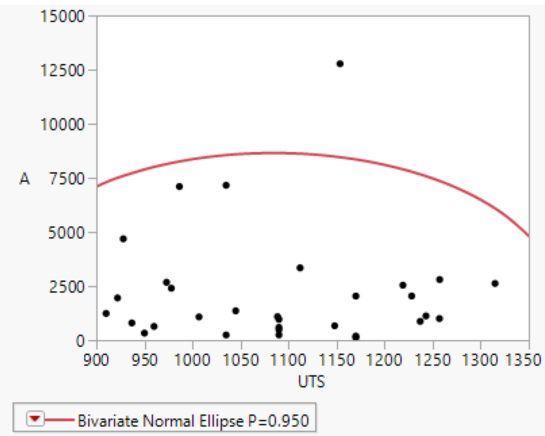

Bivariate Normal Ellipse P=0.950

Variable	Mean	Std Dev	Correlation	Signif. Prob	Number
UTS	1090.145	117.3299	-0.02139	0.9091	31
A	2168.155	2649.174			

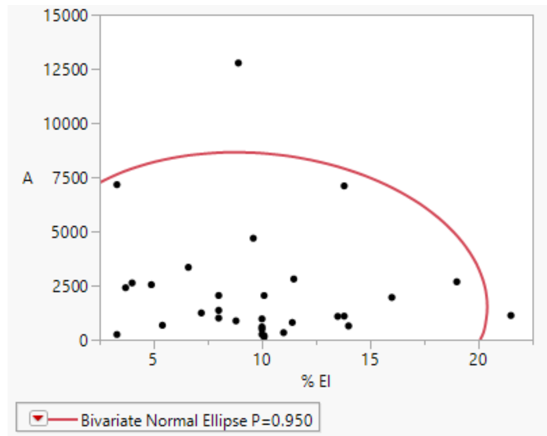

Bivariate Normal Ellipse P=0.950

Variable	Mean	Std Dev	Correlation	Signif. Prob	Number
% El	9.853871	4.311995	-0.10272	0.5824	31
A	2168.155	2649.174			

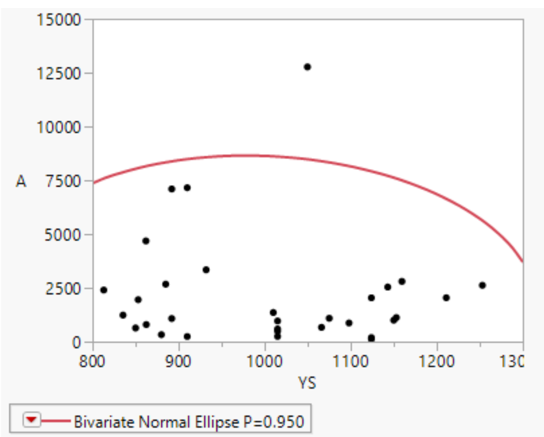

Bivariate Normal Ellipse P=0.950

Variable	Mean	Std Dev	Correlation	Signif. Prob	Number
YS	1005.708	127.0714	-0.08776	0.6388	31
A	2168.155	2649.174			

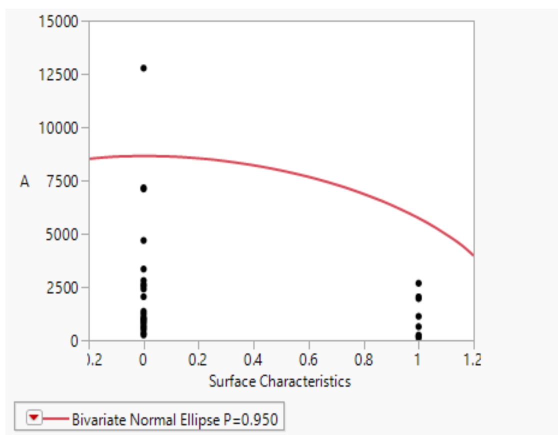

Bivariate Normal Ellipse P=0.950

Variable	Mean	Std Dev	Correlation	Signif. Prob	Number
Surface Characteristics	0.258065	0.444803	-0.2362	0.2008	31
A	2168.155	2649.174			

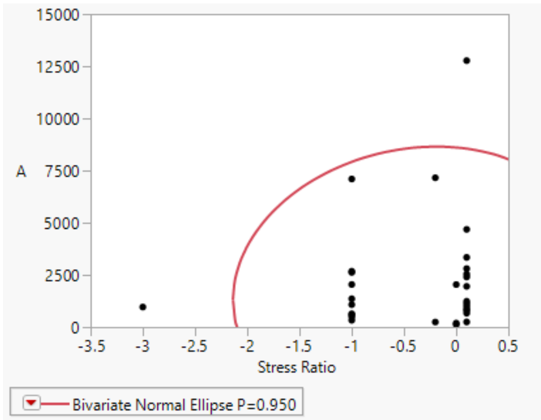

Bivariate Normal Ellipse P=0.950

Variable	Mean	Std Dev	Correlation	Signif. Prob	Number
Stress Ratio	-0.41935	0.701626	0.133223	0.4749	31
A	2168.155	2649.174			

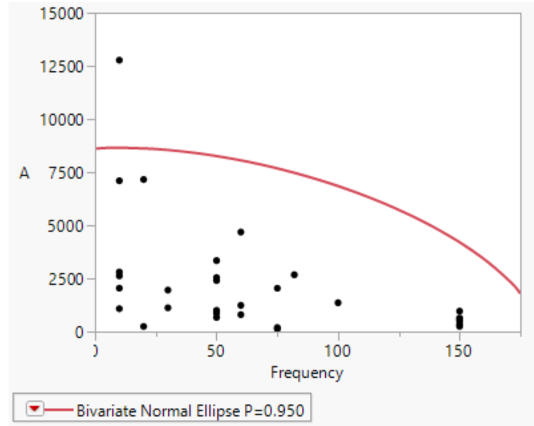

Bivariate Normal Ellipse P=0.950

Variable	Mean	Std Dev	Correlation	Signif. Prob	Number
Frequency	63.12903	49.7177	-0.44031	0.0132*	31
A	2168.155	2649.174			

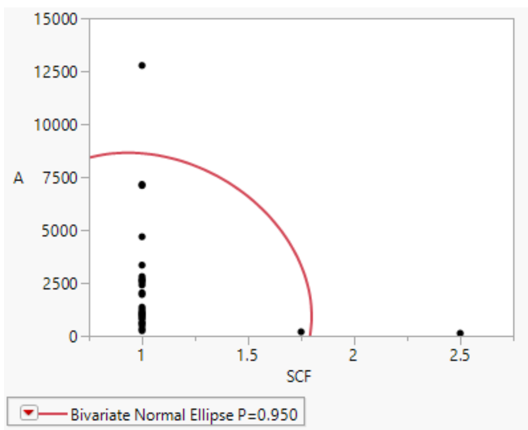

Bivariate Normal Ellipse P=0.950

Variable	Mean	Std Dev	Correlation	Signif. Prob	Number
SCF	1.072581	0.297164	-0.19249	0.2995	31
A	2168.155	2649.174			

Equation:

$A_{\text{Predicted}} = 3649.26 - \text{Frequency} * 23.46$

The residuals obtained using this equation can be seen in Figure 5.16. The residuals seem closer to the zero line in the figure; however, they are mostly having deviations of more than 2000 units from the zero line and therefore, the estimation is not very useful to predict the A value for SLM fabricated Ti64 alloy.

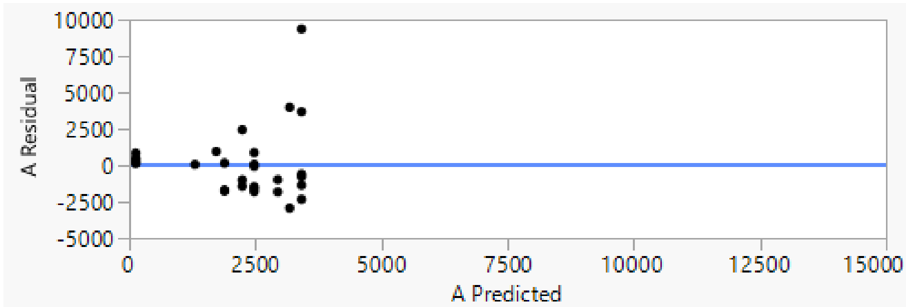

Figure 5. 16 A residuals vs A predicted for SLM fabricated Ti64 alloy

<u>‘B’</u>

Similar to the estimation of ‘A’ the results of predicting ‘B’ from available data sets are equally bad when done by muti-regression analysis as can be seen from the fit provided by JMP for estimating ‘B’ in Figure 5.17. The scatter in the predicted model can be clearly seen in Figure 5.17 indicating that the final model developed could not estimate the B value very accurately. The ‘B’ generally lies around -0.05 to -0.35 and a variation of mere 0.02 units is enough to deviate the stress values in the S-N curve by around 200 MPa.

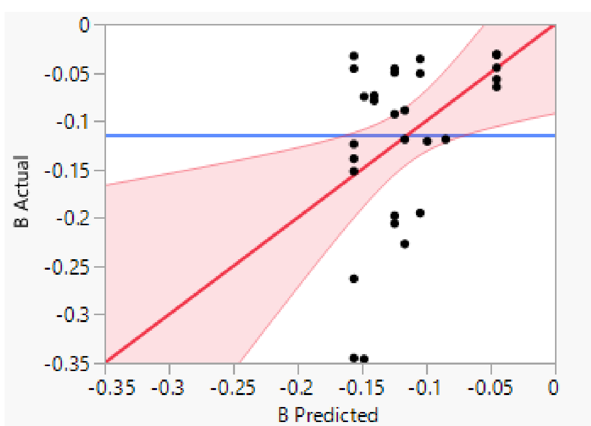

Figure 5. 17 B Actual vs B Predicted by multi-regression analysis model for SLM fabricated Ti64 alloys

Summary of Fit

RSquare	0.340185
RSquare Adj	0.139372
Root Mean Square Error	0.082407
Mean of Response	-0.11413
Observations (or Sum Wgts)	31

Analysis of Variance

Source	DF	Sum of Squares	Mean Square	F Ratio
Model	7	0.08052776	0.011504	1.6940
Error	23	0.15618973	0.006791	Prob > F
C. Total	30	0.23671748		0.1602

Parameter Estimates

Term	Estimate	Std Error	t Ratio	Prob>|t|
Intercept	-0.373822	0.18703	-2.00	0.0576
UTS	-0.00018	0.000484	-0.37	0.7125
YS	0.0003348	0.000445	0.75	0.4600
% El	0.0041157	0.004216	0.98	0.3391
Surface Characteristics	0.0122999	0.043528	0.28	0.7800
Stress Ratio	0.000872	0.025199	0.03	0.9727
Frequency	0.0008089	0.000341	2.37	0.0266*
SCF	0.0236421	0.061078	0.39	0.7023

Figure 5. 18 Initial model fit for estimating B value of SLM fabricated Ti64 alloys

Summary of Fit

RSquare	0.196951
RSquare Adj	0.16926
Root Mean Square Error	0.080963
Mean of Response	-0.11413
Observations (or Sum Wgts)	31

Analysis of Variance

Source	DF	Sum of Squares	Mean Square	F Ratio
Model	1	0.04662185	0.046622	7.1124
Error	29	0.19009564	0.006555	Prob > F
C. Total	30	0.23671748		0.0124*

Parameter Estimates

Term	Estimate	Std Error	t Ratio	Prob>|t|
Intercept	-0.164185	0.023743	-6.92	<.0001*
Frequency	0.0007929	0.000297	2.67	0.0124*

Figure 5. 19 Significant covariates for estimating B value for SLM fabricated Ti64 alloy

From the initial regression analysis, it can be seen that none of the covariates are significant except for Frequency and the intercept also shows insignificant results as can be seen in

Figure 5.18. The final regression model developed by JMP shows that only frequency influences the ‘B’ value and shows a linear correlation of 0.44 as can be seen from Figure 5.19. The bivariate plots again show that there is no linear behavior of the covariates with ‘B’ value, see Table 5.6.

Table 5. 6 Bi-variate plots for estimating B value for SLM fabricated Ti64 alloy

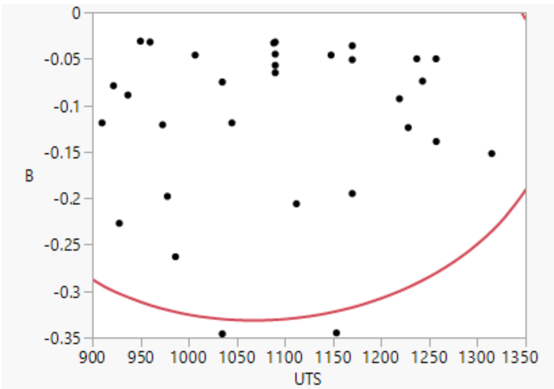

Bivariate Normal Ellipse P=0.950

Bivariate Normal Ellipse P=0.950

Variable	Mean	Std Dev	Correlation	Signif. Prob	Number
UTS	1090.145	117.3299	0.079295	0.6715	31
B	-0.11413	0.088829			

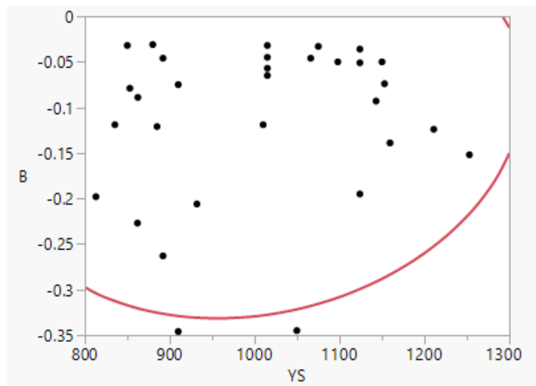

Bivariate Normal Ellipse P=0.950

Bivariate Normal Ellipse P=0.950

Variable	Mean	Std Dev	Correlation	Signif. Prob	Number
YS	1005.708	127.0714	0.159743	0.3907	31
B	-0.11413	0.088829			

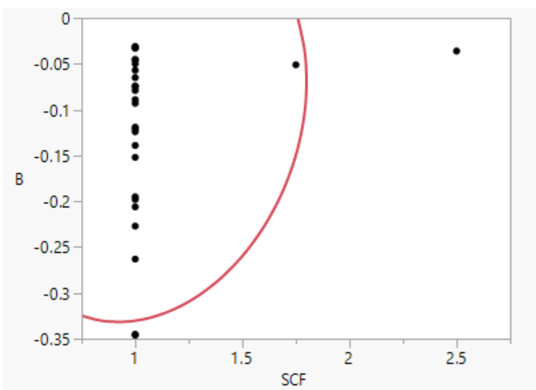

Bivariate Normal Ellipse P=0.950

Bivariate Normal Ellipse P=0.950

Variable	Mean	Std Dev	Correlation	Signif. Prob	Number
SCF	1.072581	0.297164	0.207778	0.2620	31
B	-0.11413	0.088829			

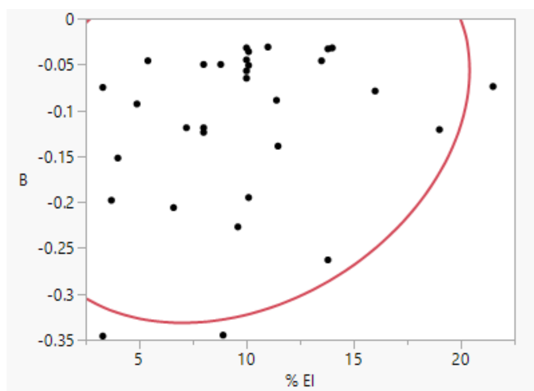

Bivariate Normal Ellipse P=0.950

Bivariate Normal Ellipse P=0.950

Variable	Mean	Std Dev	Correlation	Signif. Prob	Number
% El	9.853871	4.311995	0.268077	0.1448	31
B	-0.11413	0.088829			

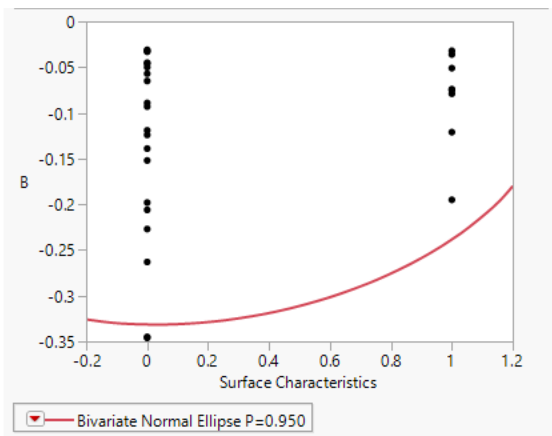

Bivariate Normal Ellipse P=0.950

Variable	Mean	Std Dev	Correlation	Signif. Prob	Number
Surface ...	0.258065	0.444803	0.210937	0.2547	31
B	-0.11413	0.088829			

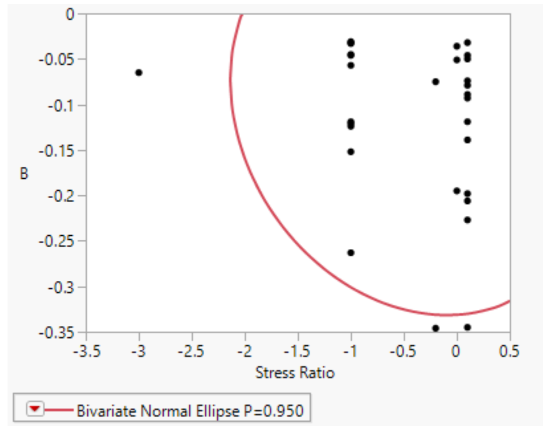

Bivariate Normal Ellipse P=0.950

Variable	Mean	Std Dev	Correlation	Signif. Prob	Number
Stress Ratio	-0.41935	0.701626	-0.1905	0.3047	31
B	-0.11413	0.088829			

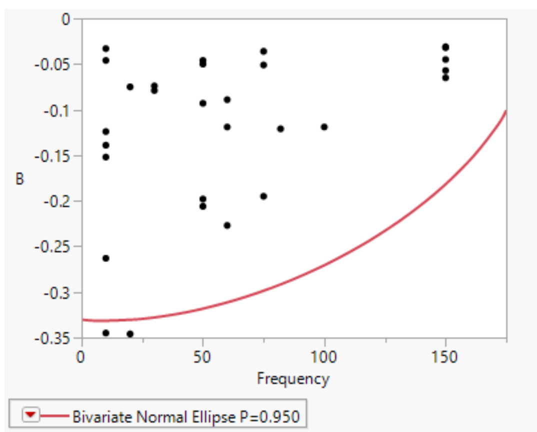

Bivariate Normal Ellipse P=0.950

Variable	Mean	Std Dev	Correlation	Signif. Prob	Number
Frequency	63.12903	49.7177	0.443792	0.0124*	31
B	-0.11413	0.088829			

Equation:

$$B_{\text{Predicted}} = -0.164 + 0.000793 * \text{Frequency}$$

The B residuals related to the above equation can be seen from Figure 5.20.

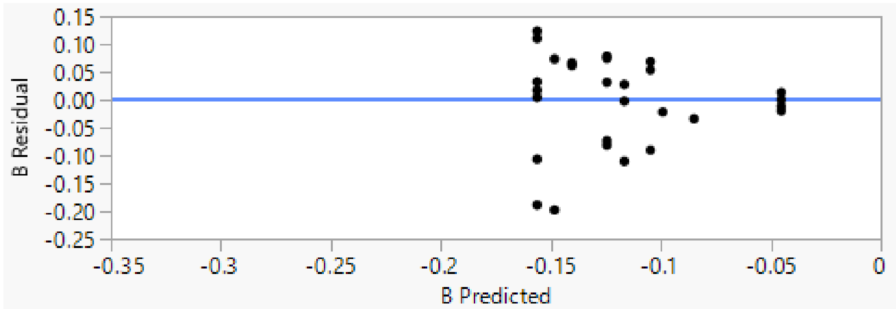

Figure 5. 20 B residuals vs B predicted for SLM fabricated Ti64 alloy

5.1.3 Fatigue EBM (Model-2)

<u>'A'</u>

The available data from EBM fatigue tests are not sufficient enough to develop a good regression fit to estimate A value. The results obtained from the regression model are discussed hereunder.

Summary of Fit

RSquare	0.098078
RSquare Adj	-0.11006
Root Mean Square Error	1887.489
Mean of Response	2536.03
Observations (or Sum Wgts)	33

Analysis of Variance

Source	DF	Sum of Squares	Mean Square	F Ratio
Model	6	10072644	1678774	0.4712
Error	26	92627984	3562615	Prob > F
C. Total	32	102700628		0.8233

Parameter Estimates

Term		Estimate	Std Error	t Ratio	Prob>|t|
Intercept	Biased	63.854089	2593.28	0.02	0.9805
UTS		-4.397328	13.34512	-0.33	0.7444
YS		7.7600131	13.36296	0.58	0.5664
% El		-21.30776	96.73791	-0.22	0.8274
Surface characteristic		362.87471	764.6648	0.47	0.6391
Stress ratio		-465.28	803.4328	-0.58	0.5675
Frequency		-0.104875	0.107203	-0.98	0.3369
SFC	Zeroed	0	0	.	.

Summary of Fit

RSquare	0.050347
RSquare Adj	0.019714
Root Mean Square Error	1773.732
Mean of Response	2536.03
Observations (or Sum Wgts)	33

Analysis of Variance

Source	DF	Sum of Squares	Mean Square	F Ratio
Model	1	5170716	5170716	1.6435
Error	31	97529911	3146126	Prob > F
C. Total	32	102700628		0.2093

Parameter Estimates

Term	Estimate	Std Error	t Ratio	Prob>|t|
Intercept	-423.9093	2329.404	-0.18	0.8568
YS	3.3872834	2.642191	1.28	0.2093

Figure 5. 21 Initial and final model fit for estimating A value of EBM fabricated Ti64 alloys

From the initial analysis of the regression model, SFC is zeroed out and therefore, needs to be removed from the analysis equation, see Figure 5.21. RSquare Adj is -ve and none of the covariates are significant and hence, they are sequentially eliminated from the analysis equation and the model is built again with the left covariates. However, no significant covariates are observed in this case. Therefore, it can be said that no linear regression model can be developed for estimating the A value of EBM fabricated Ti64 alloys.

<u>'B'</u>

Similar to the estimation of A value, no model could be built for estimating B value. The initial and final fits for the estimation model of B value can be seen in Figure 5.22.

Summary of Fit

RSquare	0.125966
RSquare Adj	-0.07573
Root Mean Square Error	0.08137
Mean of Response	-0.12876
Observations (or Sum Wgts)	33

Analysis of Variance

Source	DF	Sum of Squares	Mean Square	F Ratio
Model	6	0.02481010	0.004135	0.6245
Error	26	0.17214796	0.006621	Prob > F
C. Total	32	0.19695806		0.7091

Parameter Estimates

Term		Estimate	Std Error	t Ratio	Prob>|t|
Intercept	Biased	-0.13763	0.111797	-1.23	0.2293
UTS		0.0001823	0.000575	0.32	0.7538
YS		-0.000248	0.000576	-0.43	0.6698
% El		0.0047001	0.00417	1.13	0.2700
Surface characteristic		-0.018149	0.032965	-0.55	0.5866
Stress ratio		0.0265026	0.034636	0.77	0.4511
Frequency		4.4833e-6	4.622e-6	0.97	0.3409
SFC	Zeroed	0	0	.	.

Summary of Fit

RSquare	0.067153
RSquare Adj	0.037061
Root Mean Square Error	0.076986
Mean of Response	-0.12876
Observations (or Sum Wgts)	33

Analysis of Variance

Source	DF	Sum of Squares	Mean Square	F Ratio
Model	1	0.01322631	0.013226	2.2316
Error	31	0.18373175	0.005927	Prob > F
C. Total	32	0.19695806		0.1453

Parameter Estimates

Term	Estimate	Std Error	t Ratio	Prob>|t|
Intercept	-0.187206	0.041358	-4.53	<.0001*
% El	0.0045086	0.003018	1.49	0.1453

Figure 5. 22 Initial and final model fit for estimating B value of EBM fabricated Ti64 alloys

None of the covariates were found significant for a linear regression model for estimating the B value of EBM fabricated Ti64 alloys. The intercept becomes significant at the last step, however, that just indicates that B value would stay constant for all the scenarios. Therefore, B value for EBM fabricated Ti64 alloys can't be explained by linear regression.

5.1.4 Tensile DMLS (Model-1)

<u>Ultimate Tensile Strength:</u>

The output of the tensile DMLS regression model for estimating the ultimate tensile strength of Ti64 alloys is shown in Figure 5.23.

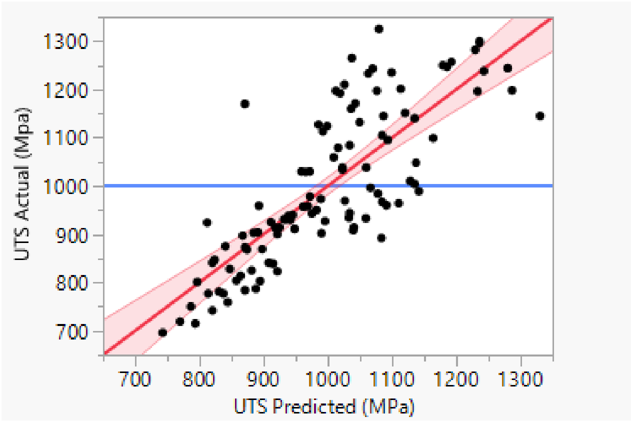

Figure 5. 23 UTS Actual vs UTS Predicted by multi-regression analysis model for DMLS fabricated Ti64 alloys

Following the same procedure as for the previous processes, the initial and the final regression model results are shown in Figure 5.24. It can be seen that the scanning speed, the laser power, and the heating temperature were observed to be significant according to the analysis of the available data for DMLS fabricated Ti64 alloy.

Equation:

$UTS_{Predicted}$ = 1184.1314 -0.2527 * Scanning Speed + 1.0964 * Laser Power – 0.2686 * Heating Temperature

Summary of Fit

RSquare	0.687512
RSquare Adj	0.666066
Root Mean Square Error	93.04441
Mean of Response	1001.945
Observations (or Sum Wgts)	110

Analysis of Variance

Source	DF	Sum of Squares	Mean Square	F Ratio
Model	7	1942794.9	277542	32.0589
Error	102	883040.7	8657	Prob > F
C. Total	109	2825835.7		<.0001*

Parameter Estimates

Term		Estimate	Std Error	t Ratio	Prob>|t|
Intercept	Biased	1471.9509	134.8435	10.92	<.0001*
Scanning Speed		-0.25915	0.026469	-9.79	<.0001*
Laser Power		1.167184	0.298063	3.92	0.0002*
Powder Layer Thickness	Biased	-7.365602	3.887802	-1.89	0.0610
Heating Temp		-0.241792	0.029829	-8.11	<.0001*
Heating Time		14.818003	12.86838	1.15	0.2522
Hiped or not		55.880175	135.2397	0.41	0.6803
Hatch Space[100]	Biased	-127.3179	47.89951	-2.66	0.0091*
Hatch Space[120]	Zeroed	0	0	.	.

Summary of Fit

RSquare	0.659526
RSquare Adj	0.64989
Root Mean Square Error	95.27132
Mean of Response	1001.945
Observations (or Sum Wgts)	110

Analysis of Variance

Source	DF	Sum of Squares	Mean Square	F Ratio
Model	3	1863713.5	621238	68.4437
Error	106	962122.2	9077	Prob > F
C. Total	109	2825835.7		<.0001*

Parameter Estimates

Term	Estimate	Std Error	t Ratio	Prob>|t|
Intercept	1184.1315	50.14096	23.62	<.0001*
Scanning Speed	-0.252731	0.02665	-9.48	<.0001*
Laser Power	1.0964574	0.243263	4.51	<.0001*
Heating Temp	-0.268593	0.026136	-10.28	<.0001*

Figure 5. 24 Initial and final model fit for estimating UTS of DMLS fabricated Ti64 alloys

The residuals obtained from the equation mentioned above are shown in Figure 5.25

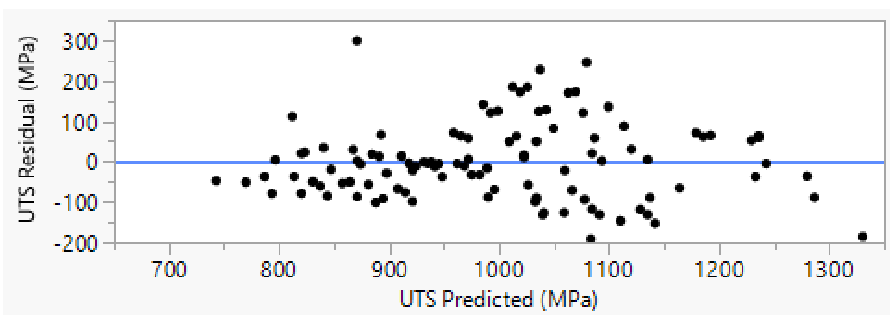

Figure 5. 25 UTS residuals vs UTS predicted for DMLS fabricated Ti64 alloy

<u>Yield Strength</u>

The output of the tensile DMLS regression model for estimating the yield strength of Ti64 alloys is shown in Figure 5.26. After zeroing out powder layer thickness initially and following the same procedure only scanning speed, laser power, and heating temperature were found to be significant and the regression analysis results are shown in Figure 5.27.

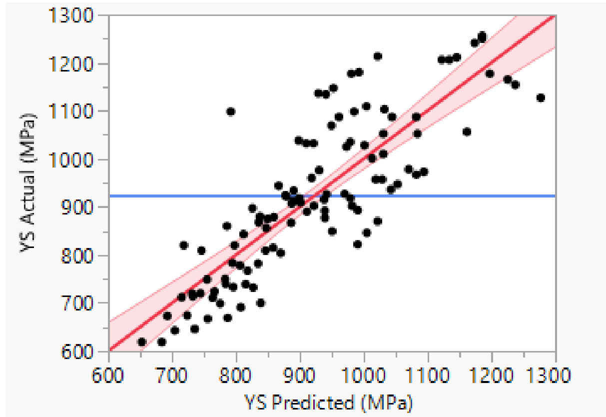

Figure 5. 26 YS Actual vs YS Predicted by multi-regression analysis model for DMLS fabricated Ti64 alloys

Summary of Fit

RSquare	0.734189
RSquare Adj	0.715947
Root Mean Square Error	89.45482
Mean of Response	924.9636
Observations (or Sum Wgts)	110

Analysis of Variance

Source	DF	Sum of Squares	Mean Square	F Ratio
Model	7	2254463.1	322066	40.2474
Error	102	816220.8	8002	Prob > F
C. Total	109	3070683.9		<.0001*

Parameter Estimates

Term		Estimate	Std Error	t Ratio	Prob>|t|
Intercept	Biased	1222.7416	95.06527	12.86	<.0001*
Scanning Speed		-0.258694	0.025447	-10.17	<.0001*
Laser Power		1.1734885	0.286564	4.10	<.0001*
Hatch Space[100]	Biased	-54.74773	47.70744	-1.15	0.2538
Hatch Space[120]	Biased	-78.3666	74.75626	-1.05	0.2970
Powder Layer Thickness	Zeroed	0	0	.	.
Heating Temp		-0.323775	0.028678	-11.29	<.0001*
Heating Time		-14.82409	12.37193	-1.20	0.2336
Hiped or not		-109.8075	130.0222	-0.84	0.4004

Summary of Fit

RSquare	0.713886
RSquare Adj	0.705788
Root Mean Square Error	91.0404
Mean of Response	924.9636
Observations (or Sum Wgts)	110

Analysis of Variance

Source	DF	Sum of Squares	Mean Square	F Ratio
Model	3	2192118.3	730706	88.1606
Error	106	878565.5	8288	Prob > F
C. Total	109	3070683.9		<.0001*

Parameter Estimates

Term	Estimate	Std Error	t Ratio	Prob>|t|
Intercept	1154.5774	47.91424	24.10	<.0001*
Scanning Speed	-0.258188	0.025466	-10.14	<.0001*
Laser Power	0.9972885	0.23246	4.29	<.0001*
Heating Temp	-0.311411	0.024976	-12.47	<.0001*

Figure 5. 27 Initial and final model fit for estimating YS of DMLS fabricated Ti64 alloys

Equation:

$$YS_{\text{Predicted}} = 1151.577 - 0.2582 * \text{Scanning Speed} + 0.9973 * \text{Laser Power} - 0.3114 * \text{Heating Temperature}$$

The residuals obtained after fitting the model for the above-shown equation are presented in Figure 5.28

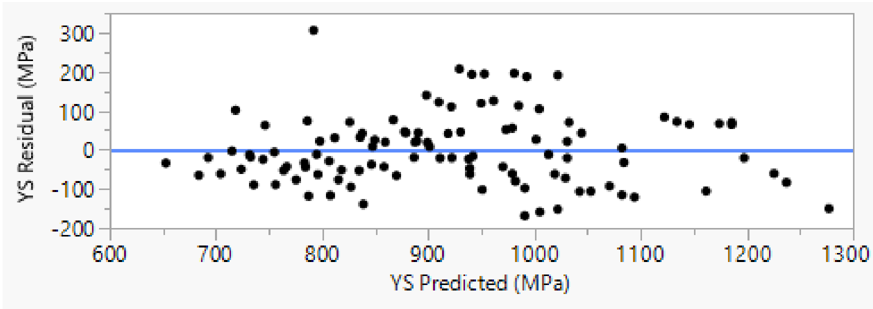

Figure 5. 28 YS residuals vs YS predicted for DMLS fabricated Ti64 alloy

<u>Elongation</u>

The results obtained after the multi-regression model fit for the elongation in the DMLS process are shown in Figure 5.29.

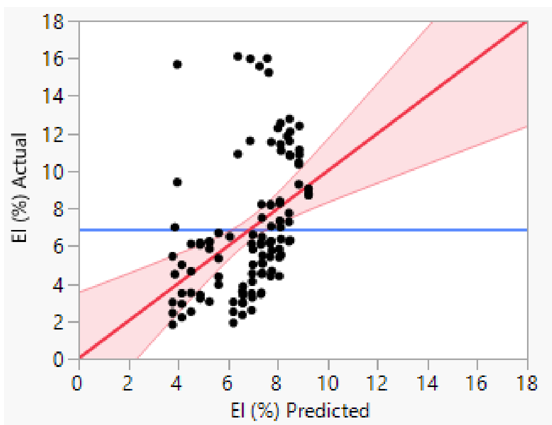

Figure 5. 29 El Actual vs El Predicted by multi-regression analysis model for DMLS fabricated Ti64 alloys

Figure 5.30 shows the initial and final model fits for the estimation of elongation in DMLS fabricated Ti64 alloys. The significant covariants, in this case, were scanning speed and heating time only.

Equation:

$El_{Predicted}$ = 6.0614 - 0.001844 * Scanning Speed + 0.00392 * Heating Temperature

Summary of Fit

RSquare	0.370259
RSquare Adj	0.327041
Root Mean Square Error	2.932773
Mean of Response	6.875091
Observations (or Sum Wgts)	110

Analysis of Variance

Source	DF	Sum of Squares	Mean Square	F Ratio
Model	7	515.8221	73.6889	8.5673
Error	102	877.3179	8.6012	Prob > F
C. Total	109	1393.1399		<.0001*

Parameter Estimates

Term		Estimate	Std Error	t Ratio	Prob>|t|
Intercept	Biased	-2.348171	3.116711	-0.75	0.4529
Scanning Speed		-0.002305	0.000834	-2.76	0.0068*
Laser Power		0.0148693	0.009395	1.58	0.1166
Hatch Space[100]	Biased	0.1189722	1.564087	0.08	0.9395
Hatch Space[120]	Biased	-0.888208	2.450881	-0.36	0.7178
Powder Layer Thickness	Zeroed	0	0	.	.
Heating Temp		0.0061664	0.00094	6.56	<.0001*
Heating Time		1.9337796	0.405613	4.77	<.0001*
Hiped or not		2.0757438	4.262773	0.49	0.6273

Summary of Fit

RSquare	0.185012
RSquare Adj	0.169779
Root Mean Square Error	3.257474
Mean of Response	6.875091
Observations (or Sum Wgts)	110

Analysis of Variance

Source	DF	Sum of Squares	Mean Square	F Ratio
Model	2	257.7483	128.874	12.1452
Error	107	1135.3917	10.611	Prob > F
C. Total	109	1393.1399		<.0001*

Parameter Estimates

Term	Estimate	Std Error	t Ratio	Prob>|t|
Intercept	6.061406	0.996549	6.08	<.0001*
Scanning Speed	-0.001844	0.000907	-2.03	0.0446*
Heating Temp	0.0039224	0.000893	4.39	<.0001*

Figure 5. 30 Initial and final model fit for estimating the El of DMLS fabricated Ti64 alloys

The residuals obtained after comparing the model equation and actual experimental values can be seen from Figure 5.31.

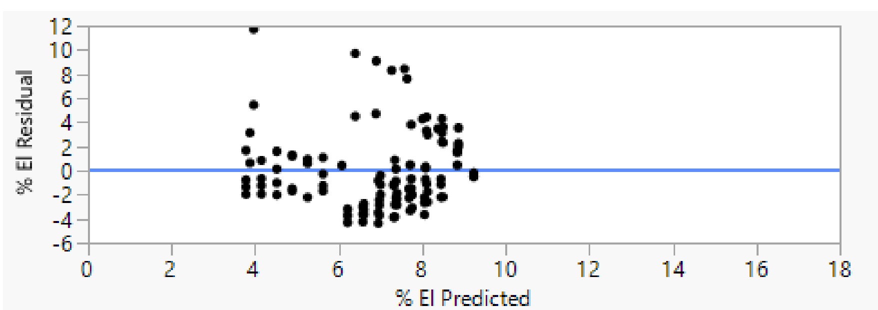

Figure 5. 31 El residuals vs El predicted for DMLS fabricated Ti64 alloy

5.2 Results for ANN Model

As mentioned before, the ANN model incorporates two hidden layers accompanied by 16 nodes in the first and 64 in the other. This section presents the results obtained by the ANN models for tensile and fatigue properties of the Ti64 fabricated by various AM processes.

5.2.1 Tensile SLM (Model-1)

The R-curve obtained from the ANN estimation model for estimating the tensile behavior of SLM fabricated Ti64 alloy is presented in Figure 5.32. A total of 49 datasets from Table 4.1 with necessary input and output values were used for building the model. As discussed earlier, 'nntool' from MATLAB was used to train the model based on Bayesian regularization. The individual R-values obtained from the predicted output values and the actual output values are presented in Table 5.7

Table 5. 7 Individual correlation values for tensile output parameters for SLM fabricated Ti64 alloy

	UTS	YS	El
Correlation (R)	0.966231	0.967153	0.924921

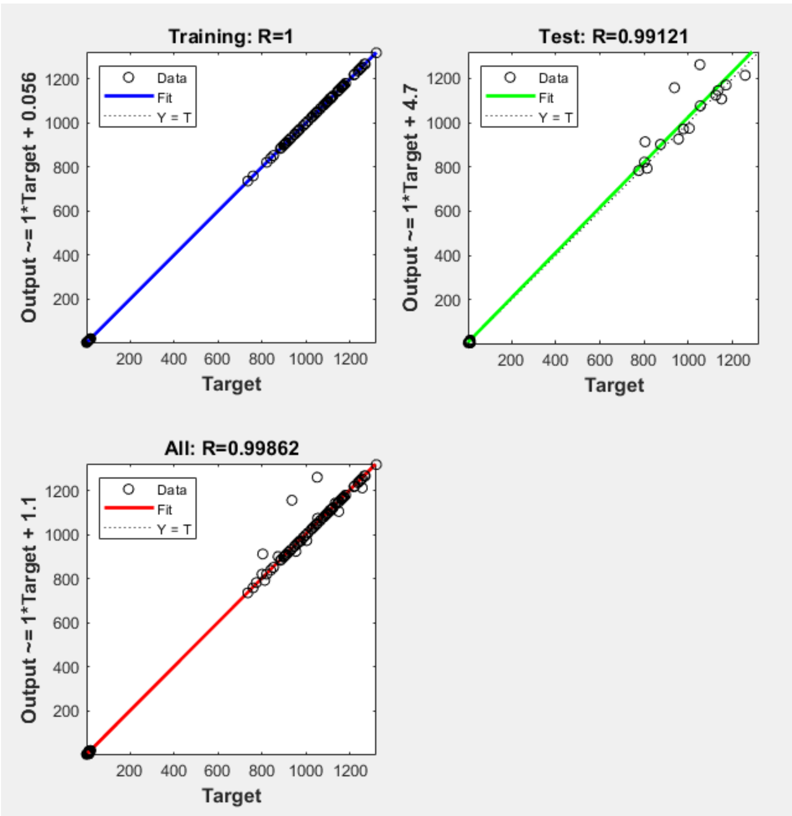

Figure 5. 32 Performance of the ANN model for tensile behavior of SLM fabricated Ti64 alloy

Since the model is built on 16 nodes in the first hidden layer and 64 nodes in the second, to develop an equation in the matrix form becomes a little tedious, however, the residuals obtained from the predicted output data are presented below individually for each of the output parameters.

Figure 5.33 shows the residuals for UTS while Figure 5.34 presents the YS residuals obtained after comparing the actual output to the predicted output of the ANN model. The residuals for the elongation can be seen in Figure 5.35. The predicted values with a large deviation from the actual values resulted in large residual values.

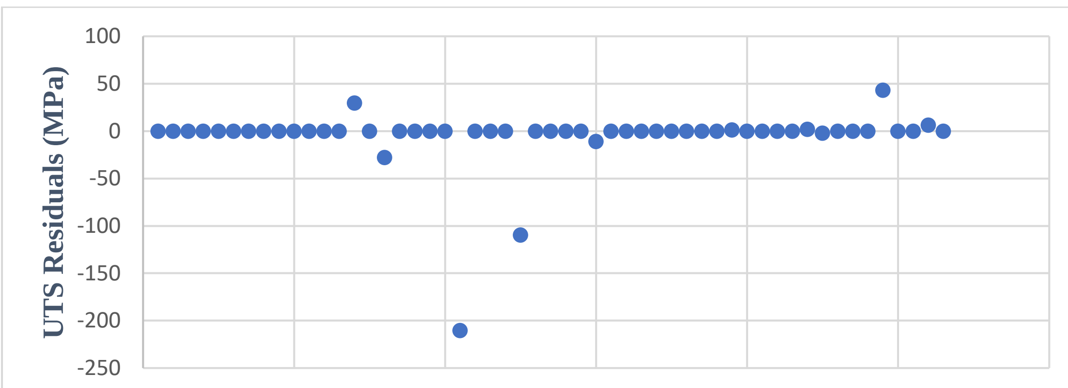

Figure 5. 33 UTS residuals for the ANN model for SLM fabricated Ti64 alloy

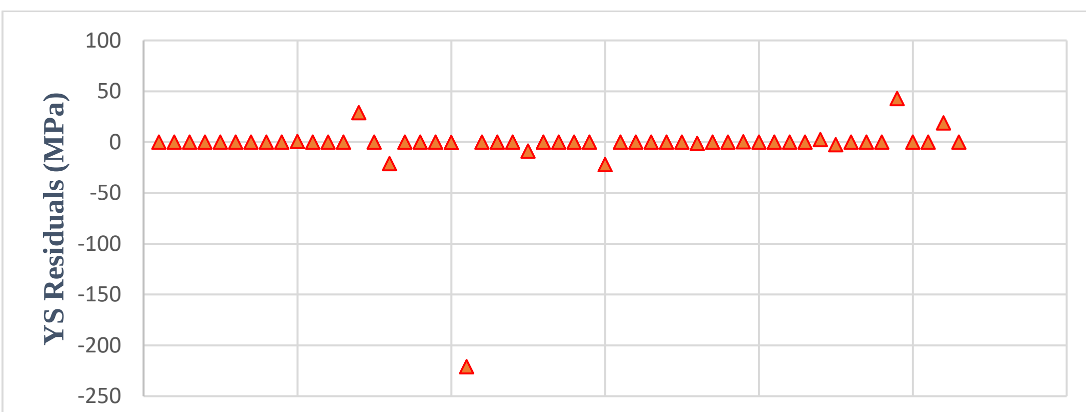

Figure 5. 34 YS residuals for the ANN model for SLM fabricated Ti64 alloy

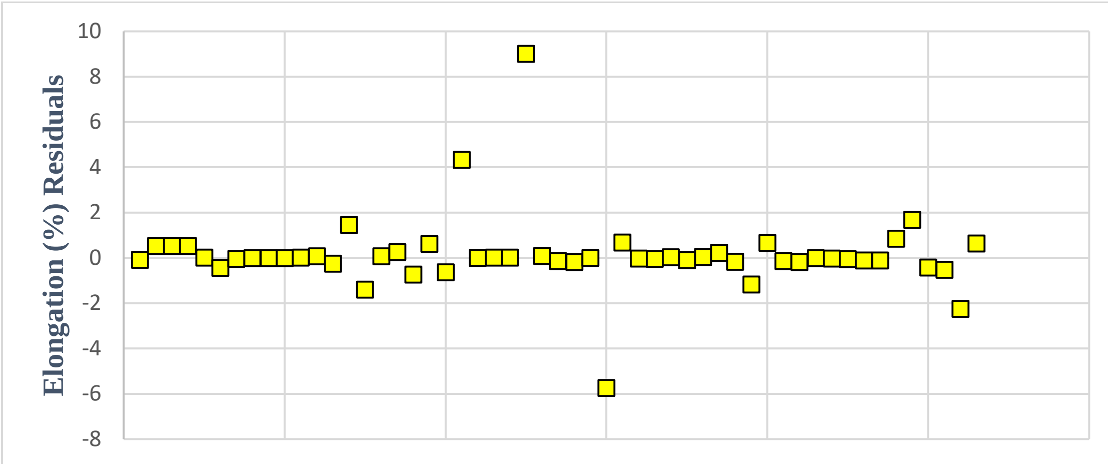

Figure 5. 35 Elongation residuals for the ANN model for SLM fabricated Ti64 alloy

It can be seen from the above analysis that the prediction model for SLM fabricated Ti64 alloy, Model-1, shows very good results and attain an overall R-value of 0.991 for testing the data. The deviations observed from the zero line for all the UTS, YS, and El are minimal and only a few anomalies are observed to get larger deviations. For the UTS, maximum deviation observed was around -200 MPa while most of the deviations averaged round the zero line. Same behavior was observed in the YS data with the largest deviation of about -200 MPa. In the case of elongation, a few cases showed very high deviations (+9%, -6%) while the remaining deviations lied around ±2%.

5.2.2 Fatigue SLM (Model-2)

The fatigue ANN model from SLM fabricated Ti64 alloy was built using 25 datasets from Table 4.2. The correlation value for the experimental output values and the predicted output values can be seen from Figure 5.36 and the individual correlation response of A and B values can be found in Table 5.8.

Table 5. 8 Individual correlation values for fatigue output parameters for SLM fabricated Ti64 alloy

	A	B
Correlation (R)	0.94473	0.9273

Since the model is developed on a heavy architecture of layers and nodes, therefore, formulating and presenting an equation is not easy. The residuals obtained after comparing the predicted and actual experimental values for A and B are shown in Figure 5.37 and Figure 5.38 respectively.

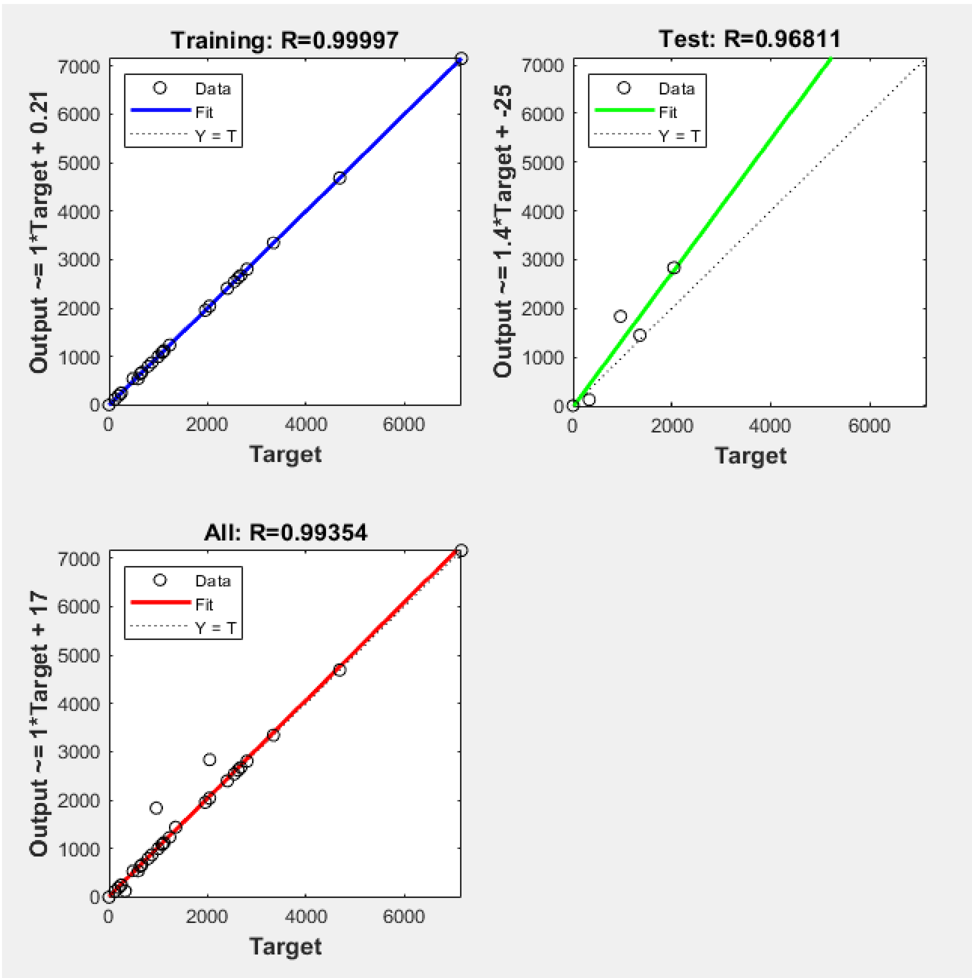

Figure 5. 36 Performance of the ANN model for fatigue behavior of SLM fabricated Ti64 alloy

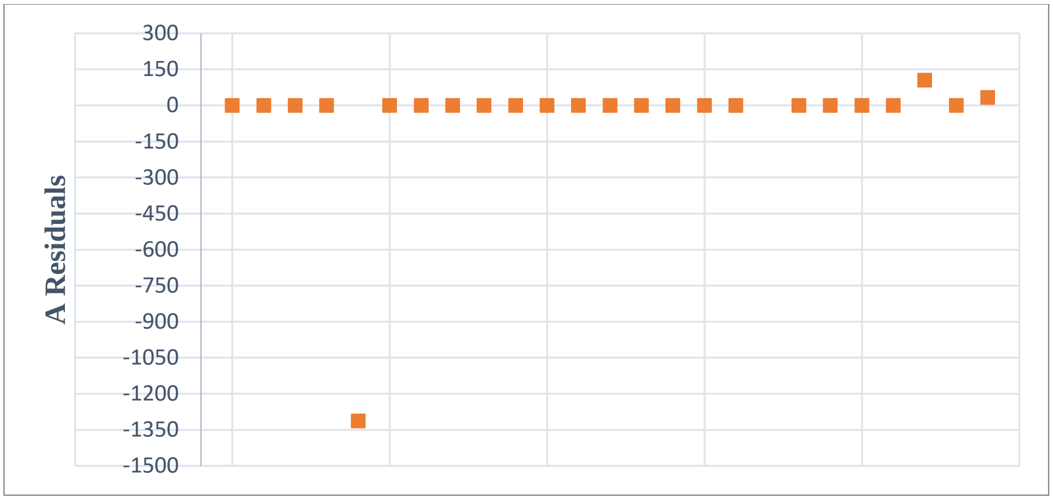

Figure 5. 37 A residuals for the ANN model for SLM fabricated Ti64 alloy

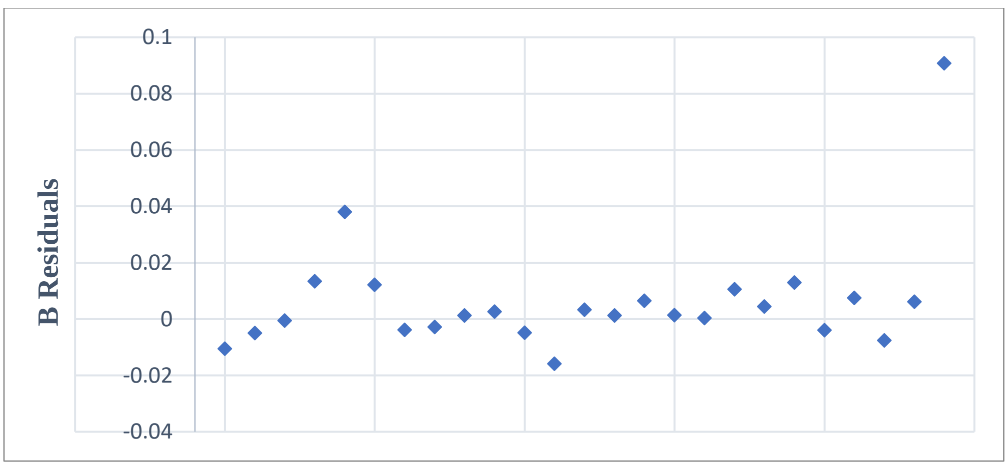

Figure 5. 38 B residuals for the ANN model for SLM fabricated Ti64 alloy

While modeling for the fatigue behavior of SLM fabricated Ti64 alloy, it was noticed that the A value converged around the zero line for most of the observations ($R \approx 0.94$) and similar to the model for tensile behavior, a few observations were deviated. The maximum and only deviation for A value was observed to be around -1300. In the case of B value (R-value ≈ 0.92), the deviation curve was scattered quite evenly in the range of -0.02 to 0.02 which still puts up a window of about -200 MPa to +200 MPa while predicting the S-N curve (considering no deviation in A value). The maximum deviation for B value was recorded to be around +0.09. However, the results developed are far better than those obtained for the multi-regression analysis.

5.2.3 Fatigue EBM (Model-2)

From Table 4.3, 33 datasets, having all the input and output parameter information, were extracted and an ANN model was built on MATLAB using nntool similar to previous cases. The correlation plot obtained after training and testing the model is presented in Figure 5.39 and the individual correlation values for each of the output parameters can be found in Table 5.9.

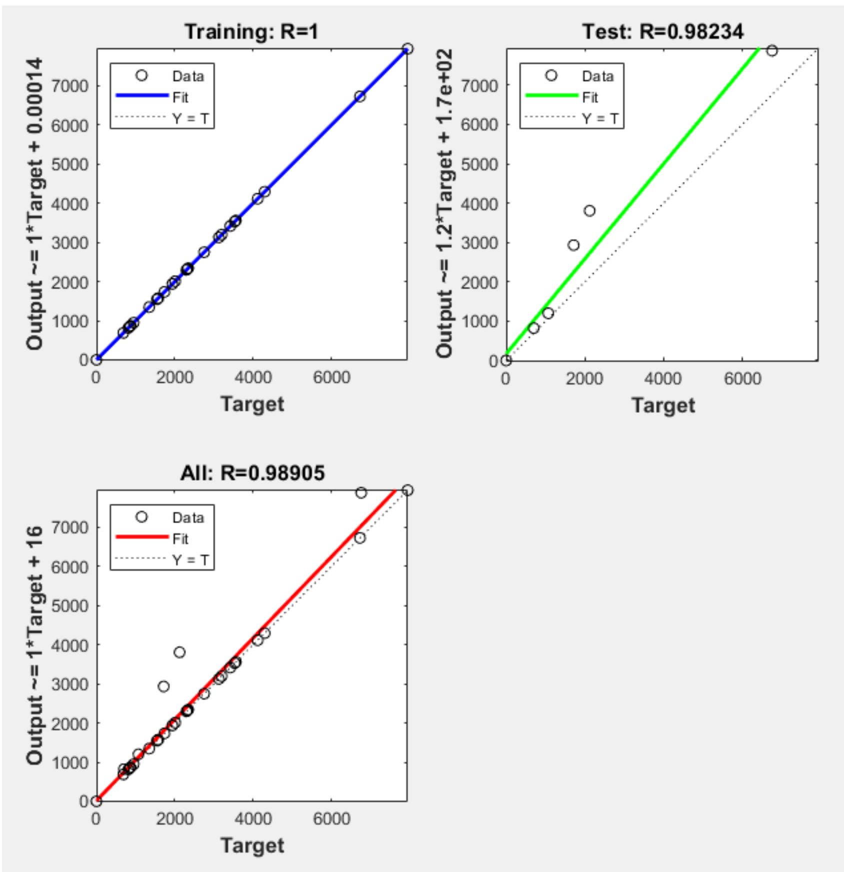

Figure 5. 39 Performance of the ANN model for fatigue behavior of EBM fabricated Ti64 alloy

Table 5. 9 Individual correlation values for fatigue output parameters for EBM fabricated Ti64 alloy

	A	B
Correlation (R)	0.977714	0.968522

The residuals value information for A and B can be seen in Figure 5.40 and Figure 5.41 respectively.

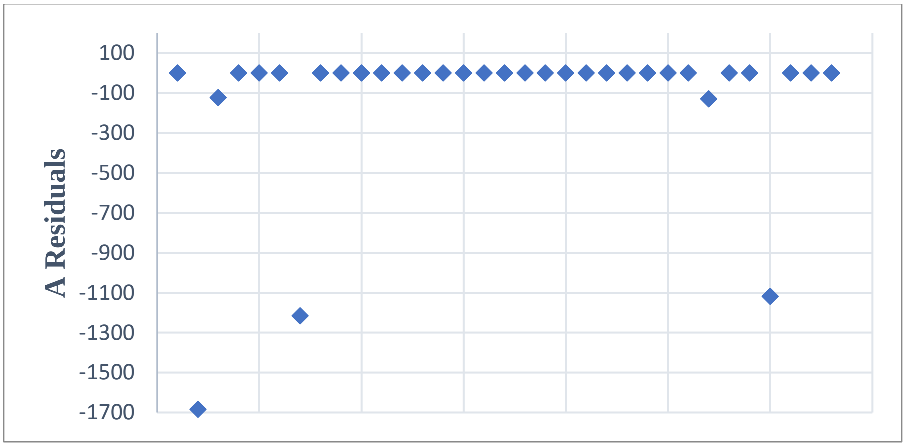

Figure 5. 40 A residuals for the ANN model for EBM fabricated Ti64 alloy

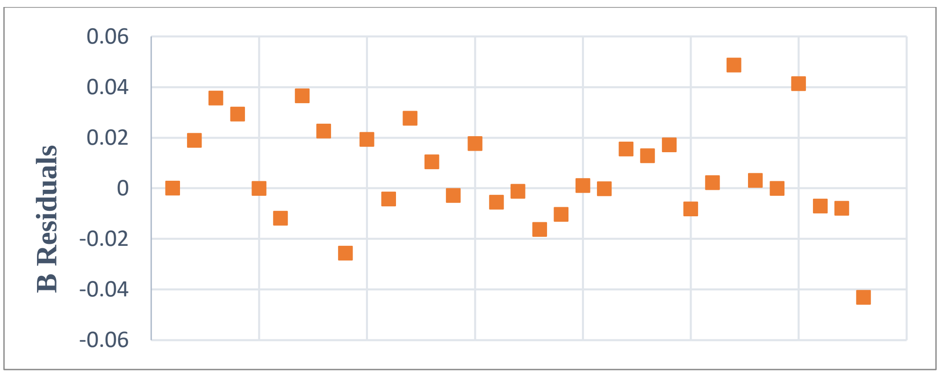

Figure 5. 41 B residuals for the ANN model for EBM fabricated Ti64 alloy

The estimation model of the fatigue behavior of EBM fabricated Ti64 could put up a deviation of ±400 MPa while plotting the S-N curve using the data developed by this model which is evident by the deviation in B value ranging from -0.04 to +0.04 (R ≈0.97) which is better than Model-2 for SLM. The effect of deviation of A value would be close to none as most of the data for estimating A value converged to result in an almost zero deviation (R ≈ 0.98). The largest deviation observed in the estimation model for A was -1700 but only for one case.

5.2.4 Tensile DMLS (Model-1)

A set of 100 data were taken from Table 4.4 and was fed to the nntool in MATLAB. The individual correlation for each of the output values is shown in Table 5.10 and the R curve obtained for the whole model can be seen from Figure 5.42.

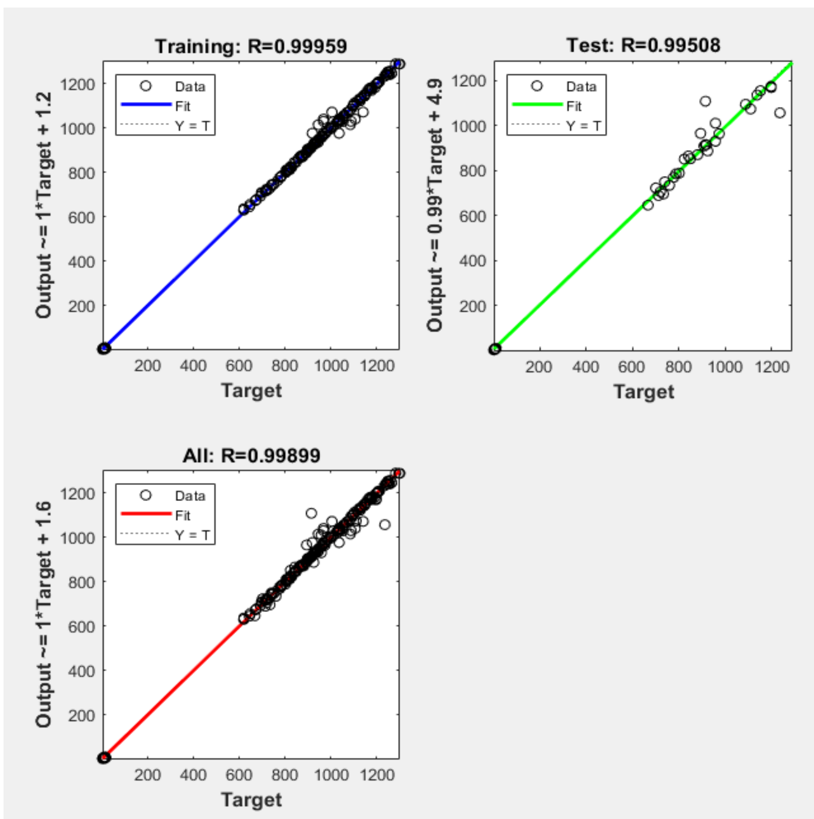

Figure 5. 42 Performance of the ANN model for tensile behavior of DMLS fabricated Ti64 alloy

Table 5. 10 Individual correlation values for tensile output parameters for DMLS fabricated Ti64 alloy

	UTS	YS	El
Correlation (R)	0.96	0.984	0.781

The residuals obtained for UTS, YS, and elongation from the nntool are shown in Figure 5.43, Figure 5.44, and Figure 5.45.

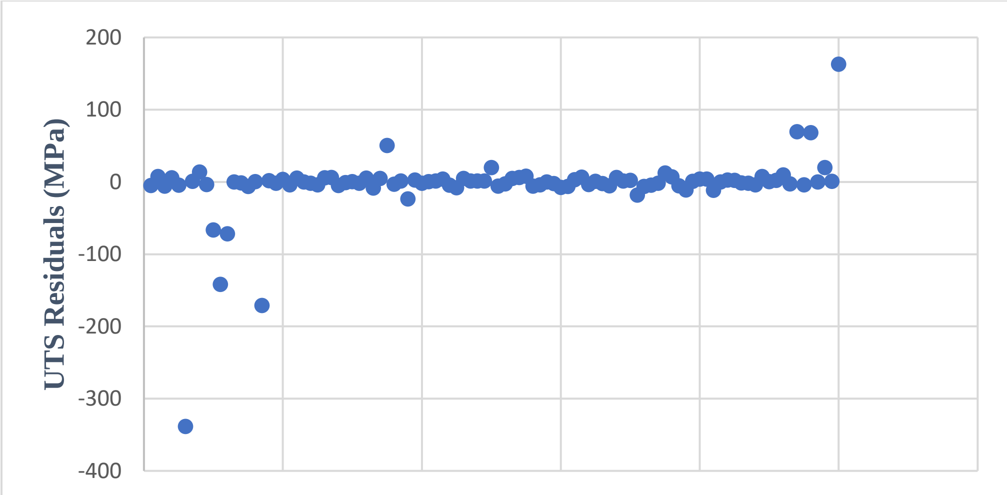

Figure 5. 43 UTS residuals for the ANN model for DMLS fabricated Ti64 alloy

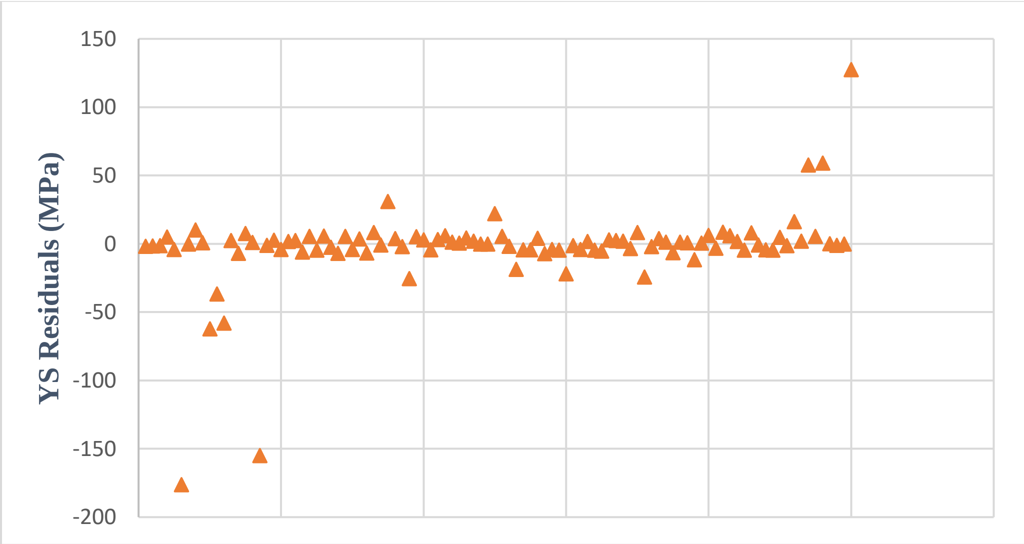

Figure 5. 44 YS residuals for the ANN model for DMLS fabricated Ti64 alloy

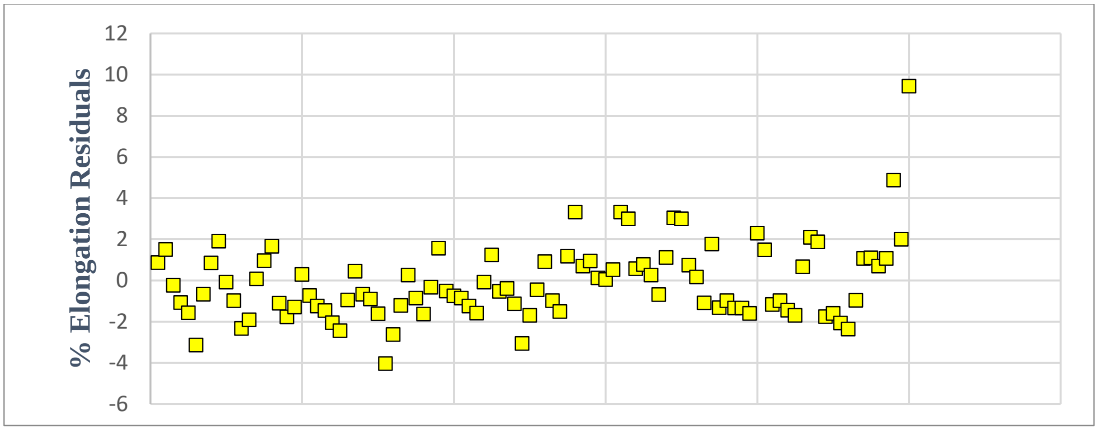

Figure 5. 45 Elongation residuals for the ANN model for DMLS fabricated Ti64 alloy

The tensile behavior prediction model for DMLS, being developed on 100 datasets, resulted in a very efficient model with an overall R-value of 0.995. The individual R-values for the UTS and YS were also close to 0.96 and 0.98 respectively and the maximum deviations observed for each of these were around +120 MPa to -350 MPa and +120 MPa to -200 MPa respectively. However, in the case of elongation, the deviations were scattered evenly around ±3 % with a maximum deviation of above +9% reflected by the R-value of just 0.78.

5.3 Model Analysis

5.3.1 Sensitivity Analysis and Input Parameter Influences for Model-1

From the above results, it is evident that the non-linear ANN model estimates the investigated parameters far better than the multi-regression analysis. The sensitivity analysis is performed to get a measure of uncertainty in the output parameters of a model with respect to the variation in input parameters. A derivative based localized sensitivity analysis is performed for each of the models where the median values of all input data are kept as the local point. Since the minimum to maximum range for each input parameter is very different, z-score normalization is done to achieve a common comparable scale. Results obtained from the sensitivity analysis for Model-1, aiming to estimate the effect of processing parameters on Ti-6Al-4V AM fabrication, are presented in this section followed by the investigation of the impact individual parameters have on the tensile behavior of the alloy. HIPed is not included in this analysis as the data collected discusses HIPed as a discrete input and sensitivity analysis works for continuous parameters.

5.3.1.1 Tensile SLM (Model-1)

As mentioned above, the median values of the data used for making up the model are considered as the local point for performing the sensitivity analysis, see Table 5.11. The variation in the input parameters for performing the sensitivity analysis is +1% and the data obtained for sensitivity analysis can be seen in Table 5.12.

Table 5. 11 Median Values of the data used for developing the SLM Model-1

S Speed (mm/s)	Power (W)	Hatch S (μm)	Layer t (μm)	H Temp (ºC)	H Time (hrs)	UTS (MPa)	YS (MPa)	El (%)
1200	200	100	30	650	3	1244.19	1142.27	4.952

Table 5. 12 Median based +1% variation in each input parameter for sensitivity analysis for SLM

	S Speed (mm/s)	Power (W)	Hatch S (μm)	Layer t (μm)	H Temp (ºC)	H Time (hrs)	UTS (MPa)	YS (MPa)	El (%)
Median	1200	200	100	30	650	3	1263.1	1160.0	7.46
S Speed	1212	200	100	30	650	3	1260.2	1159.5	7.49
Power	1200	202	100	30	650	3	1264.6	1160.5	7.43
Hatch S	1200	200	101	30	650	3	1263.2	1160.0	7.47
Layer t	1200	200	100	30.3	650	3	1262.3	1159.7	7.39
H Temp	1200	200	100	30	656.5	3	1261.4	1159.3	7.54
H Time	1200	200	100	30	650	3.03	1263.5	1160.2	7.42

Table 5. 13 Normalized results for data in Table 5.12

	S Speed	Power	Hatch S	Layer t	H Temp	H Time	UTS	YS	El
Median	-0.378	-0.378	-0.378	-0.378	-0.378	-0.378	0.325	0.274	0.044
S Speed	2.268	-0.378	-0.378	-0.378	-0.378	-0.378	-1.674	-0.998	0.722
Power	-0.378	2.268	-0.378	-0.378	-0.378	-0.378	1.348	1.508	-0.636
Hatch S	-0.378	-0.378	2.268	-0.378	-0.378	-0.378	0.399	0.388	0.295
Layer t	-0.378	-0.378	-0.378	2.268	-0.378	-0.378	-0.173	-0.411	-1.351
Temp	-0.378	-0.378	-0.378	-0.378	2.268	-0.378	-0.840	-1.392	1.632
Time	-0.378	-0.378	-0.378	-0.378	-0.378	2.268	0.615	0.631	-0.706

Table 5. 14 Results for the sensitivity analysis on the data presented for SLM Model-1

	S_UTS	S_YS	S_El
Scan speed	-0.75583	-0.48079	0.256275
Laser power	0.386528	0.466273	-0.25674
Hatch spacing	0.027754	0.043056	0.095059
Layer t	-0.18833	-0.25917	-0.52696
Heat temp	-0.4406	-0.62978	0.600369
Heat time	0.10949	0.134738	-0.28334

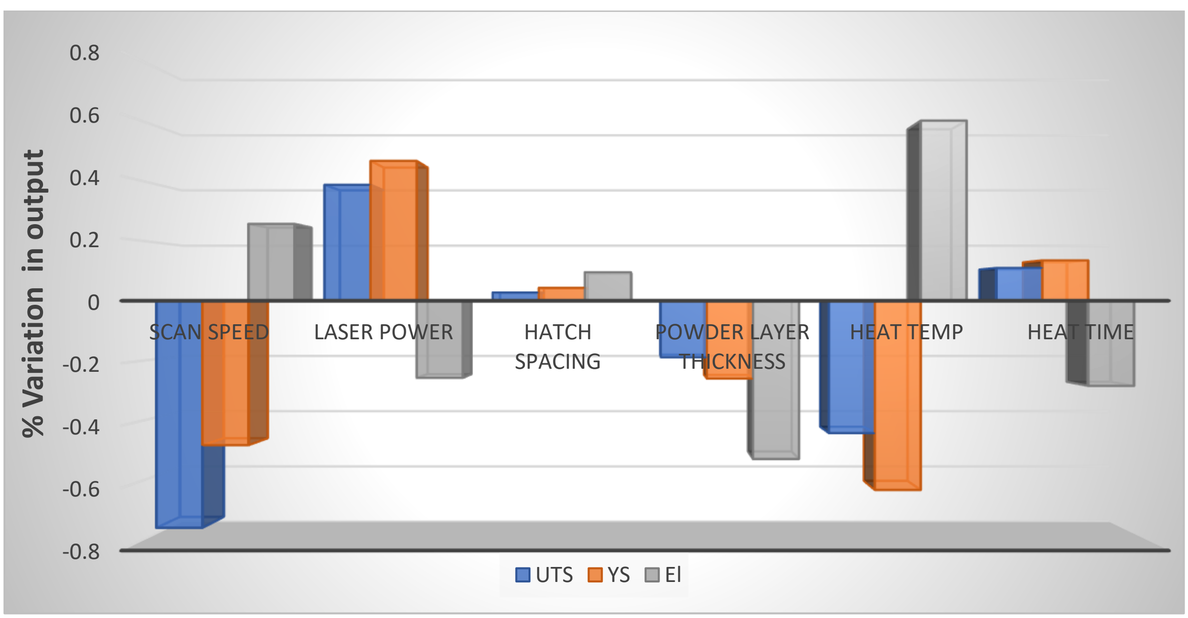

Figure 5. 46 Sensitivity analysis for +1% variation from median values for SLM Model-1

Table 5.13 shows the z-score normalized data for the data presented in Table 5.12 while Table 5.14 presents the results for the sensitivity calculation. The results obtained from the sensitivity analysis can be understood as +1% change in the input parameter is seen to be causing 'x' % variation in the output parameters where 'x' represents the values obtained in Table 5.14. These relationships are pictographically presented in Figure 5.46.

Observations from the local sensitivity analysis at the median parameters:

- Scan speed and laser power seem to be having an inverse relation to each other. A positive variation in scan speed accounts for a decrease in the strength compensated by an increased elongation, whereas, a positive variation in laser power results in increased strength on the account of decreased elongation.
- Similarly, hatch spacing, and powder layer thickness have an inverse relationship with each other at the median value of the collected data. An increase in the hatch spacing leads to an increase in all the output parameters but this trend seemed to be reversed in case of powder layer thickness. However, a 1% variation in hatch spacing leads to a mere 0.03-0.09 % variation in the output values which accounts for the minimum impact out of all the parameters discussed. In the closer analysis, discussed later, it can be seen that this small positive trend at the median value is almost equivalent to a constant trend which after a few positive units seems to follow a similar trend as powder layer thickness shows.
- Increasing heating temperature for the heat treatment process causes a reduction in the strength well compensated by an increased elongation while an advance in heat time is reflected as an increase in the strength at an expense of elongation.

These trends are localized, and the complete input parameter profile doesn't need to behave the same way it did at the median of the data. To understand the impact of each of the input parameters at an extended range, plots are developed showing the behavior of the tensile properties for the minimum to the maximum range of variation in individual input parameters whilst keeping the others at the median value. The following section discusses the results obtained for these individual process parameters.

<u>Scan speed:</u>

In the case of low scan speeds, the powder gets completely melted resulting in a stable concentrated melt pool which leads to a reduction in porosity and internal defect during the fabrication. At higher scan speeds, the melt pool has low concentration and is unstable which causes the lack of fusion defects, in turn, leading to internal cavities and the material becomes porous, therefore, the strength also decreases. In absence of any major microstructural changes, which occur in heat treatment, the loss of strength is generally resultant of an increased elongation.

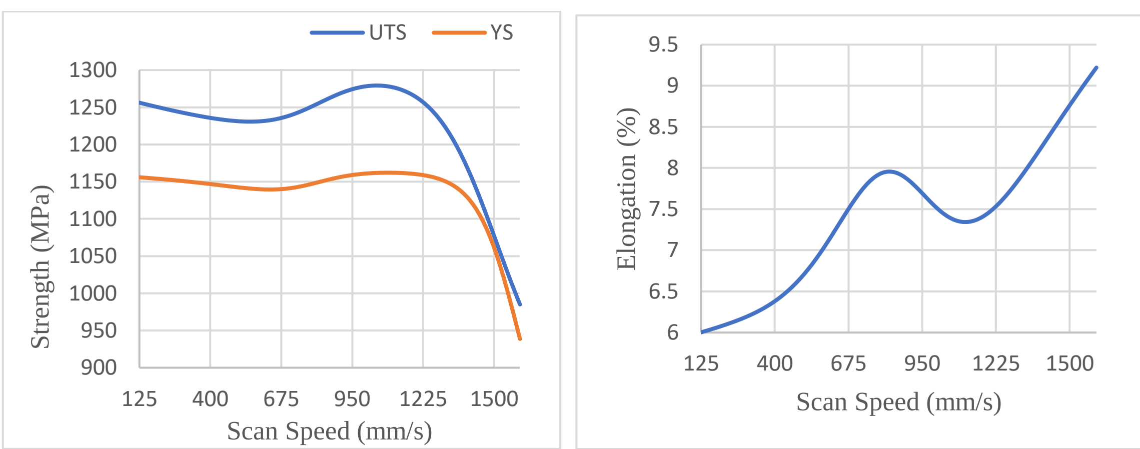

Figure 5. 47 Tensile behavior prediction vs scan speed by Model-1 for SLM

Similar trends can be seen in the plot generated by the ANN model for the scan speed parametric study of SLM fabricated Ti64 and are presented in Figure 5.47. The dips shown in the plots in the middle region could either be a model generated defect or an estimation of a sample that has an internal defect unknown without CT scan images, in either case, it is unexplanatory at this stage.

Power:

Laser power has a direct relation with the strength which is backed by the fact that an increase in laser power ensures proper melting which results in minimal porosity. This behavior can also be observed from the model output presented in Figure 5.48 where at lower power values, the strength of Ti64 is lower than the strength at higher power values. Following the general trend, elongation behaved inversely to the behavior of strength.

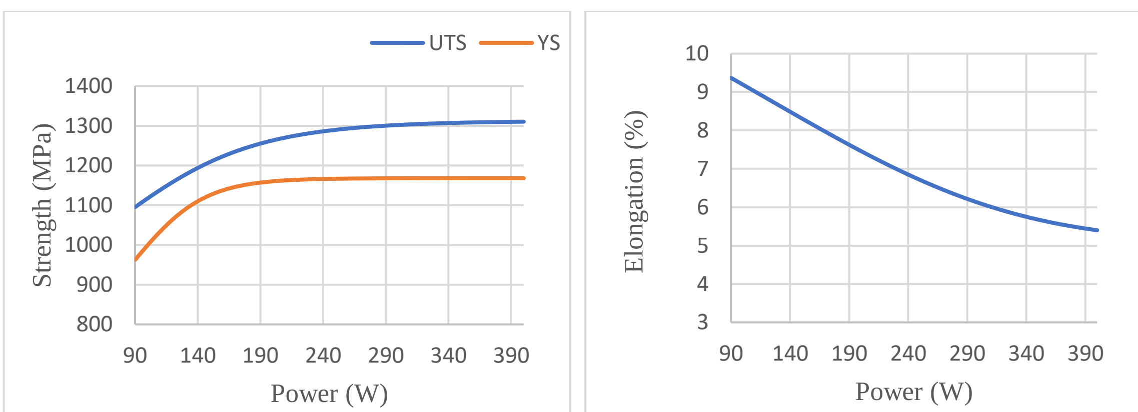

Figure 5. 48 Tensile behavior prediction vs laser power by Model-1 for SLM

Hatch Spacing:

The hatch spacing determines, how far the new round of scan begins from the previous round in the same layer. This spacing is advisable to have around half the size of the beam spot diameter because an efficient overlap between consecutive scans leads to a strong and stable melt pool. An increase in the hatch spacing beyond a certain value leads to an improper fusion of the powder in consecutive scans and generates the lack of fusion defects within the fabrication, therefore, leading to increased porosity causing a reduction in the strength. A higher value of hatch spacing demands more energy expenditure as the number of scans per layer increase however, this ensures proper melting of powder and leads to a high strength alloy. Figure 5.49 shows the predicted behavior of hatch spacing with the strength of alloy which can be comfortably backed up by the physics of hatch spacing explained above. The elongation was observed to dip in the region of a slight positive gradient for the strength behavior but as soon as the negative gradient was reached for strength, the elongation started increasing.

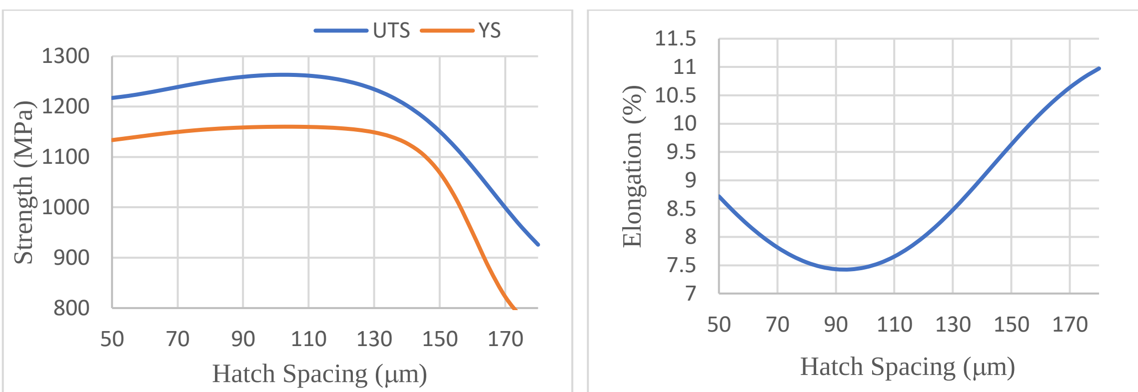

Figure 5. 49 Tensile behavior prediction vs hatch spacing by Model-1 for SLM

<u>Powder layer thickness:</u>

Powder layer thickness plays an inverse relation to the overall energy being imparted to the melt pool. An increased powder layer thickness demands more power input to perform the proper melting of the layer in each scan. For the same power, increasing the layer thickness would cause improper melting of the powder leading to a porous fabrication after solidification which would have a lower strength. On the other hand, if the layer thickness is low enough for the laser power to cause excessive penetration, keyhole pores would be generated again leading to a reduction in strength. A similar trend can also be seen in the strength vs layer thickness plot presented in Figure 5.50 where an increased powder layer thickness resulted in a decreased strength value compensating the increase in the elongation when the remaining process parameters were kept constant.

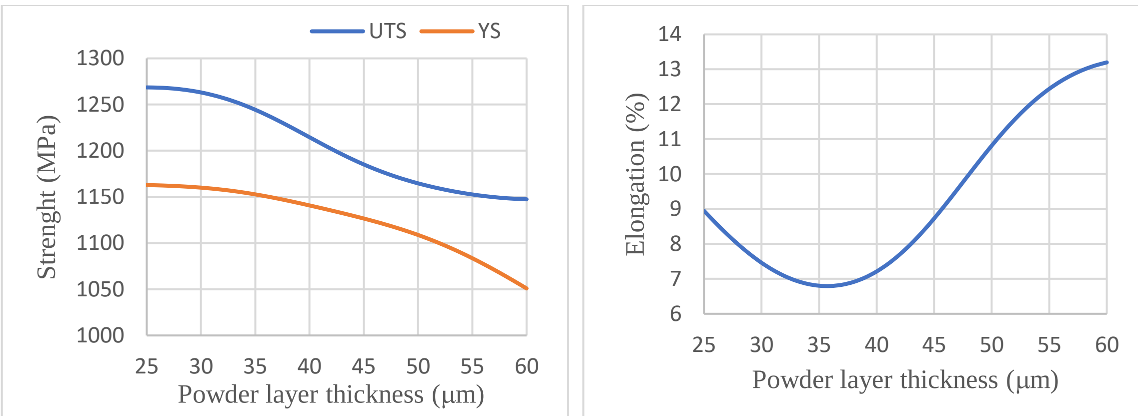

Figure 5. 50 Tensile behavior prediction vs powder layer thickness by Model-1 for SLM

<u>Heat Temperature and Heat Time:</u>

Heat temperature and time are more related to the development of an altered microstructure. The general stress-relieving process for Ti64 alloy is carried out at 650 °C for 4 hours. This heat treatment leads to the formation of larger microstructural grains of the alloy which leads to a reduction in the strength with a consequent increase in the elongation. The solution treatment, quenching, tempering, normalizing are different types of heat treatments that have their separate applications and effects on the microstructure of the grains of an alloy. These heat treatments are also accompanied by multiple parameters like the medium of heating, the medium of cooling (air-quenched, water-quenched, furnace cooling), and in a few cases, if reheating or step heating/cooling is done then the additional parameters related to those processes. This model only utilized heat temperature and heat time as the input parameters, restricted by the data available in the open literature. Also, the application of the compensating set used in this study could have developed a piece of additional information for the model which cannot replicate an actual condition for the as-fabricated alloy. Proper heat treatment leads to increased elongation and generally, this happens after heating the alloy to a certain temperature where the microstructure starts getting altered (alpha+beta phase field) and then cooled in a controlled environment. Plots presented in Figure 5.51 show similar behavior for the strength and elongation as supported by the general heat treatment procedures.

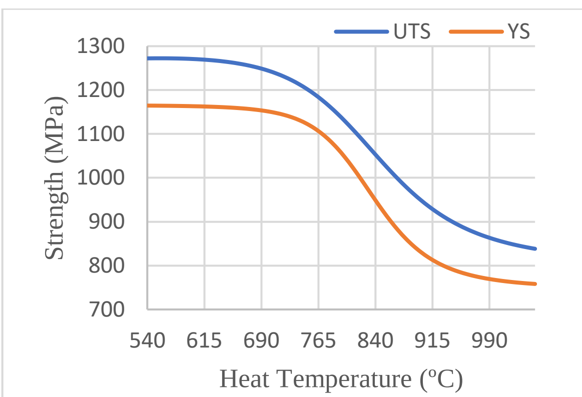

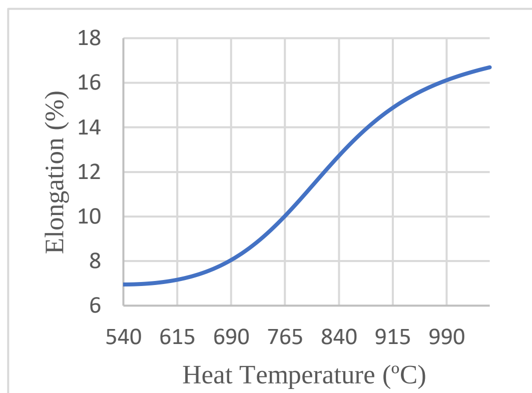

Figure 5. 51 Tensile behavior prediction vs heat temperature by Model-1 for SLM

As far as heating temperature is concerned, the model developed plots for a positive variation of heat time lead to a decline in both the strength and the elongation of the alloy which can be seen from Figure 5.52. Keeping in mind the median values for this analysis takes 650 °C as the median temperature where usually the stress-relieving process for Ti64 is operated. The relationship presented above cannot be explained at this stage as it could either be because of a microstructural variation or an internal unknown defect generated in the sample or a model generated anomaly because of the compensation sets which are given as 3-hour compensating time to fit the as-fabricated samples in the same bracket as heat-treated samples.

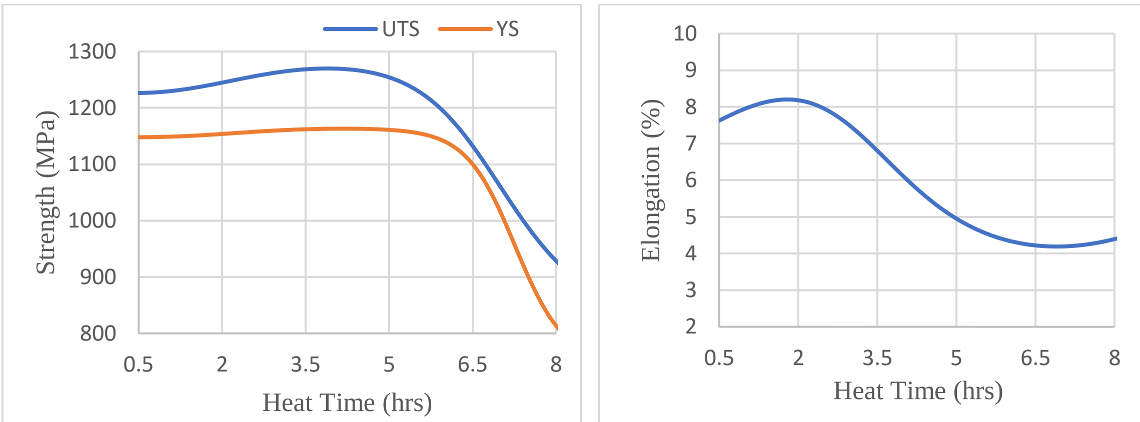

Figure 5. 52 Tensile behavior prediction vs heat time by Model-1 for SLM

5.3.1.2 Tensile DMLS (Model-1)

Similar to the analysis presented for SLM based Model-1, sensitivity analysis is performed for the Model-1 data for DMLS. The median values for the DMLS data used to build the model can be seen in Table 5.15 while Table 5.16 shows the input parameters with +1% variation to the median values which are used as the database for sensitivity analysis.

Table 5. 15 Median Values of the data used for developing the DMLS Model-1

S Speed (mm/s)	Power (W)	Hatch S (µm)	Layer t (µm)	H Temp (ºC)	H Time (hrs)	UTS (MPa)	YS (MPa)	El (%)
900	170	100	30	750	2	923.645	812.177	5.369

Similar to SLM, the +1% variated parameters presented in Table 5.16 are converted to the normalized data before performing the sensitivity calculations. The normalized data can be seen in Table 5.17 and the results of sensitivity analysis are available at Table 5.18

Table 5. 16 Median based +1% variation in each input parameter for sensitivity analysis for DMLS

	S Speed (mm/s)	Power (W)	Hatch S (µm)	Layer t (µm)	H Temp (ºC)	H Time (hrs)	UTS (MPa)	YS (MPa)	El (%)
Median	900	170	100	30	750	2	925.4	810.9	5.06
S Speed	909	170	100	30	750	2	924.1	808.6	5.02
Power	900	171.7	100	30	750	2	929.1	815.2	5.12
Hatch S	900	170	101	30	750	2	917.8	799.3	5.09
Layer t	900	170	100	30.3	750	2	924.0	808.5	5.07
H Temp	900	170	100	30	757.5	2	918.4	801.7	5.16
H Time	900	170	100	30	750	2.02	925.3	810.4	5.06

Table 5. 17 Normalized results for data in Table 5.16

	S Speed	Power	Hatch S	Layer t	H Temp	H Time	UTS	YS	El
Median	-0.378	-0.378	-0.378	-0.378	-0.378	-0.378	0.496	0.560	-0.449
S Speed	2.268	-0.378	-0.378	-0.378	-0.378	-0.378	0.160	0.137	-1.414
Power	-0.378	2.268	-0.378	-0.378	-0.378	-0.378	1.399	1.348	0.768
Hatch S	-0.378	-0.378	2.268	-0.378	-0.378	-0.378	-1.403	-1.543	0.165
Layer t	-0.378	-0.378	-0.378	2.268	-0.378	-0.378	0.130	0.137	-0.330
Temp	-0.378	-0.378	-0.378	-0.378	2.268	-0.378	-1.252	-1.109	1.698
Time	-0.378	-0.378	-0.378	-0.378	-0.378	2.268	0.469	0.470	-0.437

Table 5. 18 Results for the sensitivity analysis on the data presented for DMLS Model-1

	S_UTS	S_YS	S_El
Scan speed	-0.12719	-0.15974	-0.36472
Laser power	0.341355	0.297998	0.459948
Hatch spacing	-0.71766	-0.79486	0.23215
Layer t	-0.13835	-0.15999	0.045066
Heat temp	-0.66055	-0.63061	0.811413
Heat time	-0.01029	-0.03394	0.004587

Summary of the localized sensitivity analysis for +1% variation at the median value for DMLS Model-1, pictographically presented in Figure 5.53, can be understood as follows:

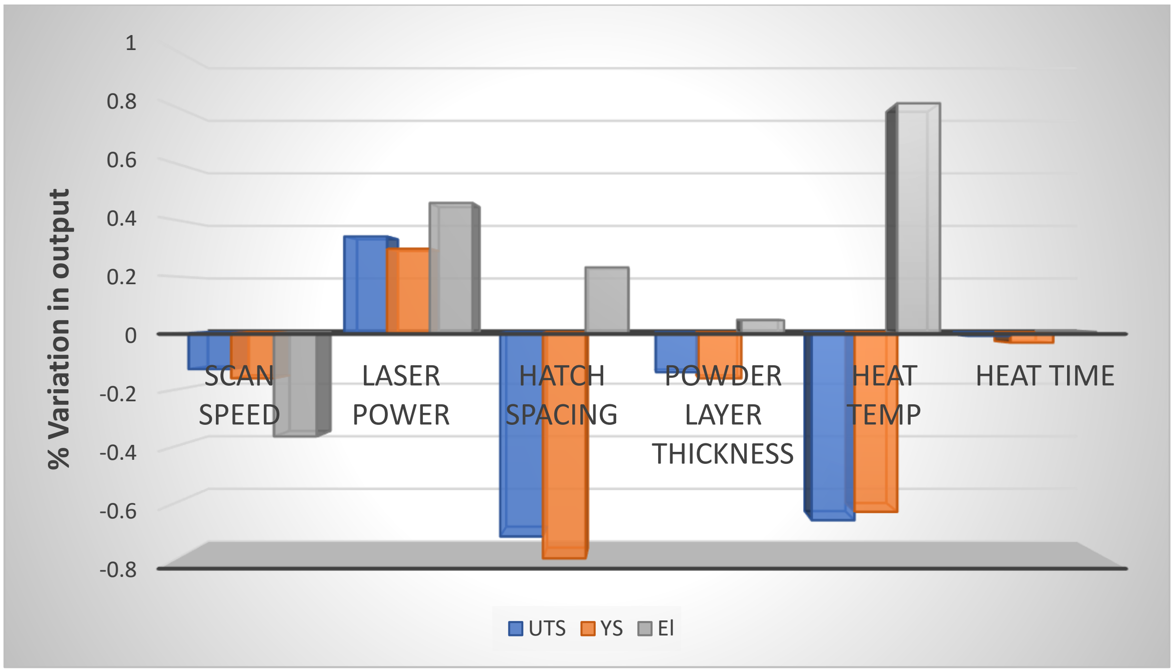

Figure 5. 53 Sensitivity analysis for +1% variation from median values for DMLS Model-1

- Laser power follows a direct relation to all the material properties whereas, the scan speed shows completely inverse trends to the laser power indicating a strong dependence on the ratio of scan speed and laser power for a DMLS fabricated Ti64 alloy
- The hatch spacing behaves closely similar to the powder layer thickness showing a positive result for the elongation and a negative result for the strength, however, the impact of hatch variation is more significant than the layer thickness.
- Heat temperature and heat time also follow similar trends to the hatch spacing and layer thickness leading to a decline in strength and an increase in elongation for +1%

variation from the median values. The effect of heat temperature is more prominent on both the strength and elongation, whereas, heat time seems to have almost negligible variation in the output parameters.

To understand the extent of the behavior of tensile properties predicted by the model, an extended analysis of each of the input parameters is done with the strength and elongation keeping the remaining parameters constant at the median values. The results obtained from the analysis are discussed in the section below:

<u>Scan Speed:</u>

Figure 5.54 presents the results obtained from the ANN tensile model for the behavior of scan speed with the tensile properties of DMLS fabricated Ti64 for the remaining constant median values. The strength attains a maximum value for medium-range scan speeds from 500 mm/s to 600 mm/s. At very low scan speeds for DMLS, the strength is somewhat smaller which could be explained by the formation of keyhole defects due to excess melting of powder. For higher scan speeds, the strength drops below 900 MPa as a suspected result of the lack of fusion defects.

The elongation plot presented in Figure 5.54 behaves differently than the usual elongation trend of generating a positive variation in elongation for a decline in strength. Reasons for this behavior is not clear. One hypothesis is that the increased speed will introduce lack of fusion defect and both strength and ductility will reduce due to increased defect density. This hypothesis cannot be validated using the collected data and need detailed microstructure imaging observations.

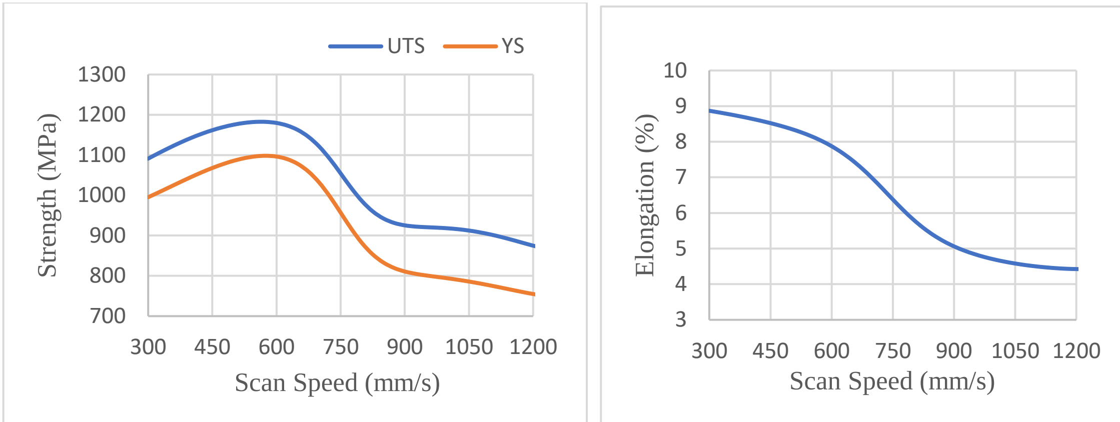

Figure 5. 54 Tensile behavior prediction vs scan speed by Model-1 for DMLS

Power:

As explained in section 5.3.1.1, the power trends shown in Figure 5.55 can be completely backed by the physics of power influence on laser fabrication. The maximum strength was obtained in the power range of 210 W to 240 W when the remaining median parameters were kept constant. This behavior is supported by the general physics for melting using the laser. At very low power values, the powder material gets insufficient heat input and is unable to completely melt the material which leads to a high porosity fabrication, in turn, resulting in a decline in the strength. However, increasing the power too much also leads to a decline in the strength of the alloy which is caused by the development of extra internal stress concentration sites in the form of keyhole pores due to excessive energy being imparted to melt the powder.

The behavior of elongation with power variation presented in Figure 5.55 also suggests that the defect mechanism is dominating in the strength and ductility trend. It is well known that the strength increase will usually accompany with ductility loss. This is in general agreement with the grain structure characteristics. For example, increased grain size during the heat treatment will cause the grain size increases and the strength will decrease with increased ductility. If both strength and ductility show the same trend, it indicates the major mechanism is the defect. If defect density increases/decreases, both strength and ductility will decrease/increases.

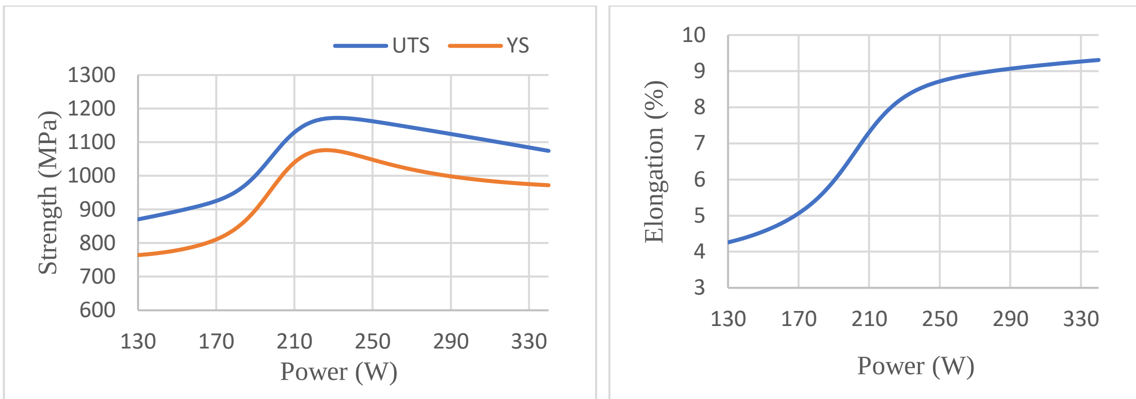

Figure 5. 55 Tensile behavior prediction vs laser power by Model-1 for DMLS

<u>Hatch Spacing:</u>

The results obtained for variation in hatch spacing from the ANN model are shown in Figure 5.56 where the strength almost showed a linearly inverse relationship to the hatch spacing for the range in which model could have best predicted the trend keeping the remaining parameters constant. The elongation showed an inverse relation to the strength as a drop in the strength was compensated with an increase in the elongation and vice versa.

This plot behavior cannot be considered as the ideal behavior of the strength and elongation for DMLS process with the hatch spacing because the model is built on 90 % hatch spacing values of 100 μm and a few 120 μm values but it can essentially be said that the increment in hatch spacing results in an increment in elongation and a decrement of the strength.

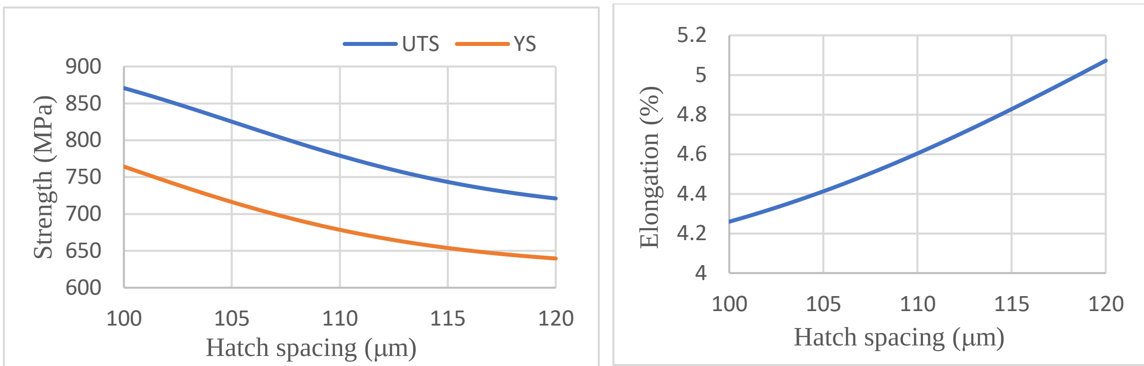

Figure 5. 56 Tensile behavior prediction vs hatch spacing by Model-1 for DMLS

<u>Powder layer thickness:</u>

Similar to the trend shown by the hatch spacing, the powder layer thickness was almost linearly inverse to the strength of the alloy, and the elongation was again compensated positively for a negative variation in the strength, see Figure 5.57.

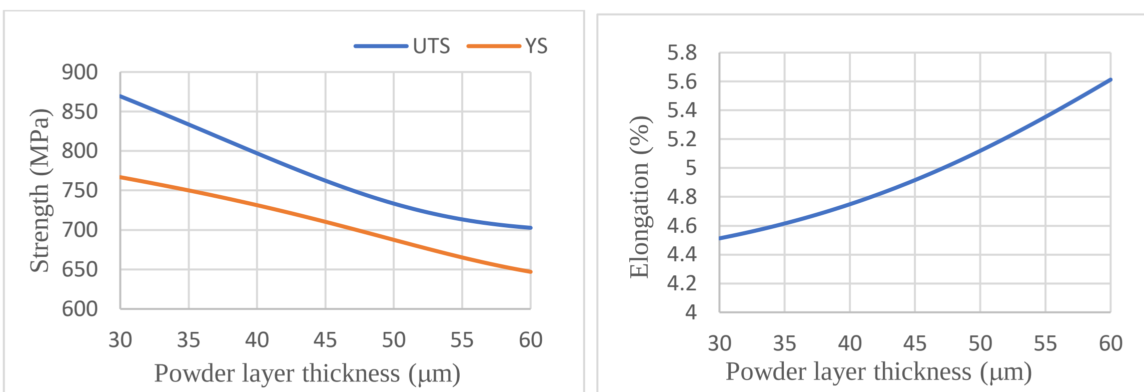

Figure 5. 57 Tensile behavior prediction vs powder layer thickness by Model-1 for DMLS

Again, similar to the case for the hatch spacing, the model is mostly built on a powder layer thickness of 30 μm and a few cases of 60 μm, therefore, valuable information for the trend of powder layer thickness with the strength and elongation is still missing but an increase in the layer thickness reduces the strength and increases the elongation of the fabrication.

Heat Temperature and Heat Time:

The results obtained from the heat temperature variation against the tensile behavior of DMLS fabricated Ti64 are shown in Figure 5.58 where it can be seen that the trends for strength and elongation are quite similar to those observed for SLM heat temperature variation. A decline in strength was obtained above and around the alpha+beta phase field heating which was naturally compensated by an increase in the elongation. Heat time showed an inverse relationship with the strength and direct relation with the elongation which is quite different than SLM heat time behavior.

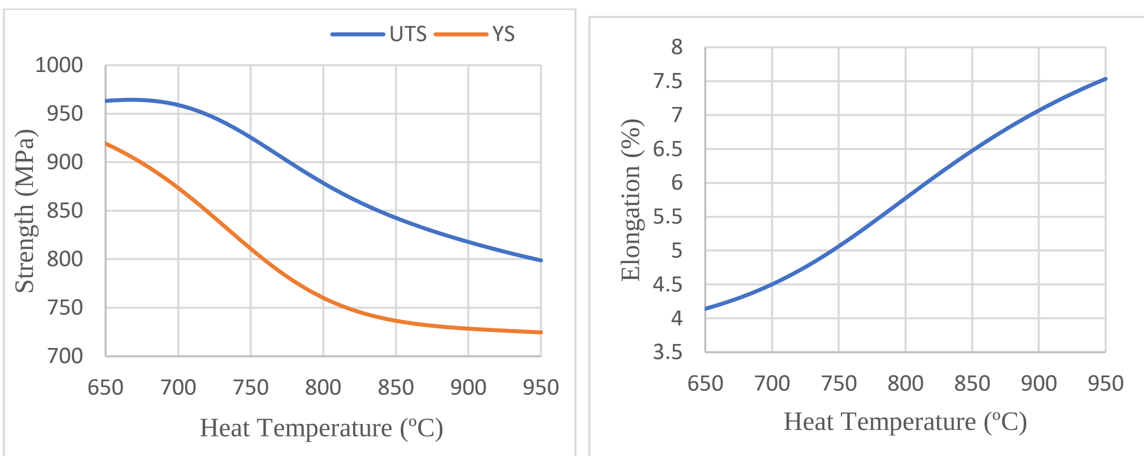

Figure 5. 58 Tensile behavior prediction vs heat temperature by Model-1 for DMLS

Figure 5.59 shows the variation occurred in the tensile properties for the minimum to the maximum range of heat time when the remaining process parameters were kept constant at the median values. A decline in the strength was compensated by an increment in the elongation however, the trend observed for these variations is quite different than the ones obtained for heat time variation with the SLM process.

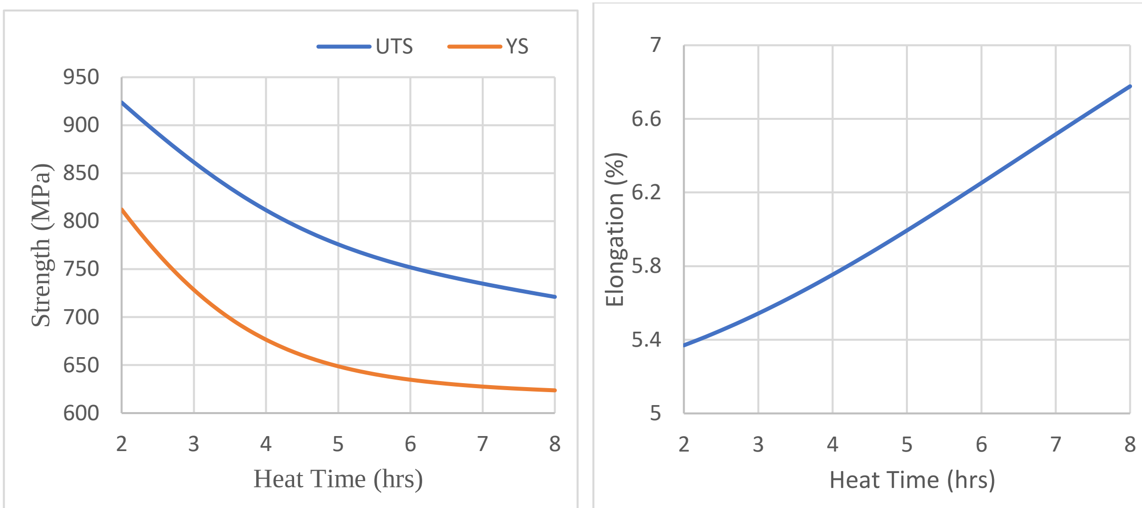

Figure 5. 59 Tensile behavior prediction vs heat time by Model-1 for DMLS

5.3.2 Fatigue Life Factor Analysis for Model-2

As mentioned earlier, the sensitivity analysis is performed to understand the impact of a continuous parameter on the output parameters of a model. In the case of the fatigue models, the absence of sufficient data makes up the input parameters close to discrete data sets, and therefore to analyze the fatigue model efficiency, instead of a sensitivity analysis, a fatigue life factor analysis is carried out. Fatigue life factor is the ratio of the predicted number of cycles to the actual number of cycles. A fatigue life factor of 2 is detrimental to an excellent prediction while a factor of 3 accounts for a good prediction. In the following section, logarithmic values of the actual vs predicted number of cycles are plotted.

5.3.2.1 Fatigue SLM (Model-2)

Figure 5.60 shows the predicted fatigue life values obtained from the estimated model in regard to the actual fatigue life of SLM fabricated Ti64. The blue dotted line represents a 100% accurate prediction while the yellow band declares the fatigue life factor of 2 expressing an excellent prediction up to a 50% variation in estimating failure cycles. The orange and red bands are life factors of 5 and 15.

Table 5. 19 Percentage allocation of the prediction cycles in fatigue life factor bands for SLM

Life factor band	Predicted values (%)
2	18.7
5	58.9
15	75.9
Outside	24.1

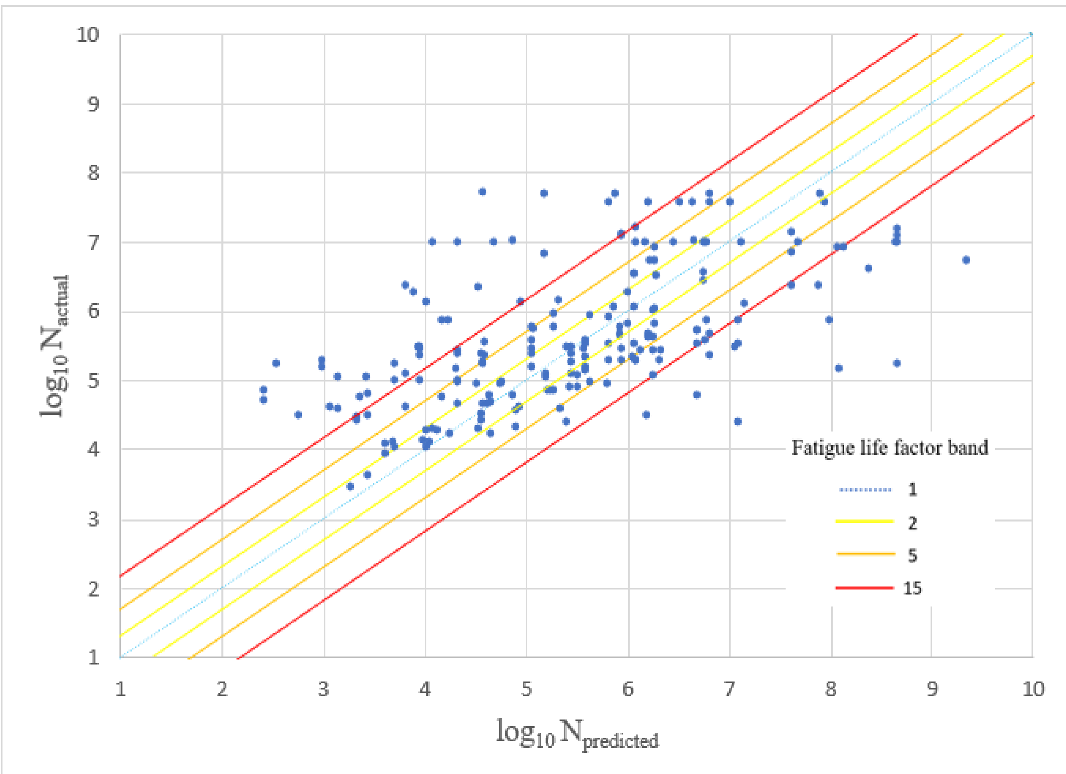

Figure 5. 60 Actual vs predicted life cycles for fatigue model of SLM

Table 5.19 shows the percentage of the prediction cycles in each of the fatigue life factor band. Only 18.7% of the predicted fatigue cycle values fall under the excellent prediction band and ever for a fatigue life factor of 15, only 75.9% predicted cycle values come under the umbrella. The trained model individual R-values, in this case, were 0.94 and 0.92 for A and B respectively. Possible explanations to the scattered trends in Figure 5.60 are explained at the end of this section.

5.3.2.2 Fatigue EBM (Model-2)

Fatigue life factor analysis is also performed for EBM based model. The results of each of the S-N datasets available are plotted in Figure 5.61. The life factor bands of 2, 5, and 15 are shown in yellow, orange, and red colors similar to the ones in SLM fatigue life analysis plots. Table 5.20 shows the percentage of the predicted cycles in each of the fatigue life factor bands.

Table 5. 20 Percentage allocation of the prediction cycles in fatigue life factor bands for DMLS

Life factor band	Predicted values (%)
2	32.7
5	60.2
15	76.3
Outside	23.7

It can be seen that for EBM fatigue estimations, the predicted number of cycles fall fairly away from the excellent prediction regime. A 32.7% population was recorded to be under the excellent prediction regime which is certainly higher than the same for the SLM based Model-2. Nearly 60% of the predictions fall under the fatigue life factor of 5 while almost 24% datasets were a part of outside a life factor of 15 band. The recorded R-value for the EBM based Model-2 was nearly 0.97 for both the A and B values even so the scatter in the predicted values and actual values are easily noticeable.

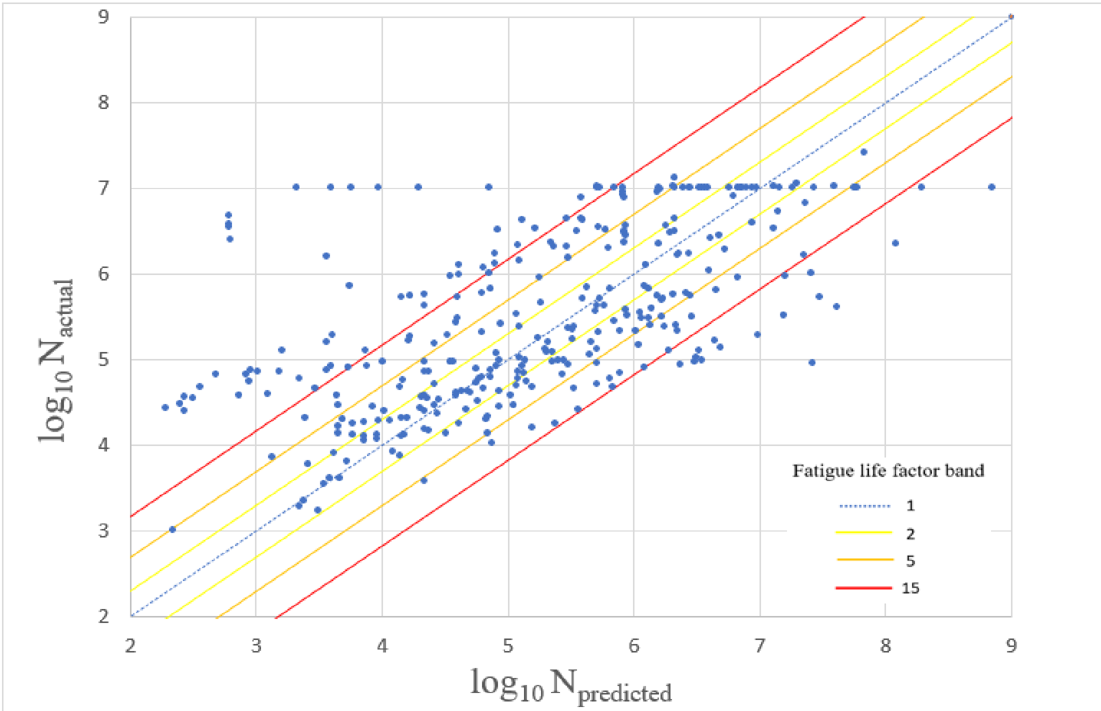

Figure 5. 61 Actual vs predicted life cycles for fatigue model of DMLS

<u>Possible explanations of the scattered behavior of the fatigue analysis plots:</u>

Supported by the high R-values is the fact that the model predicted somewhat accurate values to what was fed as a target parameter to it. However, the target parameters are determined by a power-law estimation of the fatigue S-N curves. This estimation does not necessarily follow through each of the S-N points but is an estimation such that the deviation from each of the points is minimum. Now the fatigue estimation models are developed after considering the A and B values as the target value. The predictions made by the model result in a very close estimation of these A and B values, but the target values are not the accurate data values for the S-N curve and therefore an R value of 1 would also lead to major deviations in the fatigue life factor analysis. To get a better estimation from the model, a target value that satisfies the actual experimental outputs is required.

As mentioned earlier a variation as minimum as 0.02 units in the B value is an equivalent of creating a variation of 200 MPa in the corresponding ‘stress’ value considering the A value is same and this, in turn, leads to huge deviations for a ‘cycle’ value and that adds up to another reason for the deviations.

CHAPTER – 6

CONCLUSIONS AND FUTURE WORKS

6.1 Conclusion

The work reported in this thesis focuses on the estimation of mechanical properties of additively manufactured Ti-6Al-4V through different AM processes such as SLM, EBM, and DMLS. Due to constraints of availability of data in the open domain, two models have been proposed for the estimation of output parameters. Model-1 estimates the Ultimate Tensile Strength (UTS), Yield Strength (YS), and Elongation (El) from the identified process parameters for a specific AM process, whereas Model-2 determines Fatigue strength from input variables viz. UTS, YS, and El, etc.

Due to the insufficiency of data satisfying the input and output parameters considered in this study, Model-1 for the EBM process and Model-2 for the DMLS process could not be developed.

The prediction has subsequently been carried out through two different models. One is based on linear multi regression analysis and the other is based on non-linear Artificial Neural Network (ANN). The multi-regression analysis was tried, however, the correlations obtained for those fits weren't accurate enough to declare a definite linear relationship of process parameters and tensile behavior of Ti64 alloy. ANN-based model, on the other hand, shows better performance in the current study. From the correlation obtained after analyzing the data with linear regression and ANN model, it is confirmed that the tensile behavior of Ti64 behaves non-linearly with the processing parameters selected in this study, see Table 6.1.

In the case of Model-2 for the SLM process, although, regression analysis developed an R-value of 0.4 for both the output parameters A and B with frequency as the significant covariate, the F-test results rejected the usefulness of the model and therefore rejecting the possibility of explaining the model linearly. No significant covariates were found in Model-2 fit for the EBM process. Model-2 developed by the ANN procedure showed R-value results close to 1 for each of the considered cases, see Table 6.2. The A values for both SLM and EBM presented minimal deviations from actual values, however, the B values, sensitive to the estimation of the S-N curve still showed a deviation of ±0.06 and ±0.04 in SLM and EBM which accounts for approximately, a ±600 MPa and ±400 MPa variation respectively in y-axis while plotting the estimated S-N curve.

Table 6. 1 R-values from Model-1 estimations for varied AM processes

AM Process	R-value							
	Multi-regression				Artificial Neural Network			
	UTS	YS	El	Model	UTS	YS	El	Model
SLM	0.737	0.508	0.501	NA	0.9662	0.9671	0.9249	0.9912
EBM	NA	NA	NA	NA	NA	NA	NA	NA
DMLS	0.8056	0.8402	0.4111	NA	0.96	0.984	0.781	0.9951

Table 6. 2 R-values from Model-2 estimations for varied AM processes

AM Process	R-value					
	Multi-regression			Artificial Neural Network		
	A	B	Model	A	B	Model
SLM	0.4074*	0.4111*	NA	0.9447	0.9273	0.9681
EBM	-	-	-	0.9777	0.9685	0.9823
DMLS	NA	NA	NA	NA	NA	NA

* F-Test rejected the usefulness of the model

Due to the non-linearity and the involvement of each of the datasets in model building for ANN models, the model fit equations work with complex matrices making it difficult to develop a relationship of the individual input with individual output. Therefore, to better understand the model behaviors localized sensitivity analysis was performed for Model-1, and fatigue life factor analysis was performed for Model-2. Both SLM and DMLS based Model-1 came up with almost similar results for the sensitivity analysis at the median values. However, the important finding was that in both cases, power and scan speed showed inverse relations to each other, almost canceling out each other's effect which enlightens the fact that the ratio of scan speed to the laser power could be a very important factor in laser-based AM. Effect of powder layer thickness and hatch spacing also agreed with the general physics, however, in the case of DMLS, hatch space and powder layer thickness behavior could not be explored efficiently due to the lack of sufficient variations in the data. The fatigue life factor analysis gave almost 75% predictions under a life factor of 15 and only 30% and 18% population were recorded in fatigue factor of 2 for EBM and SLM based Model-2 respectively. It cannot be denied that the ANN based models developed are worked on a very preliminary concept of Bayesian regularization provided by MATLAB. However, a custom-built model on python could result in a potential output.

6.2 Future Works

From this study, the mechanical properties of Ti-6Al-4V alloy can be estimated efficiently using the ANN modeling method. No doubt, the error margins still exist but an increase in the database could lead to more efficient models. An ANN model estimating the fatigue properties from taking in inputs from the tensile properties opens up a vast horizon of future development in this stream. For enabling it to reach that level, a few assurances need to be done. Some of the necessary upgrades related to this study are discussed hereunder.

6.2.1 Predicting Model-2 using Model-1

It was observed that Model-1 predictions done by ANN in the case of SLM and DMLS fabricated Ti-6Al-4V alloy resulted in high correlation values with the outputs: UTS, YS, and elongation. Fatigue testing of a sample takes long experiment time and therefore a model that could predict the fatigue properties of a material would certainly be a useful entity. A high-efficiency Model-1 can be used to develop inputs for Model-2 and this way, the dataset for developing Model-2 can be increased. Since there is not enough published data on the fatigue properties of a material that fits in all the input parameters needed for a model building, such an approach can be used to successfully utilize all the potential published data.

6.2.2 Missing Data Imputation

This is also a method to increase the potential database for building the ANN model. Such an approach can be directly used to get a prediction value for any missing modeling parameters based on the data collected itself. Hierarchical Bayesian data Augmentation (HBDA) has been observed to result in a good performance when concerned about small sample size therefore, it fits in perfectly to work with small sample size fatigue data [134]. Another way that this imputation can be used is by finding the missing parameters from the Model-1 database. This ensures an efficient Model-1, in turn, more database for developing Model-2. Thus, Model-2 performance can be increased either by using an imputed database directly or by imputing the Model-1 database and then using that to find input parameters for Model-2 as mentioned in section 6.2.1. One such example of imputed data (in red) is shown in Table 6.3 in which, missing data from Table 4.1 has been imputed.

Table 6. 3 Missing data imputation from Table 4.1

S Speed (mm/s)	Laser P (W)	Hatch S (μm)	t (μm)	H Temp (°C)	H Time (hrs)	UTS (MPa)	YS (MPa)	El (%)
1250	200	80	30	820	1.5	1045	1010	8
1600	250	60	30	650	4	1170	1124	10.1
710	175	120	30	800	2	1032.946	964.6178	11.03882
200	200	180	50	As-fabricated		1035	910	3.3
960	120	100	30	As-fabricated		1237	1098	8.8
540	120	100	30	As-fabricated		1257	1150	8
400	120	100	30	As-fabricated		1148	1066	5.4
1260	120	100	30	As-fabricated		1112	932	6.6
1500	120	100	30	As-fabricated		978	813	3.7
1000	200	50	50	As-fabricated		1243	1153	21.5
1000	200	50	50	930	2	922	853	16
1250	200	120	40	845.53	1.914	973	885	19
1250	170	100	30	650	3	1059.336	978.5825	10.23914
1250	200	120	40	As-fabricated		1051	736	11.9
1250	200	120	40	700	1	1115	1051	11.3
1250	200	120	40	900	2	988	908	9.5
1250	200	120	40	900	2	973	885	19
1250	170	100	30	650	3	1057.378	975.6595	10.27161
1250	170	100	30	650	3	1058.226	973.8105	10.24577
1250	170	100	30	650	4	1219	1143	4.89
800.0837	172.5901	114.7444	30	As-fabricated		1314.9	1253	4
1290.65	262.4317	100.8487	30	800	2	1228.1	1211	8
1436.215	257.0825	91.08253	30	1050	2	986.4	892	13.8
1369.607	257.8571	93.2493	30	920	2	1088.5	1075	13.8
1450.244	260.1483	90.0301	30	1050	2	1006.8	892	13.5
1137.544	187.1853	90.10967	30	800	4	936.9	862.4	11.4
1037.889	285.9793	92.012	60	800	4	910.1	835.4	7.2
1177.792	320.8649	94.43266	60	900	2	928	862	9.6
1775.986	400	50	60	740	1.5	1082.11	984.3119	14.9
1767.992	400	50	60	1200	1.5	941.6	888.3029	11.9
1794.057	400	50	60	900	1.5	1090.7	992.5457	17.9
2667.078	500	64.93681	30	670	5	1090	1015	10
2665.572	500	70.19402	30	920	2	960	850	14
908.6497	275.0513	99.37406	60	350	2	1153.58	1049.7	8.91
1044.419	305.6927	96.87061	60	420	2	1257.22	1159.46	11.47

1092.732	196.2666	90.02537	31.98	670	5	1090	1015	10
1150.238	206.001	89.115	32.73	670	5	1090	1015	10
1111.392	196.3042	89.32966	31.96	670	5	1090	1015	10
1193.011	211.097	86.10534	32.85	920	5	950	880	11
1841.853	400	32.5	60	850	2	912	847.5	4.5
1060.98	200	100.6331	30	650	2	1140	1070	10.29709
1067.983	200	99.68976	30	650	2	1140	1070	10.57116
1000	400	160	50	700	1	1052	951	3.5
1200	280	140	30	704	1	1093.02	1050.51	15.27
710	175	120	30	447.66	2.133	1150	1054	9
686	375	120	90	191.51	0.969	1141	1135	1
1029	375	120	60	400	2	1250	1168	11.4
600	200	75	25	650	2	1174	1037	8.4
600	200	75	25	920	4	998	920	15.6
1600	250	60	30	As-fabricated		1271	1115	7.3
225	195	132.879	50	As-fabricated		1095	990	8.1
1600	250	60	30	As-fabricated		1267	1110	7.28
1600	250	60	30	540	5	1223	1118	5.36
1600	250	60	30	850	2	1004	955	12.84
1600	250	60	30	850	5	965	909	2
1600	250	60	30	1015	0.5	874	801	13.45
1600	250	60	30	1020	2	840	760	14.06
1600	250	60	30	705	3	1082	1026	9.04
1600	250	60	30	940	1	948	899	13.59
1600	250	60	30	1015	0.5	902	822	12.74
225	157	100	50	730	2	1052	937	9.6
225	157	100	50	As-fabricated		1117	967	8.9
600	100	105	30	725	8	959	950	9.4
600	100	105	30	974	8	912	902	10.09
600	100	105	30	827	4	911	906	9.51
600	100	105	30	1025	4	804	775	14.1
600	100	105	30	As-fabricated		1170.4	1101.68	7.98
710	175	120	30	640	4	1256	1152	3.9
710	175	120	30	As-fabricated		1321	1166	2
375	100	130	30	As-fabricated		1181	1037	7
1000	150	70	30	As-fabricated		1221	1088	6.9
1124.724	213.2761	95.98979	30	650	4	1156	1132	8
1216.953	235.0701	101.2743	30	890	2	998	964	6
745.4036	145.5085	111.9272	30	As-fabricated		1216	1125	6
710	175	120	30	As-fabricated		1213.3	1096	2.5
500	110	103.0716	50	As-fabricated		1246	1150	1.4
1200	280	140	30	920	0.5	1079	1029	11
1200	340	120	60	920	0.5	974	881	13
1200	280	140	30	650	3	1237	1161	7.6
1200	340	120	60	650	3	1222	1151	9.8
1250	250	125	30	As-fabricated		1250	1163	10.3
1250	250	125	30	730	2	1134	1054	13

1250	250	125	30	900	2	1046	889	19.2
375	100	130	30	As-fabricated		1220	1120	6.799
125	90	130	30	As-fabricated		1250	1125	6
125	90	130	30	750	2	1000	920	12
375	100	130	30	As-fabricated		1220	1120	6.603
58	42	30	50	As-fabricated		1117	967	8.9

6.2.3 Ideal Black Box Modeling

The results from sensitivity analysis agrees quite well with the general physics and this raises a possibility of an ideal black box which could be developed following the same approach where outputs can be used as inputs and the processing parameters can be estimated from the desired mechanical properties. Developing such a model would be a little tedious because, for the model working in the reverse direction, it would have to find more output variables when less inputs are given to the model. On top of this, less data availability toughens the procedure for developing the model. So, imputation and prediction from Model-1 mentioned in section 6.2.1 and 6.2.2 could be proven quite useful for building this black box.

6.2.4 Other areas of exposure

Another additive manufacturing process employed to work with metals and alloys is Direct Energy Deposition (DED). A Successful model development for Powder Bed Fusion technologies opens up a door for developing models for DED processes like Laser Engineered Net Shaping (LENS), Direct Metal Deposition (DMD), Fused Deposition Modeling (FDM), and Direct Laser Fabrication (DLF), see section 2.2.2.1. Depending upon the data available for the AM material, this method could be used to develop prediction models for mostly used additive manufacturing materials and that could potentially be used to develop a simulation software for additive manufacturing processes specifically. The ideal black box modeling mentioned in section 6.2.3 could be utilized for the development of such a software.

REFERENCES

[1] D. Banerjee and J. C. Williams, “Perspectives on titanium science and technology,” *Acta Mater.*, vol. 61, no. 3, pp. 844–879, 2013, doi: 10.1016/j.actamat.2012.10.043.

[2] M. A. Imam and F. H. Froes, “Low cost titanium and developing applications,” *Jom*, vol. 62, no. 5. pp. 17–20, 2010, doi: 10.1007/s11837-010-0069-8.

[3] G. Lütjering and J. C. Williams, *Titanium*, Edition, 2. Springer, 2007.

[4] I. Gibson and D. W. Rosen, *Additive Manufacturing Technologies*. Springer, 2019.

[5] R. Bogue, “3D printing: The dawn of a new era in manufacturing?,” *Assem. Autom.*, vol. 33, no. 4, pp. 307–311, 2013, doi: 10.1108/AA-06-2013-055.

[6] R. Hague, I. Campbell, and P. Dickens, “Implications on design of rapid manufacturing,” vol. 217, pp. 25–30.

[7] T. Pereira, J. V. Kennedy, and J. Potgieter, “A comparison of traditional manufacturing vs additive manufacturing, the best method for the job,” *Procedia Manuf.*, vol. 30, pp. 11–18, 2019, doi: 10.1016/j.promfg.2019.02.003.

[8] M. Baumers, C. Tuck, R. Hague, I. Ashcroft, and R. Wildman, “A Comparative Study of Metallic Additive Manufacturing Power Consumption,” vol. 21, no. 2009, pp. 427–441, 2010.

[9] L. C. Ardila *et al.*, “Effect of IN718 recycled powder reuse on properties of parts manufactured by means of Selective Laser Melting,” *Phys. Procedia*, vol. 56, no. C, pp. 99–107, 2014, doi: 10.1016/j.phpro.2014.08.152.

[10] H. P. Tang, M. Qian, N. Liu, X. Z. Zhang, G. Y. Yang, and J. Wang, “Effect of Powder Reuse Times on Additive Manufacturing of Ti-6Al-4V by Selective Electron Beam Melting,” *Jom*, vol. 67, no. 3, pp. 555–563, 2015, doi: 10.1007/s11837-015-1300-4.

[11] M. Attaran, “The rise of 3-D printing: The advantages of additive manufacturing over traditional manufacturing,” *Bus. Horiz.*, vol. 60, no. 5, pp. 677–688, 2017, doi: 10.1016/j.bushor.2017.05.011.

[12] I. Inagaki, T. Takechi, Y. Shirai, and N. Ariyasu, “Application and features of titanium for the aerospace industry,” *Nippon Steel Sumitomo Met. Tech.*, vol. 106, no. 106, pp. 22–27, 2014, [Online]. Available: https://www.nipponsteel.com/en/tech/report/nssmc/pdf/106-05.pdf.

[13] H. Fujii, K. Takahashi, and Y. Yamashita, “Application of titanium and its alloys for automobile parts,” *Nippon Steel Tech. Rep.*, no. 88, pp. 70–75, 2003.

[14] M. Peters, J. Kumpfert, C. H. Ward, and C. Leyens, “Titanium alloys for aerospace applications,” *Adv. Eng. Mater.*, vol. 5, no. 6, pp. 419–427, 2003, doi:

10.1002/adem.200310095.

[15] J. Breme, E. Eisenbarth, and V. Biehl, "Titanium and its Alloys for Medical Applications," *Titan. Titan. Alloy.*, pp. 423–451, 2005, doi: 10.1002/3527602119.ch16.

[16] K. Vanmeensel *et al.*, *Additively manufactured metals for medical applications*. Elsevier Inc., 2018.

[17] N. Mitsuo, "Mechanical properties of biomedical titanium alloys," *Mater. Sci. Eng. A*, vol. 243, no. 1–2, pp. 231–236, 1998, [Online]. Available: http://www.sciencedirect.com/science/article/pii/S092150939700806X.

[18] K. Wang, "The use of titanium for medical applications in the USA," *Mater. Sci. Eng. A*, vol. 213, no. 1–2, pp. 134–137, 1996, doi: 10.1016/0921-5093(96)10243-4.

[19] A. D. Dobrzańska-Danikiewicz, T. G. Gaweł, and W. Wolany, "Ti6Al4V titanium alloy used as a modern biomimetic material," *Arch. Mater. Sci. Eng.*, vol. 76, no. 2, pp. 150–156, 2015.

[20] T. C. Kontis, "Modern implants: Surgical and injectable," *Facial Plast. Surg.*, vol. 32, no. 5, p. 471, 2016, doi: 10.1055/s-0036-1588012.

[21] P. Wan, L. Tan, and K. Yang, "Surface Modification on Biodegradable Magnesium Alloys as Orthopedic Implant Materials to Improve the Bio-adaptability: A Review," *J. Mater. Sci. Technol.*, vol. 32, no. 9, pp. 827–834, 2016, doi: 10.1016/j.jmst.2016.05.003.

[22] T. Novakov, M. J. Jackson, G. M. Robinson, W. Ahmed, and D. A. Phoenix, "Laser sintering of metallic medical materials—a review," *Int. J. Adv. Manuf. Technol.*, vol. 93, no. 5–8, pp. 2723–2752, 2017, doi: 10.1007/s00170-017-0705-3.

[23] J. M. Anderson, "Future challenges in the in vitro and in vivo evaluation of biomaterial biocompatibility," *Regen. Biomater.*, vol. 3, no. 2, pp. 73–77, 2016, doi: 10.1093/RB/RBW001.

[24] Z. Sheikh, P. J. Brooks, O. Barzilay, N. Fine, and M. Glogauer, "Macrophages, foreign body giant cells and their response to implantable biomaterials," *Materials (Basel).*, vol. 8, no. 9, pp. 5671–5701, 2015, doi: 10.3390/ma8095269.

[25] X. Wang *et al.*, "Topological design and additive manufacturing of porous metals for bone scaffolds and orthopaedic implants: A review," *Biomaterials*, vol. 83, pp. 127–141, 2016, doi: 10.1016/j.biomaterials.2016.01.012.

[26] B. Vandenbroucke and J. P. Kruth, "Selective laser melting of biocompatible metals for rapid manufacturing of medical parts," *Rapid Prototyp. J.*, vol. 13, no. 4, pp. 196–203, 2007, doi: 10.1108/13552540710776142.

[27] F. A. Shah, A. Snis, A. Matic, P. Thomsen, and A. Palmquist, "3D printed

Ti6Al4V implant surface promotes bone maturation and retains a higher density of less aged osteocytes at the bone-implant interface," *Acta Biomater.*, vol. 30, pp. 357–367, 2016, doi: 10.1016/j.actbio.2015.11.013.

[28] N. M. Baloyi, A. P. I. Popoola, and S. L. Pityana, "Microstructure, hardness and corrosion properties of laser processed Ti6Al4V-based composites," *Trans. Nonferrous Met. Soc. China (English Ed.*, vol. 25, no. 9, pp. 2912–2923, 2015, doi: 10.1016/S1003-6326(15)63917-6.

[29] M. Peters, J. Hemptenmacher, J. Kumpfert, and C. Leyens, *Structure and Properties of Titanium and Titanium Alloys*. 2005.

[30] M. J. Donachie, *Titanium: A Technical Guide*, vol. 3, no. 2. 2015.

[31] J. M. Cordeiro and V. A. R. Barão, "Is there scientific evidence favoring the substitution of commercially pure titanium with titanium alloys for the manufacture of dental implants?," *Mater. Sci. Eng. C*, vol. 71, pp. 1201–1215, 2017, doi: 10.1016/j.msec.2016.10.025.

[32] H. L. Freese, M. G. Volas, and J. R. Wood, "Metallurgy and Technological Properties of Titanium and Titanium Alloys," pp. 25–51, 2001, doi: 10.1007/978-3-642-56486-4_3.

[33] K. J. Qiu *et al.*, "Microstructure, mechanical properties, castability and in vitro biocompatibility of Ti-Bi alloys developed for dental applications," *Acta Biomater.*, vol. 15, pp. 254–265, 2015, doi: 10.1016/j.actbio.2015.01.009.

[34] G. Terlinde, G. Fischer, and O. F. Metallwerke, *Titanium and Titanium Alloys: Fundamentals and Applications*. 2003.

[35] ASTM International, "Standard Specification for Titanium-6Aluminum-4Vanadium Alloy Castings for Surgical Implants (UNS R56406)," *Astm F1108-04*, vol. 04, no. Reapproved 2009, pp. 1–4, 2010, doi: 10.1520/F1108-04R09.2.

[36] A. K. Swarnakar, O. Van Der Biest, and B. Baufeld, "Thermal expansion and lattice parameters of shaped metal deposited Ti-6Al-4V," *J. Alloys Compd.*, vol. 509, no. 6, pp. 2723–2728, 2011, doi: 10.1016/j.jallcom.2010.12.014.

[37] G. Lütjering, "Influence of processing on microstructure and mechanical properties of (α + β) titanium alloys," *Mater. Sci. Eng. A*, vol. 243, no. 1–2, pp. 32–45, 1998, doi: 10.1016/s0921-5093(97)00778-8.

[38] R. Pederson, "Microstructure and Phase Transformation of Ti-6Al-4V," Lulea University of Technology, 2002.

[39] Y. Fan, W. Tian, Y. Guo, Z. Sun, and J. Xu, "Relationships among the Microstructure, Mechanical Properties, and Fatigue Behavior in Thin Ti6Al4V," *Adv. Mater. Sci. Eng.*, vol. 2016, 2016, doi: 10.1155/2016/7278267.

[40] F. J. Gil, M. P. Ginebra, J. M. Manero, and J. A. Planell, "Formation of α-

Widmanstätten structure: Effects of grain size and cooling rate on the Widmanstätten morphologies and on the mechanical properties in Ti6Al4V alloy," *J. Alloys Compd.*, vol. 329, no. 1–2, pp. 142–152, 2001, doi: 10.1016/S0925-8388(01)01571-7.

[41] J. Chesnutt, A. Thompson, and J. C. Williams, "Influence of Metallurgical Factors on the Fatigue Crack Growth Rate in α-β Titanium Alloys," *Rockwell Int. Thousand Oaks Calif Sci. Cent.*, 1978.

[42] R. K. Nalla, R. O. Ritchie, B. L. Boyce, J. P. Campbell, and J. O. Peters, "Influence of microstructure on high-cycle fatigue of Ti-6Al-4V: Bimodal vs. lamellar structures," *Metall. Mater. Trans. A*, vol. 33, no. 3, pp. 899–918, Mar. 2002, doi: 10.1007/s11661-002-0160-z.

[43] Y. M. Hu, W. Floer, U. Krupp, and H. J. Christ, "Microstructurally short fatigue crack initiation and growth in Ti-6.8Mo-4.5Fe-1.5Al," *Mater. Sci. Eng. A*, vol. 278, no. 1–2, pp. 170–180, 2000, doi: 10.1016/S0921-5093(99)00575-4.

[44] S. Birosca, J. Y. Buffiere, F. A. Garcia-Pastor, M. Karadge, L. Babout, and M. Preuss, "Three-dimensional characterization of fatigue cracks in Ti-6246 using X-ray tomography and electron backscatter diffraction," *Acta Mater.*, vol. 57, no. 19, pp. 5834–5847, 2009, doi: 10.1016/j.actamat.2009.08.009.

[45] A. ANTONYSAMY, "Microstructure, Texture and Mechanical Property Evolution during Additive Manufacturing of Ti6Al4V Alloy for Aerospace Applications," University of Manchester, 2012.

[46] R. F. Housholder, "Molding process," no. 19, p. 15, 1981, [Online]. Available: https://patents.google.com/patent/US4247508B1/en.

[47] H. Kodama, "Automatic method for fabricating a three-dimensional plastic model with photo-hardening polymer," *Rev. Sci. Instrum.*, vol. 52, no. 11, pp. 1770–1773, 1981, doi: 10.1063/1.1136492.

[48] F. Prinz *et al.*, *Rapid prototyping in Europe and Japan*, vol. 1. 1997.

[49] R. H. Crawford and J. J. Beaman, *Solid freeform fabrication*, vol. 36, no. 2. 2002.

[50] C. W. Hull, "Apparatus for Production of Three-Dmensonal Objects By Stereo Thography," *Patent*, no. 19, p. 16, 1984, [Online]. Available: https://patents.google.com/patent/US4575330A/en.

[51] S. Crump, "Apparatus and method for creating three-dimensional objects," *Patent*, 1992, [Online]. Available: https://patents.google.com/patent/US5121329A/en.

[52] C. R. Deckard, R. Rock, and J. Joseph, "Method for Selective Laser Sintering With Layerwise Cross-Scanning," no. 19, p. 12, 1992, [Online]. Available: https://patents.google.com/patent/US5155324A/de15.

[53] S. Liu and Y. C. Shin, "Additive manufacturing of Ti6Al4V alloy: A review,"

Mater. Des., vol. 164, p. 107552, 2019, doi: 10.1016/j.matdes.2018.107552.

[54] X. Yan and P. Gu, "A review of rapid prototyping technologies and systems," *CAD Comput. Aided Des.*, vol. 28, no. 4, pp. 307–318, 1996, doi: 10.1016/0010-4485(95)00035-6.

[55] J. R. Hönnige *et al.*, "Residual stress and texture control in Ti-6Al-4V wire + arc additively manufactured intersections by stress relief and rolling," *Mater. Des.*, vol. 150, no. 2017, pp. 193–205, 2018, doi: 10.1016/j.matdes.2018.03.065.

[56] M. J. Bermingham, L. Nicastro, D. Kent, Y. Chen, and M. S. Dargusch, "Optimising the mechanical properties of Ti-6Al-4V components produced by wire + arc additive manufacturing with post-process heat treatments," *J. Alloys Compd.*, vol. 753, pp. 247–255, 2018, doi: 10.1016/j.jallcom.2018.04.158.

[57] A. Sola and A. Nouri, "Microstructural porosity in additive manufacturing: The formation and detection of pores in metal parts fabricated by powder bed fusion," *J. Adv. Manuf. Process.*, vol. 1, no. 3, pp. 1–21, 2019, doi: 10.1002/amp2.10021.

[58] J. Robinson, I. Ashton, P. Fox, E. Jones, and C. Sutcliffe, "Determination of the effect of scan strategy on residual stress in laser powder bed fusion additive manufacturing," *Addit. Manuf.*, vol. 23, no. February, pp. 13–24, 2018, doi: 10.1016/j.addma.2018.07.001.

[59] V. Griffiths, J. P. Scanlan, M. H. Eres, A. Martinez-Sykora, and P. Chinchapatnam, "Cost-driven build orientation and bin packing of parts in Selective Laser Melting (SLM)," *Eur. J. Oper. Res.*, vol. 273, no. 1, pp. 334–352, 2019, doi: 10.1016/j.ejor.2018.07.053.

[60] L. Thijs, F. Verhaeghe, T. Craeghs, J. Van Humbeeck, and J. P. Kruth, "A study of the microstructural evolution during selective laser melting of Ti-6Al-4V," *Acta Mater.*, vol. 58, no. 9, pp. 3303–3312, 2010, doi: 10.1016/j.actamat.2010.02.004.

[61] J. P. Kruth, M. Badrossamay, E. Yasa, J. Deckers, L. Thijs, and J. Van Humbeeck, "Part and material properties in selective laser melting of metals," *16th Int. Symp. Electromachining, ISEM 2010*, pp. 3–14, 2010.

[62] X. Liu, P. K. Chu, and C. Ding, "Surface modification of titanium, titanium alloys, and related materials for biomedical applications," *Mater. Sci. Eng. R Reports*, vol. 47, no. 3–4, pp. 49–121, 2004, doi: 10.1016/j.mser.2004.11.001.

[63] B. Vrancken, "Study of Residual Stresses in Selective Laser Melting," Arenberg Doctoral School, 2016.

[64] B. Wysocki, P. Maj, R. Sitek, J. Buhagiar, K. J. Kurzydłowski, and W. Święszkowski, "Laser and electron beam additive manufacturing methods of fabricating titanium bone implants," *Appl. Sci.*, vol. 7, no. 7, pp. 1–20, 2017, doi: 10.3390/app7070657.

[65] J. Delgado, J. Ciurana, and C. A. Rodríguez, "Influence of process parameters on

part quality and mechanical properties for DMLS and SLM with iron-based materials," *Int. J. Adv. Manuf. Technol.*, vol. 60, no. 5–8, pp. 601–610, 2012, doi: 10.1007/s00170-011-3643-5.

[66] R. Konečná, G. Nicoletto, A. Bača, and L. Kunz, "Microstructure, defects and fractoghaphy of Ti6Al4V alloys produced by SLM and DMLS," *Powder Metall. Prog.*, vol. 15, no. 86, pp. 86–93, 2015, [Online]. Available: http://www.imr.saske.sk/pmp/issue/ss_2015/PMP_Vol15_ss_p_086-093.pdf.

[67] EOS, "EOSINT M 280 technical brochure," 2015. [Online]. Available: http://www.eos.info/systeme_loesungen/metall/systeme_und_zubehoer/eosint_m280.

[68] D. Agius, K. I. Kourousis, and C. Wallbrink, "A review of the as-built SLM Ti-6Al-4V mechanical properties towards achieving fatigue resistant designs," *Metals (Basel).*, vol. 8, no. 1, 2018, doi: 10.3390/met8010075.

[69] A. H. Chern *et al.*, "A review on the fatigue behavior of Ti-6Al-4V fabricated by electron beam melting additive manufacturing," *Int. J. Fatigue*, vol. 119, pp. 173–184, 2019, doi: 10.1016/j.ijfatigue.2018.09.022.

[70] M. Izadi, A. Farzaneh, M. Mohammed, I. Gibson, and B. Rolfe, "A review of laser engineered net shaping (LENS) build and process parameters of metallic parts," *Rapid Prototyp. J.*, no. November 2019, 2020, doi: 10.1108/RPJ-04-2018-0088.

[71] A. Guzanová, G. Ižaríková, J. Brezinová, J. Živčák, D. Draganovská, and R. Hudák, "Influence of build orientation, heat treatment, and laser power on the hardness of Ti6Al4V manufactured using the DMLS process," *Metals (Basel).*, vol. 7, no. 8, 2017, doi: 10.3390/met7080318.

[72] F. Cao, T. Zhang, M. A. Ryder, and D. A. Lados, "A Review of the Fatigue Properties of Additively Manufactured Ti-6Al-4V," *Jom*, vol. 70, no. 3, pp. 349–357, 2018, doi: 10.1007/s11837-017-2728-5.

[73] A. V. Manzhirov and S. A. Lychev, "Mathematical modeling of additive manufacturing technologies," *Lect. Notes Eng. Comput. Sci.*, vol. 2, pp. 1404–1409, 2014.

[74] X. Qi, G. Chen, Y. Li, X. Cheng, and C. Li, "Applying Neural-Network-Based Machine Learning to Additive Manufacturing: Current Applications, Challenges, and Future Perspectives," *Engineering*, vol. 5, no. 4, pp. 721–729, 2019, doi: 10.1016/j.eng.2019.04.012.

[75] M. Fousová, D. Vojtěch, K. Doubrava, M. Daniel, and C. F. Lin, "Influence of inherent surface and internal defects on mechanical properties of additively manufactured Ti6Al4V alloy: Comparison between selective laser melting and electron beam melting," *Materials (Basel).*, vol. 11, no. 4, 2018, doi: 10.3390/ma11040537.

[76] J. M. ZURADA, *Introduction to Artificial Neural Systems*. 1992.

[77] B. Van Hooreweder, R. Boonen, D. Moens, J. P. Kruth, and P. Sas, "On the determination of fatigue properties of Ti6Al4V produced by selective laser melting," *Collect. Tech. Pap. - AIAA/ASME/ASCE/AHS/ASC Struct. Struct. Dyn. Mater. Conf.*, no. April, 2012, doi: 10.2514/6.2012-1733.

[78] J. Günther *et al.*, "Fatigue life of additively manufactured Ti–6Al–4V in the very high cycle fatigue regime," *Int. J. Fatigue*, vol. 94, pp. 236–245, 2017, doi: 10.1016/j.ijfatigue.2016.05.018.

[79] P. Edwards and M. Ramulu, "Fatigue performance evaluation of selective laser melted Ti-6Al-4V," *Mater. Sci. Eng. A*, vol. 598, pp. 327–337, 2014, doi: 10.1016/j.msea.2014.01.041.

[80] H. Gong, K. Rafi, H. Gu, G. D. Janaki Ram, T. Starr, and B. Stucker, "Influence of defects on mechanical properties of Ti-6Al-4V components produced by selective laser melting and electron beam melting," *Mater. Des.*, vol. 86, pp. 545–554, 2015, doi: 10.1016/j.matdes.2015.07.147.

[81] X. Zhao *et al.*, "Comparison of the microstructures and mechanical properties of Ti-6Al-4V fabricated by selective laser melting and electron beam melting," *Mater. Des.*, vol. 95, pp. 21–31, 2016, doi: 10.1016/j.matdes.2015.12.135.

[82] G. Kasperovich and J. Hausmann, "Improvement of fatigue resistance and ductility of TiAl6V4 processed by selective laser melting," *J. Mater. Process. Technol.*, vol. 220, pp. 202–214, 2015, doi: 10.1016/j.jmatprotec.2015.01.025.

[83] W. Eric, E. Claus, S. Shafaqat, and W. Frank, "High cycle fatigue (HCF) performance of Ti-6Al-4V alloy processed by selective laser melting," *Adv. Mater. Res.*, vol. 816–817, no. September 2016, pp. 134–139, 2013, doi: 10.4028/www.scientific.net/AMR.816-817.134.

[84] H. K. Rafi, T. L. Starr, and B. E. Stucker, "A comparison of the tensile, fatigue, and fracture behavior of Ti-6Al-4V and 15-5 PH stainless steel parts made by selective laser melting," *Int. J. Adv. Manuf. Technol.*, vol. 69, no. 5–8, pp. 1299–1309, 2013, doi: 10.1007/s00170-013-5106-7.

[85] S. Leuders, T. Lieneke, S. Lammers, T. Tröster, and T. Niendorf, "On the fatigue properties of metals manufactured by selective laser melting - The role of ductility," *J. Mater. Res.*, vol. 29, no. 17, pp. 1911–1919, 2014, doi: 10.1557/jmr.2014.157.

[86] K. D. Rekedal and D. Liu, "Fatigue life of selective laser melted and hot isostatically pressed Ti-6Al-4v absent of surface machining," *56th AIAA/ASCE/AHS/ASC Struct. Struct. Dyn. Mater. Conf.*, pp. 1–9, 2015, doi: 10.2514/6.2015-0894.

[87] G. Nicoletto, S. Maisano, M. Antolotti, and F. Dall'aglio, "Influence of post

fabrication heat treatments on the fatigue behavior of Ti-6Al-4V produced by selective laser melting," *Procedia Struct. Integr.*, vol. 7, pp. 133–140, 2017, doi: 10.1016/j.prostr.2017.11.070.

[88] M. Benedetti *et al.*, "The effect of post-sintering treatments on the fatigue and biological behavior of Ti-6Al-4V ELI parts made by selective laser melting," *J. Mech. Behav. Biomed. Mater.*, vol. 71, no. March, pp. 295–306, 2017, doi: 10.1016/j.jmbbm.2017.03.024.

[89] W. Xu, S. Sun, J. Elambasseril, Q. Liu, M. Brandt, and M. Qian, "Ti-6Al-4V Additively Manufactured by Selective Laser Melting with Superior Mechanical Properties," *Jom*, vol. 67, no. 3, pp. 668–673, 2015, doi: 10.1007/s11837-015-1297-8.

[90] M. Benedetti, V. Fontanari, M. Bandini, F. Zanini, and S. Carmignato, "Low- and high-cycle fatigue resistance of Ti-6Al-4V ELI additively manufactured via selective laser melting: Mean stress and defect sensitivity," *Int. J. Fatigue*, vol. 107, no. October 2017, pp. 96–109, 2018, doi: 10.1016/j.ijfatigue.2017.10.021.

[91] A. Tridello *et al.*, "VHCF response of heat-treated SLM Ti6Al4V Gaussian specimens with large loaded volume," *Procedia Struct. Integr.*, vol. 18, pp. 314–321, 2019, doi: 10.1016/j.prostr.2019.08.171.

[92] E. Wycisk, A. Solbach, S. Siddique, D. Herzog, F. Walther, and C. Emmelmann, "Effects of defects in laser additive manufactured Ti-6Al-4V on fatigue properties," *Phys. Procedia*, vol. 56, no. C, pp. 371–378, 2014, doi: 10.1016/j.phpro.2014.08.120.

[93] A. Fatemi, R. Molaei, S. Sharifimehr, N. Phan, and N. Shamsaei, "Multiaxial fatigue behavior of wrought and additive manufactured Ti-6Al-4V including surface finish effect," *Int. J. Fatigue*, vol. 100, pp. 347–366, 2017, doi: 10.1016/j.ijfatigue.2017.03.044.

[94] P. E. Carrion, A. Soltani-Tehrani, S. M. Thompson, and N. Shamsaei, "Effect of Powder Degradation on the Fatigue Behavior of Additively Manufactured As-Built Ti-6Al-4V," *Solid Free. Fabr. Proc.*, pp. 1366–1372, 2018.

[95] W. Xu *et al.*, "Additive manufacturing of strong and ductile Ti-6Al-4V by selective laser melting via in situ martensite decomposition," *Acta Mater.*, vol. 85, pp. 74–84, 2015, doi: 10.1016/j.actamat.2014.11.028.

[96] H. K. Rafi, N. V. Karthik, H. Gong, T. L. Starr, and B. E. Stucker, "Microstructures and mechanical properties of Ti6Al4V parts fabricated by selective laser melting and electron beam melting," *J. Mater. Eng. Perform.*, vol. 22, no. 12, pp. 3872–3883, 2013, doi: 10.1007/s11665-013-0658-0.

[97] L. Facchini, E. Magalini, P. Robotti, A. Molinari, S. Höges, and K. Wissenbach, "Ductility of a Ti-6Al-4V alloy produced by selective laser melting of prealloyed powders," *Rapid Prototyp. J.*, vol. 16, no. 6, pp. 450–459, 2010, doi:

10.1108/13552541011083371.

[98] B. Vrancken, L. Thijs, J. P. Kruth, and J. Van Humbeeck, “Heat treatment of Ti6Al4V produced by Selective Laser Melting: Microstructure and mechanical properties,” *J. Alloys Compd.*, vol. 541, pp. 177–185, 2012, doi: 10.1016/j.jallcom.2012.07.022.

[99] M. Simonelli, Y. Y. Tse, and C. Tuck, “Effect of the build orientation on the mechanical properties and fracture modes of SLM Ti-6Al-4V,” *Mater. Sci. Eng. A*, vol. 616, pp. 1–11, 2014, doi: 10.1016/j.msea.2014.07.086.

[100] G. M. ter Haar, T. H. Becker, and D. C. Blaine, “Influence of heat treatments on the microstructure and tensile behaviour of selective laser melting-produced TI-6AL-4V parts,” *South African J. Ind. Eng.*, vol. 27, no. 3SpecialIssue, pp. 174–183, 2016, doi: 10.7166/27-3-1663.

[101] A. Mertens *et al.*, “Mechanical properties of alloy Ti-6Al-4V and of stainless steel 316L processed by selective laser melting: Influence of out-of-equilibrium microstructures,” *Powder Metall.*, vol. 57, no. 3, pp. 184–189, 2014, doi: 10.1179/1743290114Y.0000000092.

[102] D. Agius, K. I. Kourousis, C. Wallbrink, and T. Song, “Cyclic plasticity and microstructure of as-built SLM Ti-6Al-4V: The effect of build orientation,” *Mater. Sci. Eng. A*, vol. 701, no. June, pp. 85–100, 2017, doi: 10.1016/j.msea.2017.06.069.

[103] B. Vrancken, S. Buls, J.-P. Kruth, and J. Van Humbeeck, “Preheating of Selective Laser Melted Ti6Al4V: Microstructure and Mechanical Properties,” *Proc. 13th World Conf. Titan.*, pp. 1269–1277, 2016, doi: 10.1002/9781119296126.ch215.

[104] V. Cain, L. Thijs, J. Van Humbeeck, B. Van Hooreweder, and R. Knutsen, “Crack propagation and fracture toughness of Ti6Al4V alloy produced by selective laser melting,” *Addit. Manuf.*, vol. 5, pp. 68–76, 2015, doi: 10.1016/j.addma.2014.12.006.

[105] K. I. Kourousis, D. Agius, C. Wang, and A. Subic, “Constitutive modeling of additive manufactured Ti-6Al-4V cyclic elastoplastic behaviour,” *Tech. Mech.*, vol. 36, no. 1–2, pp. 57–72, 2016, doi: 10.24352/ub.ovgu-2017-010.

[106] P. Kumar and U. Ramamurty, “Microstructural optimization through heat treatment for enhancing the fracture toughness and fatigue crack growth resistance of selective laser melted Ti–6Al–4V alloy,” *Acta Mater.*, vol. 169, no. March, pp. 45–59, 2019, doi: 10.1016/j.actamat.2019.03.003.

[107] P. Kumar, O. Prakash, and U. Ramamurty, “Micro-and meso-structures and their influence on mechanical properties of selectively laser melted Ti-6Al-4V,” *Acta Mater.*, vol. 154, pp. 246–260, 2018, doi: 10.1016/j.actamat.2018.05.044.

[108] D. Zhang *et al.*, “Effect of heat treatment on the tensile behavior of selective laser

melted Ti-6Al-4V by in situ X-ray characterization," *Acta Mater.*, vol. 189, pp. 93–104, 2020, doi: 10.1016/j.actamat.2020.03.003.

[109] D. Agius, K. I. Kourousis, and C. Wallbrink, "Elastoplastic response of as-built SLM and wrought Ti-6Al-4V under symmetric and asymmetric strain-controlled cyclic loading," *Rapid Prototyp. J.*, vol. 24, no. 9, pp. 1409–1420, 2018, doi: 10.1108/RPJ-05-2017-0105.

[110] K. I. Kourousis and D. Agius, "Uniaxial Cyclic Stress-Strain Behaviour of Ti-6Al-4V Additively Manufactured by Selective Laser Melting," no. April, 2017.

[111] H. Bikas, P. Stavropoulos, and G. Chryssolouris, "Additive manufacturing methods and modelling approaches : a critical review," 2015, doi: 10.1007/s00170-015-7576-2.

[112] P. E. Carrion, A. Soltani-Tehrani, N. Phan, and N. Shamsaei, "Powder Recycling Effects on the Tensile and Fatigue Behavior of Additively Manufactured Ti-6Al-4V Parts," *Jom*, vol. 71, no. 3, pp. 963–973, 2019, doi: 10.1007/s11837-018-3248-7.

[113] U. Ackelid, M. Svensson, and A. B. Arcam, "Additive manufacturing of dense metal parts by Electron Beam Melting," *Proc. Euro Int. Powder Metall. Congr. Exhib. Euro PM 2009*, vol. 3, pp. 1–7, 2009.

[114] X. Shui, K. Yamanaka, M. Mori, Y. Nagata, K. Kurita, and A. Chiba, "Effects of post-processing on cyclic fatigue response of a titanium alloy additively manufactured by electron beam melting," *Mater. Sci. Eng. A*, vol. 680, no. October 2016, pp. 239–248, 2017, doi: 10.1016/j.msea.2016.10.059.

[115] D. Greitemeier, F. Palm, F. Syassen, and T. Melz, "Fatigue performance of additive manufactured TiAl6V4 using electron and laser beam melting," *Int. J. Fatigue*, vol. 94, pp. 211–217, 2017, doi: 10.1016/j.ijfatigue.2016.05.001.

[116] D. Greitemeier, C. Dalle Donne, F. Syassen, J. Eufinger, and T. Melz, "Effect of surface roughness on fatigue performance of additive manufactured Ti–6Al–4V," *Mater. Sci. Technol. (United Kingdom)*, vol. 32, no. 7, pp. 629–634, 2016, doi: 10.1179/1743284715Y.0000000053.

[117] N. Hrabe, T. Gnäupel-Herold, and T. Quinn, "Fatigue properties of a titanium alloy (Ti–6Al–4V) fabricated via electron beam melting (EBM): Effects of internal defects and residual stress," *Int. J. Fatigue*, vol. 94, pp. 202–210, 2017, doi: 10.1016/j.ijfatigue.2016.04.022.

[118] E. Tiferet *et al.*, "Mapping the tray of electron beam melting of Ti-6Al-4V: Properties and microstructure," *Materials (Basel).*, vol. 12, no. 9, pp. 1–14, 2019, doi: 10.3390/ma12091470.

[119] E. Brandl, C. Leyens, and F. Palm, "Mechanical properties of additive manufactured Ti-6Al-4V using wire and powder based processes," *IOP Conf. Ser.*

Mater. Sci. Eng., vol. 26, no. 1, 2011, doi: 10.1088/1757-899X/26/1/012004.

[120] A. Kirchner *et al.*, "Mechanical properties of Ti-6Al-4V additively manufactured by electron beam melting," *Proc. Euro PM 2015 Int. Power Metall. Congr. Exhib.*, no. October, 2015.

[121] H. Khalid Rafi., N. V. Karthik, T. L. Starr, and B. E. Stucker, "Mechanical property evaluation of Ti-6Al-4V parts made using Electron Beam Melting," *23rd Annu. Int. Solid Free. Fabr. Symp. - An Addit. Manuf. Conf. SFF 2012*, pp. 526–535, 2012.

[122] A. Mohammadhosseini, D. Fraser, S. H. Masood, and M. Jahedi, "Microstructure and mechanical properties of Ti-6Al-4V manufactured by electron beam melting process," *Mater. Res. Innov.*, vol. 17, no. SUPPL 2, 2013, doi: 10.1179/1432891713Z.000000000302.

[123] Z. Liu, Z. Wang, C. Gao, R. Liu, and Z. Xiao, "Microstructure, Anisotropic Mechanical Properties and Very High Cycle Fatigue Behavior of Ti6Al4V Produced by Selective Electron Beam Melting," *Met. Mater. Int.*, no. 0123456789, 2020, doi: 10.1007/s12540-020-00664-2.

[124] M. Nakatani, H. Masuo, Y. Tanaka, and Y. Murakami, "Effect of Surface Roughness on Fatigue Strength of Ti-6Al-4V Alloy Manufactured by Additive Manufacturing," *Procedia Struct. Integr.*, vol. 19, pp. 294–301, 2019, doi: 10.1016/j.prostr.2019.12.032.

[125] P. Edwards, A. O'Conner, and M. Ramulu, "Electron beam additive manufacturing of titanium components: Properties and performance," *J. Manuf. Sci. Eng. Trans. ASME*, vol. 135, no. 6, pp. 1–7, 2013, doi: 10.1115/1.4025773.

[126] G. Nicoletto, R. Konečná, M. Frkáň, and E. Riva, "Surface roughness and directional fatigue behavior of as-built EBM and DMLS Ti6Al4V," *Int. J. Fatigue*, vol. 116, no. June, pp. 140–148, 2018, doi: 10.1016/j.ijfatigue.2018.06.011.

[127] D. B. Witkin, T. V. Albright, and D. N. Patel, "Empirical Approach to Understanding the Fatigue Behavior of Metals Made Using Additive Manufacturing," *Metall. Mater. Trans. A Phys. Metall. Mater. Sci.*, vol. 47, no. 8, pp. 3823–3836, 2016, doi: 10.1007/s11661-016-3501-z.

[128] Z. A. Mierzejewska, "Effect of laser energy density, internal porosity and heat treatment on mechanical behavior of biomedical TI6AL4V alloy obtained with DMLS technology," *Materials (Basel).*, vol. 12, no. 18, 2019, doi: 10.3390/ma12182928.

[129] G. Nicoletto, "Anisotropic high cycle fatigue behavior of Ti–6Al–4V obtained by powder bed laser fusion," *Int. J. Fatigue*, vol. 94, pp. 255–262, 2017, doi: 10.1016/j.ijfatigue.2016.04.032.

[130] Z. A. Mierzejewska, R. Hudák, and J. Sidun, "Mechanical properties and

microstructure of DMLS Ti6Al4V alloy dedicated to biomedical applications," *Materials (Basel).*, vol. 12, no. 1, 2019, doi: 10.3390/ma12010176.

[131] T. H. Becker, M. Beck, and C. Scheffer, "Microstructure and mechanical properties of direct metal laser sintered Ti-6Al-4V," *South African J. Ind. Eng.*, vol. 26, no. 1, pp. 1–10, 2015, doi: 10.7166/26-1-1022.

[132] M. Kayri, "Predictive abilities of Bayesian regularization and levenberg-marquardt algorithms in artificial neural networks: A comparative empirical study on social data," *Math. Comput. Appl.*, vol. 21, no. 2, 2016, doi: 10.3390/mca21020020.

[133] H. Okut, D. Gianola, G. J. M. Rosa, and K. A. Weigel, "Prediction of body mass index in mice using dense molecular markers and a regularized neural network," *Genet. Res. (Camb).*, vol. 93, no. 3, pp. 189–201, 2011, doi: 10.1017/S0016672310000662.

[134] J. Chen, S. Liu, W. Zhang, and Y. Liu, "Uncertainty quantification of fatigue S-N curves with sparse data using hierarchical Bayesian data augmentation," *Int. J. Fatigue*, vol. 134, p. 105511, 2020, doi: 10.1016/j.ijfatigue.2020.105511.

APPENDIX A

DATA COLLECTED DECEMBER-JUNE 2020

RAW DATA FOR FATIGUE SLM

A	B	Raw Data		Ref
		N	S	
1358.4	-0.119	3007.662	599.139	[75]
		18722.03	498.906	
		35108.18	399.385	
		83573.39	350.478	
		90255.36	319.728	
		219754.5	299.754	
		259321.1	279.846	
		392402.7	250.874	
		720878.3	249.613	
		761632.1	230.921	
		9964673	249.978	
		9961421	229.482	
		9956737	199.944	
2040.6	-0.195	4159.179	452.632	[77]
		8614.691	421.053	
		11385.44	350	
		13293.32	348.684	
		20354.61	279.817	
		26487.72	278.899	
		97325.22	173.514	
		256299	139.459	
		407940.8	132.973	
		644292.8	147.027	
		8303475	131.892	
193.77	-0.051	239039.3	103.243	[77]
		1178932	97.838	
		1510574	92.432	
124.63	-0.036	442798.7	76.307	[77]
		1350314	75.153	
		2031224	76.017	
		9921788	68.328	
2097.9	-0.128	12003.15	652.392	[78]
		16272.48	653.692	
		10663.51	699.28	
		12207.8	700.544	

A	B	Raw Data		Ref
		N	S	
2403.2	-0.198	15967.52	401.03	[80]
		27641.28	300.658	
		95056.95	252.16	
		263045.5	200.495	
		392549.4	178.573	
		703646.9	152.75	
		2661857	127.019	
		9800976	110.701	
1121.9	-0.074	12061.07	599.146	[81]
		49632.78	499.22	
		70233.25	449.567	
		9957294	348.937	
		60665.26	501.134	
1955	-0.079	1175402	649.254	[80]
		3273828	599.412	
		9878503	548.951	
2676.3	-0.121	156745.5	600.219	[82]
		212484.5	600.243	
		379821.5	600.289	
		1079029	501.043	
		5293266	501.169	
		7275484	350.28	
		13744791	350.33	
1671.6	-0.136	30983.28	500.744	[83]
		33783.29	500.851	
		58071.29	400.713	
		151011.6	301.193	
		173739.7	301.301	
		326637.2	240.692	
		483311.8	219.554	
		3391590	200.08	
		8351897	221.427	
		10034446	200.29	
		9899032	221.078	
		474862.3	240.58	

		27022.04	552.686	
		37257.94	553.786	
		14953.51	600.496	
		20969.4	601.598	
		195321	401.615	
		347041.8	401.699	
		1152588	401.874	
		89745	453.603	
		22819	453.403	
		40544.27	500.545	
		58810.75	500.6	
		83876.77	500.652	
562.6	-0.032	144540.2	442.063	[78]
		154339	342.91	
		1808749	311.313	
		10113961	274.85	
		13986600	353.814	
		20950678	383.686	
		28161163	373.117	
		44470262	343.305	
		56653069	342.359	
		80333628	311.577	
		1.55E+08	311.623	
		5E+08	267.421	
		8.01E+08	280.931	
		2.41E+09	237.687	
845.1	-0.031	49394.2	588.318	[78]
		102235.4	649.019	
		210972.5	531.62	
		1110228	530.533	
		1313532	530.544	
		5391464	618.221	
		11805402	560.113	
		1.35E+08	500.783	
		1.85E+08	472.727	
		3.01E+08	436.659	
		17600767	422.422	
		4.72E+08	471.455	
		5.43E+08	442.717	

564.49	-0.006	85826.8	448.936	[83]
		112839.2	599.251	
		113169.2	558.905	
		157174.3	524.125	
		2125413	498.141	
		2324373	473.774	
		3397733	598.556	
		4473479	559.266	
		5652489	473.793	
		9975098	519.987	
		10130866	497.959	
2542.8	-0.093	1232834	712.848	[81]
		2500743	657.744	
		2327384	627.365	
		4013573	575.904	
		8364980	606.903	
		8753349	600.384	
		9960973	548.989	
		12182501	546.786	
		15694603	546.746	
2622.3	-0.152	12758.32	699.66	[85]
		17998.97	598.98	
		43631.33	501.02	
		68327.07	403.061	
		1997964	305.782	
2043.9	-0.124	11538.06	701.02	[85]
		14327.53	649.32	
		17182.9	598.98	
		33028.72	550.68	
		61315.95	501.02	
		67800.71	452.721	
		846821.3	403.741	
7099.3	-0.263	15479.49	598.98	[85]
		19597.08	550.68	
		18350.34	501.02	
		28736.79	452.041	
		61079.32	403.741	
1092.4	-0.033	30452.8	798.98	[85]
		40540.82	773.129	

		5.27E+08	399.26	
		1.01E+09	423.373	
		6.73E+08	472.816	
7158	-0.346	3471.587	402.963	[79]
		13317.7	263.704	
		50417.27	202.963	
		93302.17	128.889	
		218246.7	94.815	
		993635.2	59.259	
243.35	-0.075	83861.6	94.815	[79]
		105244.5	128.889	
		116998	94.815	
		140660.1	93.333	
		302338.8	96.296	
		322233.7	93.333	
873.5	-0.05	19370.33	652.153	[80]
		38409.08	551.797	
		37821.32	401.136	
		90251.71	452.247	
		110776.8	551.927	
		130300.3	500.158	
		118268.9	351.056	
		183197.3	600.639	
		1420374	401.581	
		2366425	501.298	
		2317287	451.076	
		5263339	352.307	
1001.5	-0.05	24867.96	549.187	[80]
		60235.65	597.899	
		148906	449.894	
		174850.8	399.621	
		338369.4	550.151	
		510021.4	598.232	
		467504.9	698.52	
		665128.1	648.954	
		1019410	650.859	
		5553333	348.756	
		10094615	398.994	
669.11	-0.046	26964.45	494.472	[80]

		57415.09	748.639	
		171497.2	720.748	
		1336425	696.939	
1080.5	-0.046	30452.8	798.98	[85]
		40540.82	773.129	
		57415.09	748.639	
		171497.2	720.748	
		1336425	696.939	
		17860.32	649.32	
		24429.2	598.98	
		31288.31	550.68	
		301598.4	501.02	
		765827.5	452.041	
798.16	-0.089	27139.27	401.199	[86]
		29377.11	401.212	
		87857.53	300.942	
		95759.59	299.859	
		198091.6	241.246	
		198091.6	228.621	
		197410.3	218.191	
		273843.5	220.99	
		318663.4	229.248	
		9884971	224.325	
		9884971	211.7	
1237.3	-0.119	14348.74	499.348	[86]
		16468.69	499.371	
		33833.78	400.137	
		30722.66	350.171	
		101885.6	300.967	
		117342.1	280.681	
		123140.2	249.95	
		218151.3	250.044	
		243575.7	239.633	
		297447	231.981	
		342571.3	239.689	
		9987661	233.658	
		9884971	200.722	
4685.4	-0.227	24986.06	496.622	[86]
		42731.72	397.297	

		21367.27	346.923	
		43293.37	346.225	
		44816.31	397.234	
		89745.07	547.193	
		278564.1	446.108	
		191401.3	296.188	
		1940990	396.911	
		10169031	349.249	
		10093634	295.889	
		10159673	273.919	
3343.8	-0.206	10943.32	597.939	[80]
		19866.06	497.573	
		45122.51	398.804	
		106025.6	298.469	
		127358.7	298.492	
		283618.4	250.724	
		335673.8	149.521	
		507919.7	149.572	
		3448408	198.457	
		3616265	198.463	
2603.8	-0.125	13514.78	845.231	[112]
		8646.641	824.554	
		15079.41	831.69	
		85560.41	601.489	
		223600.7	597.686	
		473349.9	599.028	
		123964.6	478.289	
		630391.6	484.21	
		765213.2	468.739	
		832489.9	478.423	
806.94	-0.144	25655.55	173.549	[87]
		70196.55	198.881	
		97303.54	174.233	
		87956.72	124.937	
		647482.6	124.253	
		1492111	98.92	
1203.1	-0.14	25499.19	249.366	[87]
		159731.1	299.423	
		215900	249.395	

		52280.17	398.48	
		56387.61	398.48	
		179982.8	296.791	
		144353.7	296.791	
		287009.8	268.412	
		257784.9	295.608	
		413715.7	256.588	
		463461.5	245.946	
		525858.9	217.568	
		567119.1	228.209	
		716018	235.304	
		1414234	241.216	
		9978942	235.304	
671.68	-0.101	23904.49	249.546	[87]
		66515.67	249.546	
		219012	198.881	
		597228.3	173.891	
		685617.5	174.233	
		1009742	148.901	
		645306.6	124.253	
		380394.2	198.881	
		5833194	174.576	
		7897423	148.901	
		9895519	149.585	
		9995961	108.505	
639.66	-0.032	52183.95	498.718	[88]
		67827.46	498.718	
		64281.4	448.077	
		108588.8	448.718	
		105130.3	424.419	
		221725.5	424.419	
		188039.4	398.837	
		252784.2	399.419	
		52240885	398.256	
		6890184	374.257	
		48086863	374.257	
		48253594	348.515	
964.33	-0.065	230271	447.761	[90]
		348546.9	447.697	

		352294	173.832	
		593716.3	199.054	
		1981671	149.026	
		3286206	98.998	
		9849417	198.976	
		9902557	224.081	
		9955984	123.699	
		9955984	100.76	
		9902557	73.88	
491.01	-0.045	53974.96	350	[88]
		74031.85	350	
		46830.69	300.373	
		92969.56	300.373	
		101460.5	300.373	
		160787.9	276.119	
		252274.8	276.119	
		275315.1	276.119	
		227093.3	226.347	
		192571.9	250	
		280594.4	249.701	
		13575335	249.701	
		50203030	226.347	
		50025495	200	
1807.6	-0.142	25044.75	500.347	[92]
		28788.02	500.318	
		61543.79	400.519	
		73017.68	399.767	
		152195.4	299.973	
		148389.2	299.261	
		369291.6	248.893	
		516543.9	250.257	
		760051.9	217.202	
		760051.9	214.334	
		9874167	220.97	
		9936884	208.783	
		9936884	193.729	
1061.2	-0.047	24358	800.854	[92]
		28284.74	750.208	
		66693.39	599.83	

		589633	399.729	
		938766.6	399.658	
		1184529	349.706	
		16578261	349.391	
		35746885	324.574	
		35746885	299.299	
595.67	-0.057	155238.3	349.948	[90]
		199879.6	349.918	
		144631.7	300.506	
		249669.5	300.441	
		266627.9	300.433	
		381749.3	276.5	
		549346.5	275.996	
		583701.8	276.457	
		433174.6	250.319	
		583701.8	250.289	
		12617925	249.977	
		494018.4	226.61	
		35566638	226.638	
		35746885	199.118	
249.75	-0.032	174378.5	200	[90]
		280452.6	176.627	
		297991.7	176.627	
		316627.7	176.923	
		319845	150	
		782570.7	150	
		35746885	150	
		420233.5	144.937	
		474438.6	144.937	
		35566638	144.937	
		35566638	139.451	
330.37	-0.031	38355.97	249.669	[90]
		77171	249.669	
		73782.86	249.669	
		48336.76	226.159	
		63682.16	225.828	
		79709.64	225.828	
		157832.3	213.576	
		950830.9	213.245	

		71635.29	599.837	
		43715.93	575.587	
		105108.3	501.581	
		2571342	576.033	
		3847126	550.368	
		4555265	530.727	
		3400279	515.572	
		10000000	484.688	
250.82	-0.018	601730.6	172.061	[91]
		646939.2	209.49	
		994024.2	181.772	
		1215496	191.726	
		2269768	238.779	
		2241279	195.483	
		4563441	180.327	
		2.73E+08	184.608	
		1.03E+09	201.122	
		1.03E+09	181.328	
		1.02E+09	159.211	
		1.02E+09	146.75	
		2.17E+08	170.707	
		3.8E+08	171.68	

		911676.2	199.338	
		6086297	199.338	
		50853615	199.007	
		49775813	188.265	
3170.8	-0.218	3589.729	619.975	[94]
		18409.9	373.744	
		525118.7	120.477	
		9767633	123.116	
12772	-0.345	9736.304	515.257	[89]
		13105.8	514.866	
		34797.53	342.491	
126491	-0.551	43713.61	347.771	[93]
		84798.17	267.177	
		96458.77	203.383	
		122534.6	203.364	
2804.9	-0.139	129040.7	514.286	[89]
		179846.5	514.286	
		305902.1	515.966	
		240866.4	515.966	
		2847348	344.538	
		3664493	344.538	

APPENDIX B

DATA COLLECTED DECEMBER-JUNE 2020

RAW DATA FOR FATIGUE EBM

A	B	Raw Data		Ref
		N	S	
3526.9	-0.115	505714.5	800.903	[81]
		2804229	600.546	
		9862757	574.271	
		1251437	700.544	
2122.6	-0.107	18039.58	800.215	[81]
		87732.46	600.346	
		193314.3	500.951	
		1606878	450.759	
		9864674	400.497	
		46728.81	700.544	
701.49	-0.013	18611.31	751.865	[80]
		27296.41	702.324	
		68182.26	701.332	
		75560.73	652.859	
		30534.23	602.062	
		75560.73	552.584	
		50095.32	501.846	
		92799.5	452.333	
		152249.5	501.979	
		155120.6	552.67	
		125130.5	652.919	
		201492.8	651.874	
		653756.2	702.704	
		752086.4	653.134	
		1558468	552.946	
		986086	477.96	
		3512683	602.63	
		3750045	602.637	
		4605598	602.662	
812.32	-0.017	25158.04	626.586	[80]
		46810.56	701.867	
		104331.1	702.061	
		382342.8	677.32	
		428604	652.646	

A	B	Raw Data		Ref
		N	S	
2297	-0.082	1923075	702.364	[115]
		3908809	676.339	
		5177899	652.339	
		6517200	627.287	
		10524505	602.273	
		25097472	577.317	
3124.2	-0.208	19092.45	450.482	[115]
		27315.3	400.643	
		38094.68	350	
		52102.91	325.08	
		83062.15	300.161	
		130778.8	250.322	
		171051.3	225.402	
		423627.7	199.678	
		1694025	150.643	
		9996716	124.92	
1937.1	-0.125	13764.5	625.31	[116]
		13676.82	576.18	
		21667.07	576.249	
		25747.25	601.363	
		37778.38	550.201	
		47550.03	526.194	
		59089.17	450.966	
		94814.17	375.776	
		148298.9	426.018	
		10000000	276.132	
1574.7	-0.158	29321.48	350	[116]
		42205.09	325.08	
		61923.73	300.965	
		67735.57	275.241	
		96260.99	250.322	
		129987.8	225.402	
		215284.6	212.54	
		296286.5	200.482	

		2473673	602.642	
688.01	-0.153	1009.385	300.828	[80]
		1719.072	200.616	
		15154	149.086	
		85316.79	99.706	
		227508.7	99.823	
		2941439	74.785	
		3646415	75.912	
854.15	-0.06	19515.12	500.054	[96]
		89677.62	375.075	
		887814.5	400.638	
		2241740	348.341	
		9970269	300.525	
		9983086	340.587	
		9982747	320.154	
1715.5	-0.099	20417.89	799.565	[113]
		34340.98	749.525	
		41287.84	699.453	
		59274.21	599.352	
		71808	598.913	
		159279.1	499.927	
		211495.5	448.378	
		214272	404.263	
		250843	404.806	
		301250.4	432.987	
		305907.6	389.879	
		9472175	421.865	
		9869602	390.977	
		9918245	375.219	
2747.9	-0.101	27803.19	898.925	[113]
		415553.4	799.601	
		561748.9	799.573	
		1153550	700.222	
		2071913	596.915	
		4200251	559.303	
		4318286	580.066	
		7675544	559.757	
		2325732	600.192	
		9980707	520.841	

		543564.6	175.563	
		633667.6	163.505	
		9993433	150.643	
4112.1	-0.183	7537.543	708.935	[117]
		11421.22	801.573	
		12580.13	800.772	
		12825.66	704.929	
		46378.52	707.195	
		56268.11	700.842	
		93008.03	598.62	
		193871.1	603.309	
		28330.62	506.841	
		42106.02	507.599	
		65677.81	410.927	
		95744.16	408.519	
		259078.4	505.859	
		385052	303.844	
		10195172	201.384	
3415.6	-0.173	7910.723	806.357	[117]
		11644.13	704.145	
		13591.37	798.389	
		24985.7	689.822	
		24745.39	606.655	
		14402.8	598.781	
		32435.29	512.374	
		45932.45	503.631	
		120738.8	412.459	
		120738.8	404.538	
		244482.4	297.547	
		661556	299.045	
		589114	504.996	
		10097114	249.702	
		10000000	197.426	
2325.4	-0.086	237495.7	706.262	[117]
		271905.3	795.756	
		293762.1	793.373	
		529699.3	793.322	
		936846.5	803.57	
		1392376	706.11	

		9983732	541.111	
1941.6	-0.131	17952.62	633.663	[113]
		28596.51	570.016	
		45223.66	506.576	
		51111.64	485.575	
		69765.84	464.117	
		78724.24	442.602	
		93357.56	401.523	
		104656.8	400.655	
		124399	421.934	
		136930.7	382.255	
		161203.7	386.03	
		325882.7	338.253	
		397402.2	305.541	
		526760.1	315.978	
		9950185	295.165	
948.64	-0.042	26842.09	687.506	[113]
		30383.09	676.584	
		39191.5	613.292	
		35460.59	666.256	
		38261.39	633.42	
		45223.66	581.328	
		59499.72	591.576	
		79675.71	559.901	
		94172.54	538.708	
		82193.29	571.095	
		126196.7	549.216	
		193144.6	569.86	
		535987.8	527.921	
		704069.7	559.53	
		83315.01	548.642	
		10080383	517.359	
1734.3	-0.124	36293.83	526.849	[113]
		60556.05	462.167	
		97103.47	420.151	
		203615.3	357.186	
		220570	377.944	
		272864.2	345.78	
		352219	325.947	

		2109790	708.451	
		3196848	601.484	
		3420604	610.191	
		10000000	609.307	
		10000000	545.149	
2300.6	-0.083	38159.71	882.926	[118]
		91269.28	883.051	
		973369.5	829.727	
		1233312	829.761	
		1288276	779.084	
		1715716	779.125	
		2284977	622.148	
		2720356	619.192	
		2968231	622.186	
		3081262	622.191	
		3622949	620.227	
		3139381	569.523	
		4367334	569.57	
		3062129	675.855	
		3341146	726.55	
		4422081	669.945	
		7508680	622.319	
		8244051	622.332	
		8939382	622.344	
		10125355	623.356	
		10000000	569.689	
		12829378	569.725	
2006.9	-0.122	16459.29	622.432	[118]
		29193.36	622.514	
		37220.7	623.543	
		95336.81	412.995	
		117092.8	415.012	
		163910.9	519.409	
		184503.8	518.432	
		669837.3	311.909	
		1943338	313.056	
		3178735	414.494	
3197.6	-0.211	4084.239	600	[121]
		13335.21	500.901	

		544225	314.043	
		571848.7	303.584	
		673766	366.259	
		1695910	293.449	
		2521774	279.484	
		10030168	255.116	
		156823.2	399.547	
		327566.2	335.65	
870.69	-0.035	25996.1	687.495	[113]
		27365.7	633.558	
		36204.09	613.435	
		46687.23	602.016	
		55455.47	569.098	
		65968.7	590.833	
		66567.54	570.775	
		71948.96	550.04	
		126607.5	548.275	
		10038122	538.974	
		10038122	518.279	
		10038122	491.071	
		10038122	432.102	
		73886.9	568.61	
		70987.55	563.285	
		10080383	506.709	
2341.2	-0.085	18544.01	1002.557	[114]
		70104.78	901.238	
		655174.1	802.805	
		1498081	701.387	
		8801745	600.154	
		10514558	583.936	
1546.3	-0.075	59978.19	699.402	[114]
		357890	599.526	
		510670.7	548.128	
		3370096	474.006	
		7832424	499.905	
		11176812	459.343	
1347	-0.066	7260.476	736.911	[114]
		20624.85	700.547	
		547662.1	596.901	

		23337.57	401.802	
		49878.88	299.099	
		368105.4	200	
		316227.8	174.775	
		594710.4	159.459	
		9920368	150.45	
		9920368	99.099	
849.2	-0.06	19548.13	500.345	[121]
		89986.61	374.812	
		883266.3	400.398	
		2240806	349.321	
		9938128	339.86	
		10000000	319.267	
		9938128	300.078	
3559	-0.223	6033.797	600	[75]
		12873.74	498.69	
		20324.36	399.127	
		33358.52	349.345	
		76926.5	299.563	
		104977.7	249.782	
		175681.4	231.441	
		239743.5	200	
		501674.4	179.913	
		487263.3	138.865	
		711738.9	149.345	
		1625438	130.131	
		10000000	124.017	
		10000000	118.777	
		9903315	99.563	
7942.7	-0.327	2195.565	621.955	[75]
		3531.859	552.316	
		6389.069	482.676	
		12921.11	340.995	
		72981.29	204.117	
6757	-0.255	17454.01	600.408	[126]
		70855.58	397.018	
		92807.07	348.267	
		204984.3	298.072	
		339759.9	246.512	

		4153627	502.49	
		10185304	448.49	
2075.1	-0.114	16483.68	699.874	[120]
		37615.43	651.327	
		85159.39	600.759	
		224160.9	550.19	
		188262.2	499.621	
		262703.6	400.506	
		10019852	348.925	
1614.5	-0.093	20373.23	798.491	[122]
		33191.41	752.153	
		40093.77	701.818	
		60374.66	598.793	
		70115.17	600.398	
		170662	500.619	
		211078.7	451.076	
		298450.1	431.47	
		211078.7	400.702	
		250991	400.738	
		303186.2	381.099	
		9913781	421.956	
		10071100	392.837	
		10071100	375.521	
		10071100	383.392	
2799.3	-0.103	28205.14	900.348	[122]
		413081.5	801.067	
		570962.2	800.91	
		1054746	698.899	
		2074577	599.73	
		4063658	552.479	
		4100007	581.481	
		7989598	550.462	
		10047956	520.673	
		9992131	540.809	
1070.7	-0.061	19981.99	549.723	[123]
		29690.86	549.74	
		35641.79	600.697	
		59623.96	550.625	
		93218.78	500.185	

		450159.7	215.858	
		2026437	187.864	
6724.1	-0.303	1945.453	689.094	[127]
		4093.122	551.388	
		8479.274	412.572	
		41834.6	275.658	
		82727.52	206.092	
		414530.8	136.843	
2303.8	-0.14	19411.8	688.372	[127]
		40265.98	550	
		55571.99	481.395	
		110985.8	412.791	
		239111.7	344.186	
		1068579	309.302	
		10095207	275.581	
4292.7	-0.226	3840.273	689.535	[127]
		10386.3	551.163	
		15759.08	481.395	
		26039.81	411.628	
		126730.4	275.581	
		1000000	189.535	
		926996.7	205.814	
2558.9	-0.088	349884.1	823.226	[119]
		1029040	799.274	
		1626380	749.472	
		2601621	698.588	
		3452374	648.814	
		3966542	674.738	
		6120906	650.887	
		6739313	624.926	
		16442518	599.921	
		22225661	598.793	
1252.2	-0.129	25822.41	398.599	[124]
		43027.4	361.746	
		56235.84	318.103	
		103786	278.341	
		166476.3	259.914	
		184341	239.547	
		256909.7	219.181	

		88325.23	600.29	
		140031.2	549.676	
		149240.4	449.714	
		279704.4	500.114	
		308453.8	449.745	
		15656538	449.799	
		17266213	400.481	
		30726408	351.133	
		42088168	400.441	
		95932631	351.275	
		5.38E+08	301.534	
		9974776	451.114	
		78796.37	500.088	
		6.41E+08	300.8	
		2.16E+09	249.705	
2419.3	-0.194	19002.79	399.569	[124]
		23004.2	358.836	
		38823.33	320.043	
		64687.93	280.28	
		107783.8	240.517	
		154100.8	219.181	
		538773.2	180.388	
		1020338	159.052	
		1267739	150.323	
		2033889	145.474	
		10042721	121.228	

		319334.4	239.547	
		362655.7	199.784	
		439334.3	209.483	
		9670222	159.052	
		9673019	179.418	
		9925730	195.905	
		9666627	132.866	
966.41	-0.034	27991.75	718.203	[124]
		41008.61	719.153	
		43347.41	678.392	
		60670.67	659.207	
		93423.55	638.008	
		84866.81	598.414	
		177955.1	598.414	
		9963551	558.514	
		9998239	519.093	
		57251.53	678.879	
		83949.4	638.147	
		9853016	578.017	
		9981099	587.716	
1305.4	-0.063	318817.5	599.43	[120]
		874561.5	524.249	
		2274205	550.357	
		7062754	474.946	
		20058431	449.725	
		7237754	499.621	